DEVELOPMENT OF CU-BASED CATALYSTS FOR CATALYTIC TRANSFER HYDROGENATION OF FURFURYL ALCOHOL TO γ-VALEROLACTONE

THANISORN RATTANAPORNCHAIWAT

A THE SUBMITTED IN PARTIAL FULFILLMENT OF THE REQUIREMENT FOR THE DEGREE OF MASTER OF SCIENCE IN APPLIED CHEMISTRY

DEPARTMENT OF CHEMISTRY SCHOOL OF SCIENCE
KING MONGKUT'S INSTITUTE OF TECHNOLOGY LADKRABANG

2023
KMITL-2023-SC-M-012-065

Thesis Title	Development of Cu-based catalysts for catalytic transfer hydrogenation of furfuryl alcohol to γ-Valerolactone
Student	Mr. Thanisorn Rattanaphonchaiwat
Student ID	64605051
Degree	Master of Science (Applied Chemistry)
Department	Chemistry
Year	2023
Thesis Advisor	Asst. Prof. Dr. Patcharaporn Weerachawanasak
Thesis Co advisor	Prof. Dr. Tawan Sooknoi

Abstract

This work studied the catalytic transfers hydrogenation (CTH) of furfuryl alcohol (FOL) to γ-valerolactone (GVL) using Cu-based catalysts. The different charges balancing cation of Y zeolite (NH_4^+Y and HY) was comparatively studied the HY (Si/Al = 3.5) shows higher catalytic performance than NH_4^+Y (Si/Al = 3.5) zeolite. Moreover, 5%Cu/Y-IE catalyst shows higher catalytic performance than 5%Cu/Y-IM. However, increasing the amount of Cu loading from 5 to 10% (10%Cu/Y-IM) led to low catalytic activity since the agglomeration of Cu particles blocking some pore of Y zeolite. Therefore, highly dispersion of Cu on phyllosilicate (CuPS) structure is one of the good candidate catalysts for CTH of FOL to GVL. The 30%CuPS exhibits high FOL conversion (71%) with low GVL yield (49.4%). Hence, various secondary metals such as Ni, Ag, and Zn were modified on CuPS to improve the catalytic performance of CTH of FOL to GVL. The 1%ZnCuPS shows the highest catalytic performance (FOL conversion 84%, GVL yield 57%) than other secondary metal catalysts at the beginning. The synergetic effect between Zn and Cu increases the strong

acid strength with high LA/BA ratio resulting to promote the highest catalytic performance. Moreover, to improve more the GVL selectivity from the solvent effect was also studied.

Keyword: Copper phyllosilicate, Catalytic Transfer Hydrogenation (CTH), Furfuryl alcohol (FOL), γ-valerolactone (GVL), Y zeolite.

ACKNOWLEDGEMENT

The authors take this opportunity to acknowledge advisors Asst. Prof. Dr. Patcharaporn Weerachawanasak and Co-Advisor Prof. Dr. Tawan Sooknoi, for the continually suggestion, graceful knowledge, and useful discussion thoughout this research. In addition, we would like to sincere appreciate chairperson and committee member, Prof. Dr. Joongjai Panpranot and Asst. Prorf.Dr. chaval Sriwong, respectively, for the opinions and the guidance with a graceful.

This work is financially supported by Office of the Permanent Secretary, Ministry of Higher Education, Science, Research and Innovation, Thailand (Grant No. RGNS 64-246). The scholarship from School of Science, King Mongkut's Institute of Technology Ladkrabang, Thailand is gratefully acknowledged.

We would like to distribute a kindness thank to the Catalytic Chemistry Research Unit members for their contribution of the ideas and facilities and most importantly their support. We would like to extend our thanks to Dr. Sanchai Kuboon and Mr. Bunyarat Rungtaweevoranit for their help and advice in working the characterization at National Nanotechnology Center (NANOTEC), support and encouragement.

Moreover, we would like to express our appreciation thanks to Department of Chemistry, Faculty of Science, King Mongkut's Institute of Technology Ladkrabang for advanced laboratory instruments, equipment, chemical and accommodation.

Last but not least, the authors would like to gracefully thank the parents and families, who give an encouragement. This thesis would not be possible without them. The thesis is dedicated for the world citizen, who want to be a technical and theoretical expert.

Mr.Thanisorn Rattanaphonchaiwat

CONTENTS

Page

CONTENTS (CONTINUED)

CONTENTS (CONTINUED)

CONTENTS (CONTINUED)

LIST OF TABLES

Table **Page**

LIST OF FIGURES

Figure **Page**

LIST OF FIGURES(CONTINUED)

CHAPTER 1
INTRODUCTION

1.1 Introduction

Nowadays, the energy and chemical industries are highly dependent on the use of fossil resources. The fossil resources play an essential role for worldwide energy use, thus the increased energy demand swiftly diminished fossil fuel resource and increasing emission of greenhouse gases. Moreover, it also affects to environment and life quality. To beyond the scope for further development, researchers are working to find alternative sources for the energy and pollution crisis. The utilization of renewable biomass to produce various chemicals is attractive considering decreasing the fossil fuel crisis. In recent years, since there has been a greater need for more environmentally friendly fuels and chemicals, research into the conversion of carbon sources into highly valued compounds has grown significantly. Because biomass is the most plentiful organic carbon source and is extensively spread, it is frequently used to manufacture biofuels and other important compounds. C5 is one of the biomass feedstocks. It is containing oxygen compounds such as furfural (FF) and furfuryl alcohol (FOL) obtained from hemicellulose is a versatile platform molecule. However, the furfural costs the same as furfuryl alcohol. The furfuryl alcohol is important compounds in the manufacture of fine chemicals such as polyurethane, polyesters, adhesives, perfumes, medicinal intermediates, vitamin C, tetrahydrofurfuryl alcohol (THFA), ethyl furfuryl ether (FE), levulinic acid (LA), and γ-valerolactone (GVL). [1]. GVL is one of the most versatile products that used as the green solvents, jet fuels, food additive, and as an efficient fuel additive. Furthermore, GVL can be transformed and upgraded to various derivatives such as methyl tetrahydrofuran , alkanes, and 1,4-pentadiol[2].

Generally, GVL is synthesized by the hydrogenation of levulinate acid and its ester by using hydrogen gas, which mostly need to operate at high pressures, which makes the methods expensive and unsuitable for industrial manufacturing. Catalytic transfer hydrogenation (CTH) is the name of the synthetic process that involved transferring hydrogen atoms while employing alcohol as a hydrogen donor under mild condition [3].This process can be operated at low pressure. However, it needs to use the specific catalysts such as Lewis and Brønsted acid catalysts. Many researchers reported a number of catalysts that are active for CTH reaction such as transition metals or metal oxides. The transition metals provide the Lewis acid properties, which has been widely used for catalyzing the hydrogen transfer due to it provide high catalytic activity and selectivity for reaction [4]. In this work, we would like to produce GVL from FOL which the reaction pathway is illustrates in **Scheme 1**. The production of GVL from FOL is a one-pot sequential process. The FOL is first transformed to LA or alkyl levulinates (AL) via hydrolysis (Scheme 1, Path a) or alcoholysis (Scheme 1, Path b) catalysed by Brønsted acids. The LA or AL compounds are then transformed to 4-hydroxypentanoic acid and 4-hydroxypentanoates. Finally, the cyclization reaction occurs, generating the GVL product from 4-hydroxypentanoic acid or 4-hydroxypentanotes. Based on this reaction, both types of acid catalysts (Lewis and Brønsted acid) are strongly influenced to control the possible reaction pathway of furfuryl alcohol transformations.[5]

Recently, the literature reviews showed the essential from furfuryl alcohol to GVL via CTH reaction. The Lewis and Brønsted acid site have an influence to control the catalytic performance of this reaction. The metal oxide catalysts containing the suitable acid properties such as Cu/Al_2O_3[6], Cu/SiO_2,[7],Cu/ZSM-5, Pt/ZrO_2, Au/ZrO_2, Au/ZrO_2+ZSM-5[8], Zr-HY-15-20, Al-HY-6 [9], etc. have been reported to be active in this reaction. Although, precious metal-based catalysts have demonstrated exceptional catalytic activity for catalytic transfer hydrogenation to GVL synthesis, their use is constrained by their high

production costs. Therefore, the efficient non noble metal catalysts especially, Cu-based catalysts have been studied and developed for the CTH reaction. [10] However, tuning of Lewis acid and Brønsted acid on catalyst is very challenging. Moreover, using non-noble metal catalysts for direct synthesis of FOL to GVL has not much reported. Therefore, it will be attractive to develop efficient, stable, and environmentally benign non-noble metal Cu catalysts for the CTH of FOL to GVL. Besides the metal active sites, type of support which facilitate the highly disperse of active metal is also affect to the catalytic activity.

The Zeolite Y is an interesting catalyst support because it occupied wide pore channels and large accessible pore volume. Moreover, it has high surface area and could be control the Al contents resulting to low or high exchangeable site of metal [11]. Therefore, the metal can modify in zeolite Y to enhance the catalytic activity. In addition, phyllosilicate is an interesting catalyst because it can give a highly disperse of metal active sites even high metal loading. High surface area of the catalysts and strong interaction between metal and silica. Furthermore, the selection of active metal such as Cu shows an excellent in hydrogenation of formyl group. Thus, Cu phyllosilicate structure consisted of both acidic sites, i) Cu ions in the octahedral layer that acts as the Lewis acid sites, and ii) the OH groups on the surface acts as the Brønsted acid sites. Tuning of both acid sites on Cu phyllosilicate for the CTH of furfuryl alcohol to GVL should be studied.

Therefore, this research aims to design and developed Cu-based catalysts for direct conversion of furfuryl alcohol to GVL. The support containing acidic property with high surface area such as zeolite Y and phyllosilicate have been used to prepared Cu-based catalysts. The functional types (NH_4^+, HY) and Si/Al ratios of zeolite Y have been studied. Moreover, the characteristic and catalytic properties of Cu-based catalysts will be

evacuated in CTH of furfuryl alcohol to GVL. Furthermore, the effect of second metals doping on Cu phyllosilicate catalyst has been investigated.

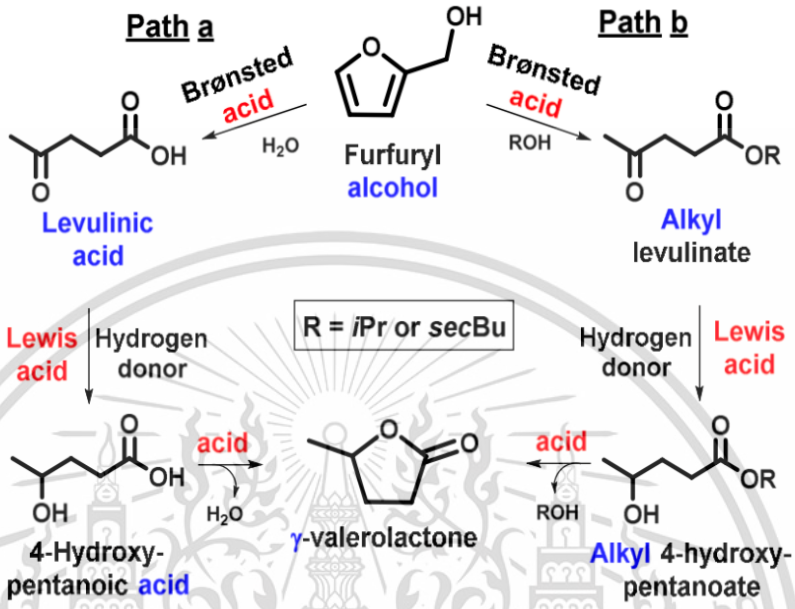

Figure 1.1 The reaction pathway of furfuryl alcohol to GVL [5].

1.2 Research objectives

1.1.1 To comparatively studied the functional types (NH_4^+Y, HY) and Si/Al ratios of zeolite Y in the catalytic transfer hydrogenation of furfuryl alcohol to GVL.

1.1.2 To design and develop Cu-based catalysts such as Cu/Y and Cu phyllosilicate catalysts for the catalytic transfer hydrogenation of furfuryl alcohol to GVL.

1.1.3 To investigate the characteristics and catalytic properties of Cu-phyllosilicate catalysts for the catalytic transfer hydrogenation of furfuryl alcohol to GVL.

1.1.4 The effect of secondary metals doping such as Ni, Zn, Ag, etc. on Cu phyllosilicate catalysts have been investigated in the catalytic transfer hydrogenation of furfuryl alcohol to GVL.

1.1.5 To investigate the effect of solvent on catalytic transfer hydrogenation of furfuryl alcohol to GVL.

1.3 Scopes of the study

1.3.1 The NH_4^+Zeolite Y and H-zeolite Y (Si/Al = 3.5) is comparatively studied in CTH of FA to GVL.

1.3.2 The HY zeolite with various Si/Al ratios (3.5, 7.5, 100) are investigated in CTH of FOL to GVL.

1.3.3 The Cu supported on HY catalysts will be prepared by ion exchanged and incipient wetness impregnation method.

1.3.4 The Cu phyllosilicate catalyst will be prepared by ammonia evaporation hydrothermal method.

1.3.5 The second metals; Ni, Ag and Zn are loading on Cu phyllosilicate catalysts by incipient wetness impregnation method.

1.3.6 All catalysts will be characterized by following techniques.

- X-ray diffraction (XRD)
- X-ray fluorescence spectroscopy (XRF)
- N_2 -physisorption (BET)
- H_2 temperature-programmed reduction (H_2-TPR)
- NH_3 temperature programed desorption (NH_3-TPD)
- X-ray photoelectron spectroscopy (XPS)
- Transmission electron microscopy (TEM)

- In situ time-resolved X-ray adsorption near -edge structure (In-situ TRXANES)
- Pyridine adsorption FTIR spectra (Py-IR)

1.3.7 All catalysts will be investigated the catalytic activity in liquid-phase selective hydrogenation of furfuryl alcohol to GVL. The effect of acidity and type of metal loading on the catalytic performance catalysts will be evaluated.

1.4 Expected Benefits

1.4.1 To obtain the highly efficiency catalysts for the liquid phase selective hydrogenation of furfuryl alcohol to GVL.

1.4.2 To understand the catalytic mechanism of Cu-based catalysts in liquid-phase selective hydrogenation of furfuryl alcohol to GVL.

CHAPTER 2

THEORY AND LITERATURE REVIEWS

2.1 Furfuryl alcohol

Furfuryl alcohol is consisted of a furan ring with a hydroxymethyl group. The furan ring is a heterocyclic organic compound, which has a five-member ring with one atom of oxygen. It can be obtained from the dehydration of sugars, which occurs in a variety of agricultural biomass such as corncobs, oat, wheat bran, and sawdust. Generally, it is a colorless liquid. However, commercial sample is slightly pale-yellow. The physical and chemical properties of furfuryl alcohol are summarized in **Table 2.1**.

Table 2.1 Physical and chemical Properties of furfuryl alcohol [12]

Properties	**Values**
Molecular formula	$C_5H_6O_2$
Structure	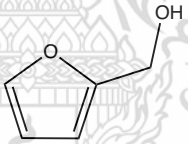
Molecular weight (g/mol)	98.1
Boiling point (°C)	170
Melting Point (°C)	-29
Flash Point (°C)	65
Vapor Pressure @20°C (mbar)	0.53
Relative density @25°C	1.135
Water solubility (g/100ml)	miscible
pH value	6
Color	Slightly pale-yellow.

Furfuryl alcohol is one of a useful chemical since it has one oxygen in furan ring which can produce the renewable energy and high values added chemicals. Generally, Industrial production of furfuryl alcohol involves hydrogenating furfural, which is

commonly made from biomass like maize cobs or sugar cane bagasse. As a green chemical, furfuryl alcohol is regarded, which produced by dehydration of pentose by using acid catalyst. Furfuryl alcohol can undergo several reactions and it gives a variety of valuable products due to the presence of hydroxymethyl group and conjugated system of double bonds in the structure. Furfuryl alcohol is a natural precursor to produce biofuels and biochemicals. In addition, furfuryl alcohol can produce many industrial products such as ranitidine, lysine, fragrance, and solvents. The main furfuryl alcohol derivatives and their applications are shown in **Figure 2.1**

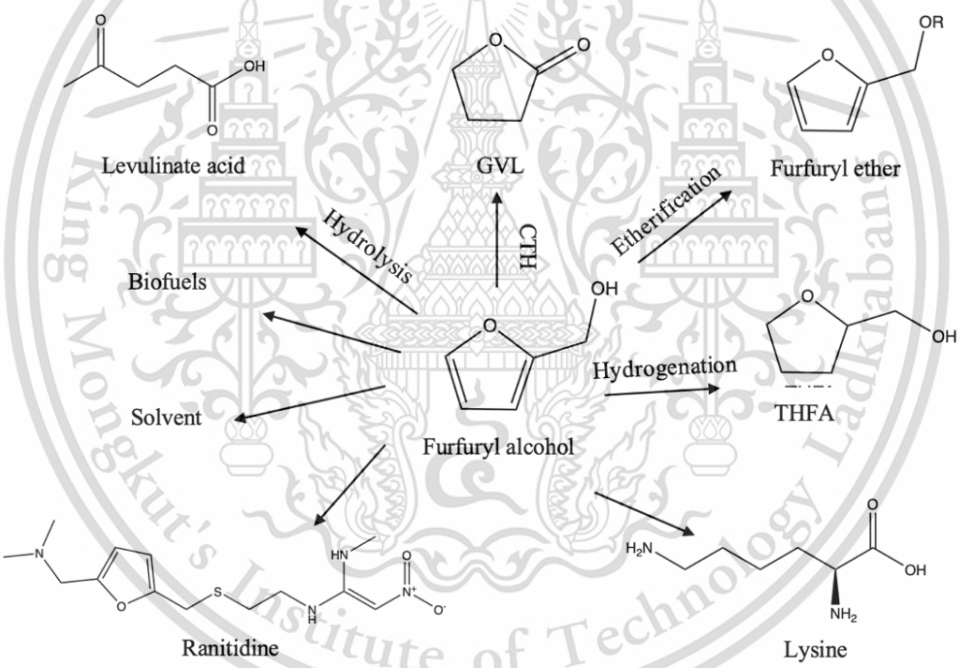

Figure 2.1 The main furfuryl alcohol derivatives and its applications [4].

2.2 γ-Valerolactone (GVL)

GVL is obtained from the hydrogenation of levulinic acid (LA). Typically, it has a high boiling point, low toxicity, and colorless liquid. In addition, it is considered as a sustainable platform molecule to produce fuel additive, jet fuels, and green solvent. GVL can be converted to dimethyl adipate, which is a monomer in the plastic industry and has potential as a gasoline due to its similar combustion energy to ethanol (29.7 MJ/kg). The physical and chemical properties of GVL illustrates in **Table 2.2.** Moreover, the high value-add chemical obtained from GVL are shown in **Figure 2.2.**

Table 2.2 Physical and chemical properties of GVL [13].

Properties	**Values**
Molecular formula	$C_5H_8O_2$
Structure	
Molecular weight	100.12
Boiling point (°C)	207-208
Melting point (°C)	-31
Appearance	Colorless liquid
Density/Specific Gravity (g/mL)	1.050

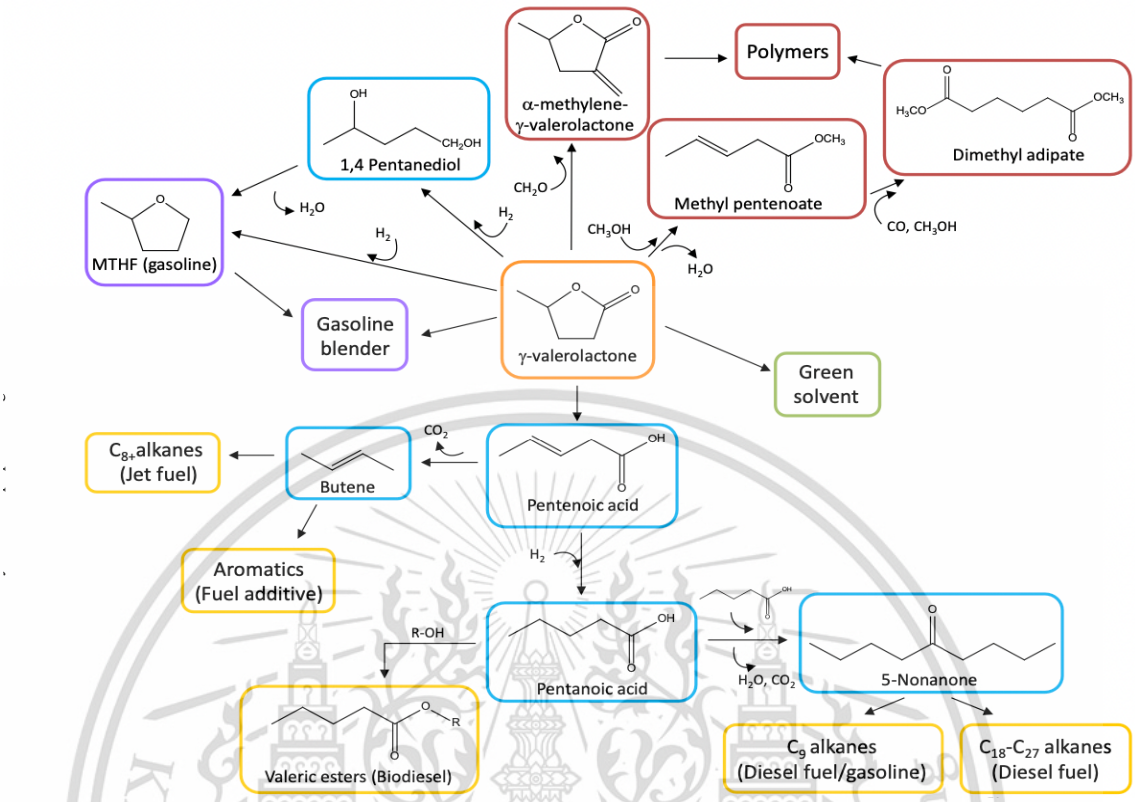

Figure 2.2 High value-added chemicals from GVL[13].

2.3 The catalytic transfer hydrogenation of furfuryl alcohol to GVL

The possible reaction pathways of catalytic transfer hydrogenation of furfuryl alcohol to GVL shows in **Figure 2.3**. There are two reaction pathways: Path A and Path B. According to path A, furfuryl alcohol can converted to Levulinic acid by using Brønsted acid catalyst and Then Levulinic acid can hydrogenated to 4-hydroxypentanoic acid by using Lewis acid catalyst. After that, 4-hydroxypentanoic acid occurs the cyclization to produce GVL. In controversy for Path B, furfuryl alcohol firstly converted to alkyl levulinate by using Brønsted acid catalyst and then it further hydrogenated to alkyl 4 hydroxy pentanoate by using Lewis acid catalysts. After that, it will be occurred lactonization to produce GVL. From this point of view, the reaction mechanism for catalytic transfer hydrogenation of furfuryl alcohol to produce GVL are complicated, and catalysts are a key

factor to control the products. Therefore, the design and development of suitable catalysts for this reaction is challenging and interesting.

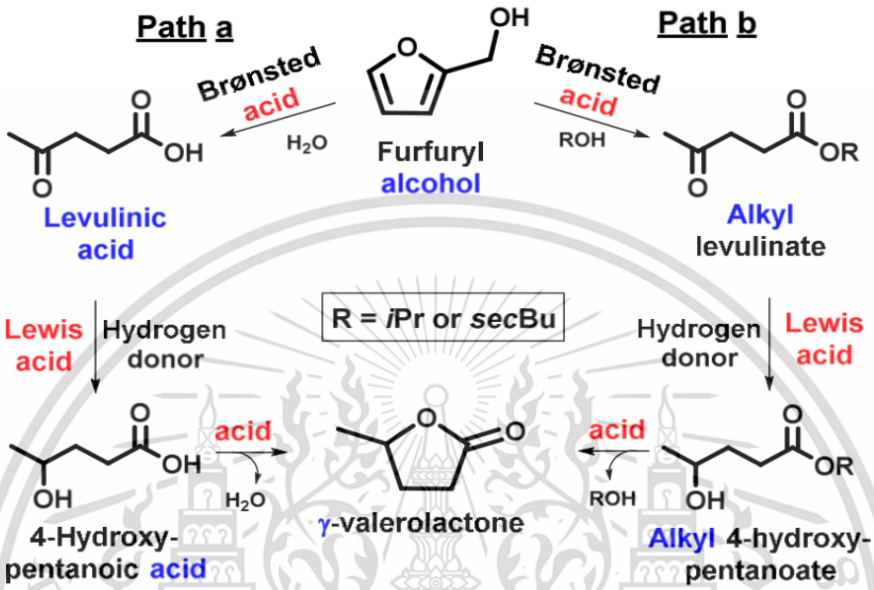

Figure 2.3 The possible reaction pathways of catalytic transfer hydrogenation of furfuryl alcohol to GVL. [5]

2.4 Zeolite Y (FAU)

The zeolite Y belongs to a family of aluminosilicate sieves with a faujasite (FAU-type) structure. Zeolite Y is an aluminosilicates mineral made from interlinked tetrahedra of AlO_4 and SiO_4. It has a relatively three-dimensional structure. The tetrahedra building unit of AlO_4 and SiO_4 are connected via double 6 rings forming a 3D porous channel structure and the pore structure led to a large cavity (supercage). [14] The zeolite Y structure are shown in **Figure 2.4.** An ammonium exchange results in NH_4Y, whereas NH_4^+ cation is ility, thus yielding the final zeolite HY. Furthermore, the structure of zeolite Y is interesting because It has wider channels and a bigger volume of accessible pores. Since it has exceptional qualities including porosity, high surface area, high stability, and strong acidity to offer both Lewis and Brønsted acid sites, crystalline zeolite Y is typically utilized

as a catalyst support. **(Figure 2.5)**. In this combination, the number and strength of the Lewis and Brønsted acid sites can vary resulting to highly obtain the GVL yield [15].

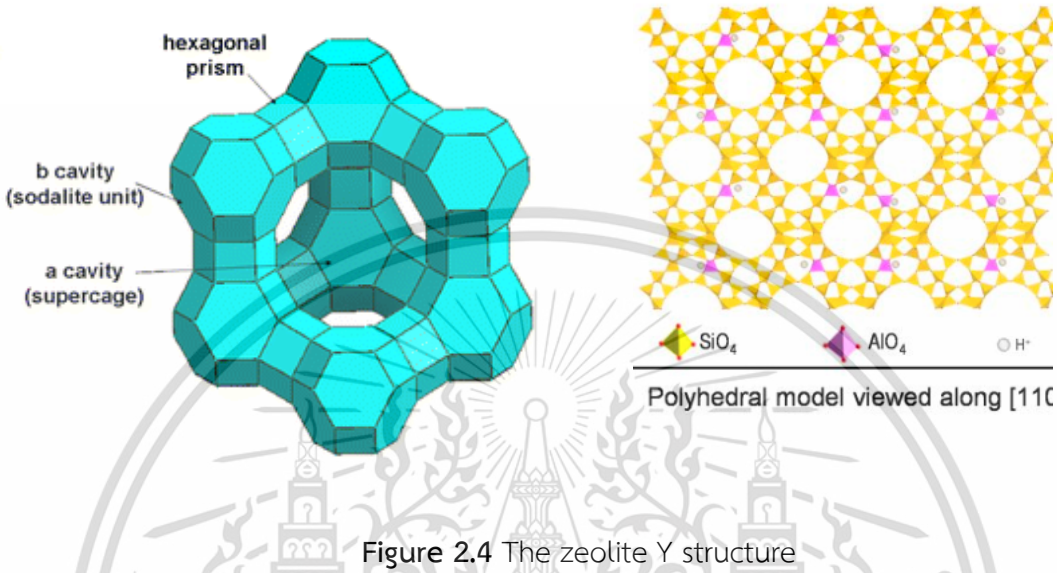

Figure 2.4 The zeolite Y structure

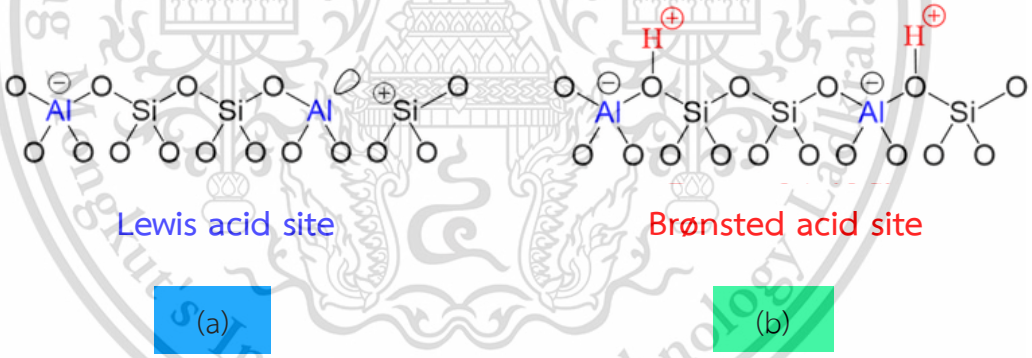

Figure 2.5 The acid sites on zeolite Y a) Lewis acid site and b) Brønsted acid site [15].

2.5 Phyllosilicate

The phyllosilicates' fundamental structure is made up of endless sheets of interconnected SiO_4^{-4} tetrahedra rings with six members. Each tetrahedron shares three of its four oxygen atoms with the other tetrahedra. This results in a $Si_2O_5^{-2}$ fundamental structural unit. as shown in **Figure 2.6a**.

Most phyllosilicates contain hydroxyl ion, OH^-, with the OH located at the center of the 6 membered rings, as shown in **Figure 2.6b**. When other cations are connected to the SiO_4 sheets, the group becomes $Si_2O_5(OH)^{-3}$ because they share the apical oxygens and the (OH) ions, which bond to the other cations in octahedral coordination. This results in the formation of an octahedral layer of cations, commonly Fe^{+2}, Mg^{+2}, or Al^{+3}, which coordinate with the O and OH ions of the tetrahedral layer. As shown in **Figure 2.6c**, the triangles become the faces of the octahedral groups that can bind to the tetrahedral layers.

The octahedral layers take on the structure of either Brucite [$Mg(OH)_3$], if the cations are +2 ions like Mg^{+2} or Fe^{+2}, or Gibbsite [$Al(OH)_3$], if the cations are +3 like Al^{+3}. In the brucite structure, all octahedral sites are occupied, and all anions are OH^-. In the Gibbsite structure every 3rd cation site is unoccupied, and all anions are OH^-.

This gives rise to 2 groups of sheet silicates:

1. the **trioctahedral** sheet silicates, such as Mg+2 or Fe+2, in which each O or OH ion is surrounded by three divalent cations.

2. The **dioctahedral** sheet silicates where each O or OH ion is surrounded by 2 trivalent cations, usually Al^{+3}.

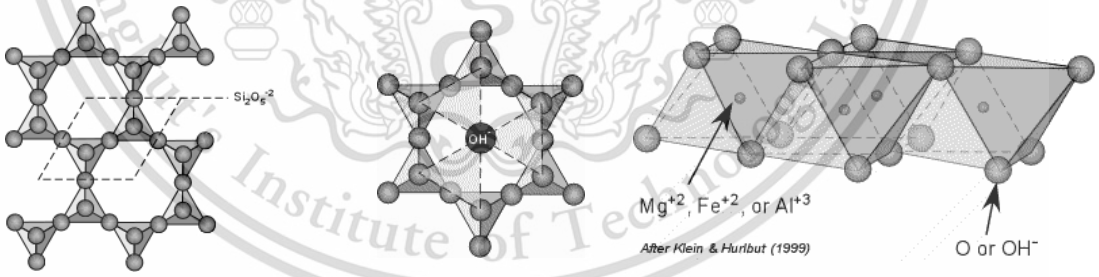

Figure 2.6 Phyllosilicate structure is consisted of a) structural unit of $Si_2O_5^{-2}$, b) OH^- located at the center of the 6 membered rings, and c) the octahedral groups bind to the tetrahedral layers [16].

The advantage of phyllosilicate for using as the catalysts are i) metal ions in the octahedral layer acts as the Lewis acid sites ii) surface OH- groups act as the Brønsted acid

site, iii) it has a high surface area when increases the metal loading, and iv) it occupied the strong interaction between metal and support. Therefore, vary metal on phyllosilicate structures such as Ni, Cu, Mg, etc. phyllosilicates are good candidate to the excellent catalytic performance for catalytic chemicals[17].

2.6 Literature review

This part is summarized the literature research which related to catalytic hydrogen transfer of furfuryl alcohol to Gamma-Valerolactone.

Haryo Pandu Winoto, et.al (2016) studied the production of γ-valerolactone from furfural by using Sn-Al-Beta zeolite [18]. The partial dealumination of Al-B eta induces the formation of a silanol nest at site where the Al was removed and leave some residual Al sites in the framework, when incorporation with tin into the dealuminated beta can be produce Sn-Al Beta zeolite, which has both framework Sn and Al sites. The furfuryl alcohol (FOL) can be etherified to furfuryl ether (FE) and subsequently undergo hydrolysis or alcoholysis to produce isopropyl levulinate (IPL) catalyzed by moderate amount of Brønsted acid sites. Nevertheless, the overall GVL selectivity depend on the higher MPV rection rates of IPL and levulinate acid (LA) with higher amount of framework Sn sites in the catalysts. Moreover, the Sn-Al beta is also more active than a physical mixture, which indicates that the Brønsted and Lewis acid sites in proximity have a synergistic effect in catalyzing this cascade reaction by using Sn-Al-Beta zeolite.

En-Cui Yang, et.al (2021) studied one-pot transformation of furfural into γ-valerolactone by using hierarchical Hf-Al-USY zeolite with balanced Lewis and Brønsted acid sites [19]. They found that H-USY worked in this reaction to convert furfural but showed a low of GVL yield that might be from the Lewis acid sites associated with extra framework Al in H-USY can catalyzed for transfer hydrogenation of IPL. As a result, show IPL was obtained as the main product due to the framework Al-related Brønsted acid site promoted transfer esterification of furfuryl alcohol. When incorporated with Hf species were the optimal Lewis acid centers to convert of FOL to GVL, which could be due to

enhance the rate of hydrogen transfer process involved in the cascade conversion as compared to Sn and Zr. From the FOL to IPL, they are suggesting that in this step Brønsted acid were more suitable for hydrolyticring opening reaction rather than Lewis acid site. The conversion from IPL to GVL proceed via the Lewis acid site framework of Hf sites.

Hongwei Zhang, et.al (2019) studied a combo Zr-HY and Al-HY zeolite catalysts for the one pot cascade transformation of biomass-derived furfural to γ-Valerolactone [9]. They found that the MPV reduction of furfural over the Zr-HY zeolites. To study from the initial rate of reaction and the conversion, For the best catalysts were Zr-HY-x-y (x is the Si/Al ratio before dealumination and y is the Si/Zr ratio after wet-impregnation). Due to from the pyridine results as shown that which had predominantly Lewis acid sites are necessary in MPV reduction, Furthermore, from NH_3-TPD show the surface acid density was the highest amongst all samples tested this suggesting that after Al removal to differences in localization of Zr^{4+} chemically nonequivalent lattice vacancies were formed. The Zr-HY have weaker acid strengths and a higher ratio of Lewis to Brønsted acid sites and show higher activity than Zr-Beta. Moreover, Zr-HY (Si/Zr 20) was attributed to a larger pore size and more hydrophobic as compared with Zr-beta (Si/Zr 12.5). the catalyst mixture with Zr-HY-15-20 and Al-HY-6 exhibited excellent activity.

Kasi Pitchumani, et.al (2011) studied catalytic transfer hydrogenation of carbonyl compounds and carbon-carbon multiple bonds by using Cu nanoparticles supported on zeolite [20]. The Y zeolite and FAU-type zeolites are appropriate hosts because they provide highly organised bigger cavities and can be employed for the assembly of metal and metal oxide nanoclusters since the pore size can limit nanoparticle growth and inhibit further aggregation of nanoparticles. Furthermore, the remarkable catalytic activity of CuNPs/Y zeolite is most likely due to the great dispersion of Cu nanoparticles on the zeolite's surface. They described a highly efficient and expeditions methodology for the chemo selective reduction of aromatic and aliphatic carbonyl compounds, as well as C-C multiple bonds, using zeolite supported Cu nanoparticles and 2-propanol.

Mohammad Reza Loghman-Estarki et.al (2012) synthesized and studied the characteristics of copper oxide nanoparticles supported on zeolite Y[21]. Copper oxide nanoparticles were created using a technique that included (i) ion exchange of copper ions into the zeolite and (ii) precipitation of copper ions within super cages made of microporous and mesoporous material. When the concentration of Cu^{2+} increases, so does the degree of exchange and the copper content in the copper ion exchange method. However, temperature is used to control the position and condition of copper oxide during precipitation and calcination of sodium hydroxide. They discovered that the copper oxide particles enclosed inside the super cage were partially oxidised at temperatures as low as 350°C. Furthermore, stoichiometric copper oxide was created.

Yao Fu, et.al (2017), studied conversion of levulinic acid and alkyl levulinates to biofuels and high valued chemical [22]. They had been proved that the production of levulinic esters from furfuryl alcohol was feasible through alcoholics reaction with strong Brønsted acid as catalyst. The catalytic performances of heterogenous are impacted by many factors, such as sizes of metal particles, surface morphology, acid density. The butyl levulinate through MPV reaction via using Lewis acid was responsible for the catalytic transfer hydrogenation process and the Brønsted acid was responsible for alcoholysis of furfuryl alcohol the combining with acid materials, that toward to produce GVL was observably by using Ru based catalyst.

Gong, et.al (2018) studied transfer hydrogenation of furfural and levulinic acid over supported copper catalyst [23]. The furfural could be adsorbed on top Cu^{+} species (Lewis acid sites) by carbonyl group via η^{1}(O)-aldehyde configuration model. The Cu^{0} species act as active centers for dehydrogenation of 2-propanol to generate active H. the TH active sites of Cu/AC should be Cu^{0}-Cu^{+} complex. For transfer hydrogenation of LA could be captured by the electrophilic Cu^{+} species, then accomplished by catalytic transfer hydrogenation through the MPV reaction at Cu catalyst.

Yongjun Xu, et.al (2020) studied the catalytic transfer hydrogenation of biomass-based furfural into 2-methylfuran over multifunctional Cu-Re bimetallic catalyst [24]. To enhance the hydrogenolysis capability of Cu-based modified by ReO dispersed on Al_2O_3 support exhibited moderate to high activity in hydrogenolysis of furfuryl alcohol to 2-MF. Because of the monometallic of Cu led to large particle sizes and thereby inhibited the activity enhancement. Thus, the influence of Re loading which created more acidic active sites on the catalyst and it change the electronic state was supposed to be the evidence for the existence of Cu-Re synergy, and for $5Cu3Re/Al_2O_3$ catalyst effectively inhibited the sintering this could be noted that the interactions between Cu-Re known as the geometric and stabilizing effect for bimetallic catalyst, which enabled the catalyst to be recycled five times.

Cheng Zhou, et. al. (2016) studied the enhancing of catalytic transfer hydrogenation of ethyl Levulinate to γ-Valerolactone over a robust Cu-Ni bimetallic Catalyst[10]. The copper catalysts exhibited excellent in catalytic transfer hydrogenation reaction for production of various organic chemicals. Nevertheless, which is low stability and easily oxidized nature of these catalysts. Thus, a second metal was introduced copper to bimetallic to enhanced catalytic activity. For the reduced catalysts showed a good dispersion of metal sites indicated that which helped to stabilize and disperse during reduction process. Moreover, the bimetallic can be improved the stability of catalyst even though the catalyst were exposed in the air. This suggesting that a metal promoter could inhibit the sintering of metal particles or change electronic properties of the active sites, resulting in more a robust and efficient catalyst.

REN Jun, et.al (2022) studied study on performance of Ag-modified layered copper silicate catalyst for hydrogenation of dimethyl oxalate to methyl glycolate [25]. The dispersion and chemical state of the Cu component can be controlled by adjusting the morphology and texture of silicon support. The lamellar copper silicate has attracted much attention due to its large specific surface area. The Ag can successfully increase the

dispersion of Cu species and prevent Cu nanoparticle aggregation and sintering. Hence, it is significantly to improve the activity and stability of the catalyst. For the TEM analysis show that after additional the amount of Ag was 5% the metal particle size of catalyst was the smallest and the dispersion of active species was the highest and this is presumably the presence of the interaction between Ag promoter and copper species could effectively inhibit agglomeration and it stay still on lamellar structure. Moreover, the interaction between Cu and Ag have effectively to improve dispersion of active Cu species and the content of Cu^{+} on the catalyst surface and the Ag can stabilize the ratio of $Cu^{+}/(Cu^{+}+Cu^{0})$ on the catalyst surface.

Lauron-Pernot, et.al (2007) prepared of the co-impregnated Cu-Zn/SiO_2 catalysts and studied an influence of the drying step on metallic particle size and on Cu^{0}-Zn^{II} interaction [26]. Through migration of ZnO species onto the copper surface, ZnII can increase dispersion of Cu particles and form active sites at the Cu-ZnOx interface. After reduction, the synthesis of mixed copper-zinc hydroxy nitrate is responsible for improved dispersion of copper metal particles. It implies that the incorporation of Zn2+ ion into the structure of copper hydroxynitrate causes copper precursor fragmentation and the production of a tiny copper particle during reduction.

Qingjie Ge, et.al (2016) prepared the silica-supported copper catalysts by different methods [27]. The silica supported copper catalysts have been studied many maneuverable methods such as impregnation (IM) , ion exchanged (IE) with tetraamine copper cations and ammonia evaporation (AE) method. The Cu/SiO2 catalyst prepared by ammonia evaporation method is believed that the formation of copper phyllosilicate also called chrysocolla. They proposed a comparative effect of Cu^{0} and Cu^{+} to the reduction of highly dispersed CuO and copper phyllosilicate respectively. The ammonia evaporation method was a suitable due to which is highly dispersion even though high copper loading also, the uniform structure that made the Lewis acid and Brønsted acid in chrysocolla structure.

From the literature reviews, the catalysts use to convert furfuryl alcohol to γ-valerolactone requires both of Lewis and Brønsted acid sites. Copper catalysts show the excellent in catalytic transfer hydrogenation of furfural and furfuryl alcohol to GVL. In addition, copper phyllosilicate (CuPS) shows a highly dispersed of copper and it can improve the selectivity of GVL by using second metal. Therefore, in our work, the Cu Y and CuPS are interesting and will be prepared for the catalytic transfer hydrogenation of furfuryl alcohol to GVL. Moreover, the effect of second metal doping on CuPS catalysts for the catalytic transfer hydrogenation of furfuryl alcohol to GVL have been studied.

CHAPTER 3

EXPERIMENTAL

3.1 Chemical

Details of the chemical used to prepare catalyst and used for the reaction study have been summarized in **Table 3.1**

Table 3.1 List of the chemicals for catalysts preparation and catalytic testing

Chemical	Grade of purity	Supplier
Zeolite NH_3Y	-	Zeolyst
Nitric acid	69.5%	CARLO ERBA
Ammonia Solution (NH_4OH)	28-30%	CARLO ERBA
Copper (II) nitrate trihydrate ($Cu(NO_3)_2 \cdot 3H_2O$)	99.50%	QRECC
Furfuryl alcohol	99.00%	Sigma Aldrich
Isopropanol	99.90%	CARLO ERBA
Methanol	99.80%	CARLO ERBA
Toluene	40.00%	CARLO ERBA
LUDOX® AS-40 colloidal silica	98.50%	Sigma Aldrich
Air zero grade das	99.99%	UIG
1% Ammonia in Helium	99.99%	Linde
Helium gas	99.99%	PRAXAIR
Hydrogen gas	99.99%	UIG
1% Hydrogen gas in Argon	99.99%	PRAXAIR
10% Hydrogen gas in Argon	99.99%	PRAXAIR
Nitrogen gas	99.99%	UIG

Distilled water	-	-

3.2 Catalysts preparation

3.2.1 Preparation of 5wt% Copper Zeolite Y Catalyst (5%Cu/Y-IE) by ion-exchanged method

Copper Zeolite Y Catalyst (Cu/Y-IE) were prepared by dissolved Copper (II) nitrate trihydrate (Cu) (Cu $(NO_3)_2 \cdot 3H_2O$) 9.664 g in 400 mL of deionized water. Then, control pH value between 3-4 by using nitric acid, to avoid the formation of metal hydroxide. After that the solution was mixed with the zeolite 4g. The suspension was stirred at 80°C in a water bath for 5h to aqueous ion exchange (AIE). The solid sample was separated from slurry using centrifugation at 9000 RPM, washed with deionized water to eliminate nitrate impurities, and dried overnight at 120°C. This procedure was performed three times using fresh copper nitrate solution each time to achieve complete ion exchange capacity. Finally, the catalyst was activated by calcination at 550°C in furnace with the heating rate of 1°C/min under 60 mL/min of air flow for 5 h. The obtained solid was denoted as 5%Cu/Y-IE catalyst.

3.2.2 Preparation of 5wt% Copper Zeolite Y Catalyst (5%Cu/Y-IM) by impregnation method

Copper Zeolite Y Catalyst (Cu/Y-IM) were prepared by dissolved Copper (II) nitrate trihydrate (Cu) (Cu $(NO_3)_2 \cdot 3H_2O$) 1.005 g in 20.5 mL of deionized water. Then The solution was slowly dropped on zeolite Y as a support (6g) until solution of Cu is used up and dried overnight at 120°C. Finally, the catalyst was activated by calcination at 550°C in furnace with the heating rate of 1°C/min under 60 mL/min of air flow for 5 h. The obtained solid was denoted as 5%Cu/Y-IM catalyst.

3.2.3 Preparation of 10wt% Copper Zeolite Y Catalyst (10%Cu/Y-IM) by impregnation method

Copper Zeolite Y Catalyst (Cu/Y-IM) were prepared by dissolved Copper (II) nitrate trihydrate (Cu) (Cu $(NO_3)_2$•$3H_2O$) 1.71 g in 35.5 mL of deionized water. Then The solution was slowly dropped on zeolite Y as a support (5g) until solution of Cu is used up and dried overnight at 120°C. Finally, the catalyst was activated by calcination at 550°C in furnace with the heating rate of 1°C/min under 60 mL/min of air flow for 5 h. The obtained solid was denoted as 10%Cu/Y-IM catalyst.

3.2.4 Preparation of 30 wt% Copper Phyllosilicate Catalyst (30%CuPS)

30 wt% Copper Phyllosilicate Catalyst (30%CuPS) were prepared by dissolved Copper (II) nitrate trihydrate (Cu $(NO_3)_2$•$3H_2O$) 9.77 g in 60 mL of distilled water. Then, 30.3 mL of ammonia solution was added and continuously stirred for 10 min with the ratio of [Cu]:[NH_3] = 1:12. After that, 11.60 mL of colloidal silica sol. (40 wt%) was added and stirred for 24 h at room temperature (pH≈11). The suspension was stirred at 80°C in a water bath to evaporation ammonia until pH value decreased from 11 to 7. The remaining mixture was then hydrothermal at 150°C for 24 h. After that, the solution was filtered and washed with distilled water, and dried at 60°C for 24 h. The obtained solid was calcined in a tube furnace at 400°C with the heating rate of 1°C/min under 60 mL/min of air flow for 4 h. The obtained solid was denoted as 30%CuPS catalyst.

3.2.5 Preparation of All secondary metal on Copper Phyllosilicate Catalysts by the incipient wetness impregnation method (Ni,Ag,Zn)

Briefly 0.2001g of $Ni(NO_3)_2$ for 1wt%NiCuPS and , 0.1378 g of (Zn $(NO_3)_2$•$6H_2O$) for 1wt%ZnCuPS was dissolved in acetone. 0.063 g of $Ag(NO_3)$ for 1wt%AgCuPS was dissolved in acetonitrile, The solution (6mL) was slowly dropped on 30%CuPS and then dried at 60 °C for 24 h. Then, the sample was calcined in air at 400°C for 4 h. The catalyst was denoted as 1wt%NiCuPS, 1wt%AgCuPS ,and 1wt%ZnCuPS catalyst respectively.

3.3 Catalyst Characterization

3.3.1 X-ray Fluorescence (XRF)

The chemical composition of catalysts can be also determined by a wavelength - dispersive X-ray fluorescence spectrometry (WD-XRF). The sample is prepared by mixing 4.5 grams of boric acid and 0.5 grams of catalyst followed by manual grinding. The mixture was packed onto the sample holder and then compressed at 150 kN. The sample was placed in the sample chamber. CuKα was employed as a source for the measurement with 50 kV. 60 mA.

3.3.2 X-ray Diffraction (XRD)

X-ray diffraction methods are the most effective methods for determining the crystal structure of materials. The sample was packed onto the sample holder and then press surface smooth. X-ray tube Copper is employed as a source for the measurement with 40 kV, 30 mA. Scan range 20-80 deg, step size 0.0200 deg.

3.3.3 N_2 Physisorption (BET)

Specific surface area of a catalyst was measured by an Autosorb (Quantachrome) instrument. Each sample (weighed approximately 0.1g) was degassed at 300°C for 12 h prior to analysis. After that, nitrogen gas was adsorbed on the surfaces of the sample at -196°C. The adsorbate pressure was fixed at 1 torr, the equilibration time of 3 min at each point, and the scaled tole, the equilibration time of 3 min at each point, and the scaled tolerances were set zero. The surface area was analyzed employing BET equation. The BJH pore size distribution was also calculated.

3.3.4 H_2-Temperature programmed reduction by hydrogen gas (H_2-TPR)

The reducibility property of metal contents can be determined by a temperature programmed reduction by H_2 gas (H_2-TPR). The measurement was performed in a quartz tube connected with a thermal conductivity detector (VICI). Prior to an analysis, the

samples (0.03 g approximately) were activated in air (flow rate of 30 mL•min^{-1}) from room temperature to 400°C at a heating rate 5°C min^{-1}, the system was naturally cooled down in the atmosphere of nitrogen gas (flow rate of 30 mL•min^{-1}) to room temperature. Then, the gas was switched to 10% H_2 in Ar at the heating rate 10°C min^{-1} from 35 to 800°C the TCD signal was calibrated employing a known mass of CuO as a standard, considering that CuO is reduced stoichiometric ally and completely to Cu and H_2O. The internal TCD calibration was performed after every run by pulsing 10% H_2/Ar in the fixed loop. The reduction profile of CuO and the use of hydrogen is equal to the number of moles of copper. The amount of metal loading is expressed as mmol of H_2 consumed per mass of a catalyst (mmol H_2/g). The copper dispersion was estimated by dissociative N_2O adsorption technique. Briefly, after the first H_2-TPR at 250°C for 2h, the sample was subsequently treated in a pure N_2O stream at 60 °C for 1h. After that the N_2O was flushed with N_2 at 60 °C for 30 min and then raised to 100 °C and hold for 30 min. Finally, the second H_2-TPR was then performed from room temperature to 250 °C, to quantify the surface Cu species. The copper dispersion (D_{Cu}) can be estimated by fraction of Cu (2nd H_2-TPR) over total Cu (1st H_2-TPR). The copper dispersion and specific copper surface area can be calculated [28].

3.3.5 NH_3-Temperature Programmed Desorption (NH_3-TPD)

The acid sites of the catalyst were identified using temperature-programmed desorption of ammonia (NH_3-TPD) measurement. Sample was preheated in the flow of air zero (30mL/min) at 400°C for 1 h and evacuated. After that, it was exposed to 20 kPa of 1% NH_3/He gas at 30°C until saturation coverage was reached. Afterward, the sample was flushed with He at room temperature for 40 min, the temperature was then increased at a linear rate of 10°C /min from 50 to 900°C under vacuum.

3.3.6 X-ray photoelectron spectroscopy (XPS)

X-ray photoelectron spectroscopy (XPS) is a useful measurement technique because it shows what elements are within a film and what other elements they are

bonded to. This means if you have a metal oxide and you want to know if the metal is in a+1 or +2 state, using XPS will allow you to find that ratio. However, at most the instrument will only probe 20 nm into a sample.

3.3.7 Pyridine adsorption FTIR spectra (Py-IR)

The nature of acid sites of phyllosilicate was further determined by pyridine adsorption FTIR spectra (Py-IR). Py-IR spectra were conducted on Bruker Equinox 55 FT-IR spectrometer equipped with mercury cadmium telluride (MTCB) detector. The powder sample was pressed into a disk and prepared in vacuum at 300°C for 1 h for the calcined sample. Then it was exposed to pyridine vapor at 30°C. The Py-IR spectra were then recorded at 200°C after vacuum for 30 min.

3.3.8 In situ time-resolved X-ray adsorption near-edge structure (*In-situ* TRXANES)

The experiments were performed at BL2.2: *In-situ* TRXAS, Synchrotron Light Research Institute (SLRI), Thailand. An energy dispersive monochromator and position sensitive detector was employed to perform XANES measurement. The Cu K-edge XANES was collected using the integration time of 2000 ms with an average of 10 scans. The oxidation state of copper composition was estimated by Linear Combination Fitting (LCF) of XANES spectra over Athena software using Cu foil, Cu_2O, CuO and $CuSO_4$ as a standard.

3.3.9 Transmission electron microscopy (TEM-EDS)

The Cu nanoparticle size was measured by transmission electron microscopy (TEM) on a JEM-2010. The sample was dispersed in ethanol and deposited on copper grids coated with transparent carbon foil and dried in vacuum.

The Cu nanoparticle size STEM with the elemental mappings images of metal was measured by transmission electron microscopy (TEM-EDS) on a JEOL : JEM-ARM200F. The

sample was dispersed in ethanol and deposited on Ni grids coated with transparent carbon foil and dried in vacuum

3.4 Catalysts Activity test

The liquid phase hydrogenation of furfuryl alcohol was carried out in a 100 ml of batch type autoclave reactor. Typically, 200 µL of furfuryl alcohol was mixed with 10 mL of isopropanol in a volumetric flask and then put it in the Teflon liner tube in an autoclave reactor. Approximately 200 mg of catalyst was added to the reactor and then closed. After that. the reactor was purged 3 times with N_2 to replace the air inside. Then, 10 bars were put of N_2 into the reactor top prevent the evaporation of gas product. After that, the reactor was heated to the reaction temperature (140°C). The stirring speed was set at 600 rpm. After reaction, the liquid products were separated from the catalyst by centrifugation. The liquid product was mixed with external standard and analyzed by gas chromatography using RTX-5 capillary column.

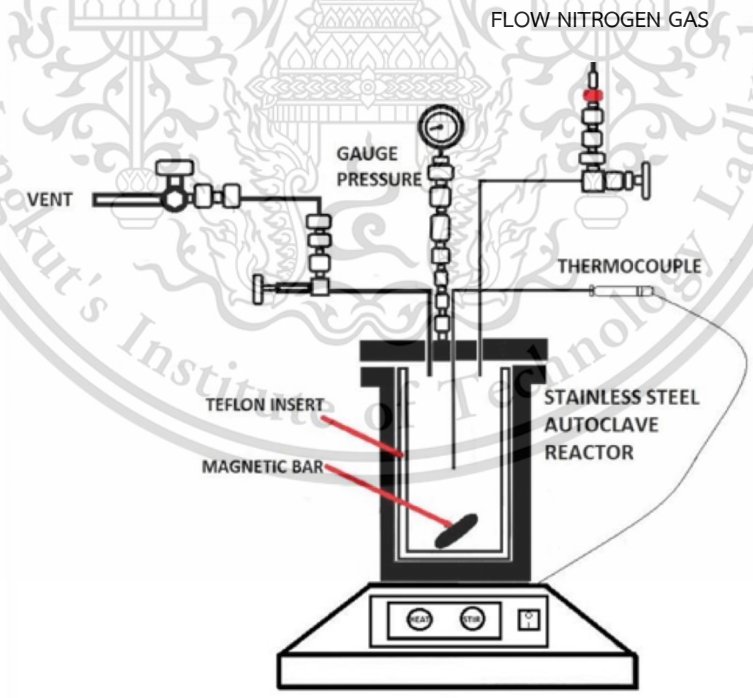

Figure 3.1 Schematic diagram of batch reactor for liquid-phase hydrogenation of furfuryl alcohol to GVL.

CHAPTER 4

Result and Discussion

PART1: To study catalytic performance of Y zeolite and Cu/Y catalysts.

4.1 Catalysts Characterization

4.1.1 X-ray diffraction pattern, XRD

The crystal structure and phase compositions of Y zeolite catalysts were determined by XRD techniques. The XRD patterns of NH_4^+Y3.5 and HY zeolites with various Si/Al ratios (3.5,7.5,100) show in **Figure 4.1.** The diffraction peaks of NH_4^+Y3.5 and all HY zeolites exhibit the same characteristic peaks at 2θ = 6.24°,10.2°,12.5°,16.0°,19.0°,21.0°,23.2°,24.0°,27.6°, 30.5°, 31.3° ,32.9° and 34.8° which were assigned to Y zeolite structure[29]. However, low crystallinity was observed on NH_4^+Y (3.5) when compared with HY (3.5) zeolite. Moreover, the high crystallinity enhanced when increased Si/Al ratios from 3.5 to 100 since the amount of Si-O-Si bonding increased when increase Si/Al ratios resulting to higher crystallinity. **Figure 4.2** shows the XRD patterns of 5%Cu/Y-IE, 5%Cu/Y-IM and 10%Cu/Y-IM catalysts after reduction at 500 °C. The crystal phase of metallic Cu^0 could be observed at 2θ = 43.2° on all catalysts [30]. It can be noted that CuO was completely reduced to metallic Cu^0 after reduction at 500 °C. Nevertheless, the diffraction pattern of Y zeolite is still observed.

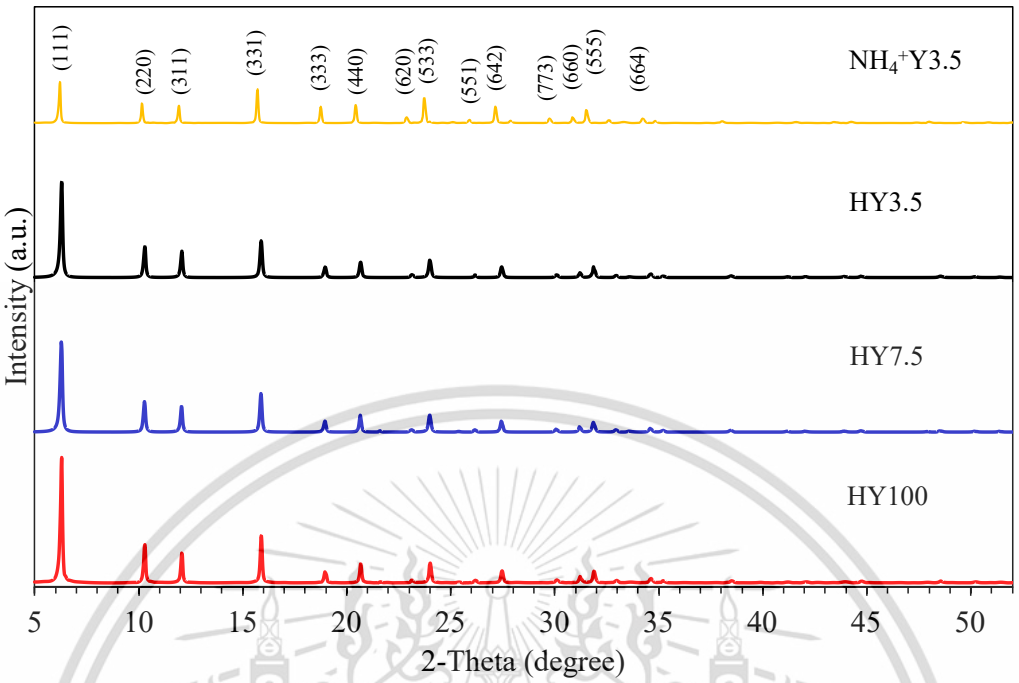

Figure 4.1. XRD patterns of NH_4^+Y (3.5) and HY zeolites (Si/Al ratio 3.5, 7.5 and 100)

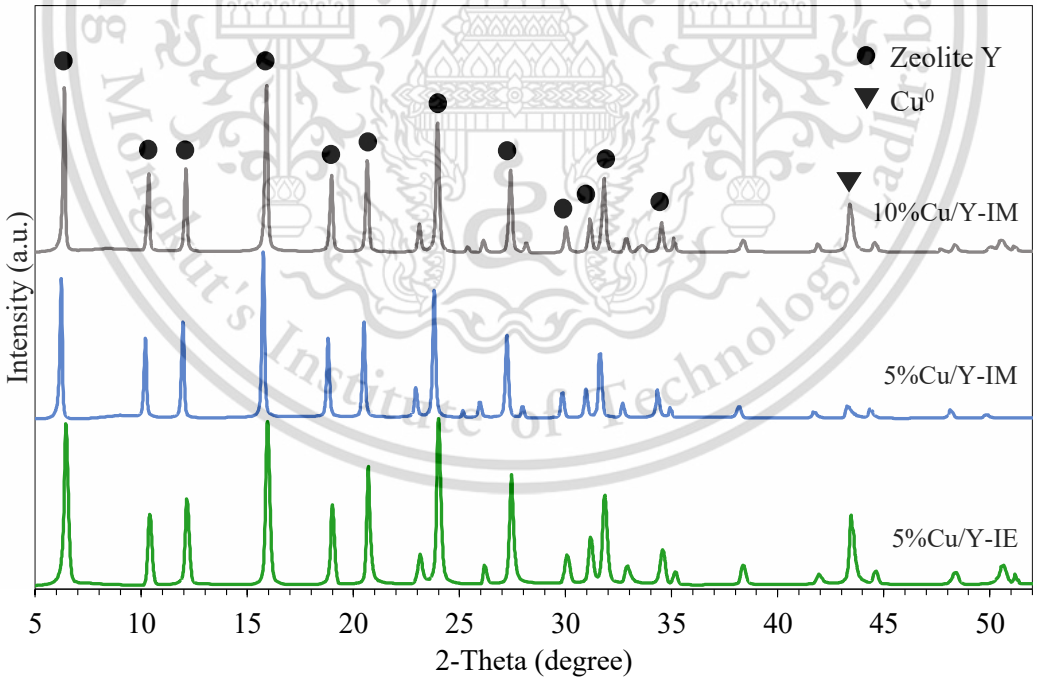

Figure 4.2. XRD patterns of 5%Cu/Y-IE , 5%Cu/Y-IM and 10%Cu/Y-IM catalysts after reduction at 500 °C.

4.1.2 H_2 Temperature program reduction (H_2-TPR)

The reduction behavior, reducibility property and dissociative N_2O adsorbed of 5%Cu/Y-IE, 5%Cu/Y-IM and 10%Cu/Y-IM catalysts can be determined by temperature program reduction of H_2 (H_2-TPR) as shown in **Figure 4.3.** For these catalysts were exhibited two reduction peaks, which is attributed to the reduction of CuO highly dispersed strongly interacting with Y zeolite as a supported [31]. In addition, these results referring to the presence of Cu species in various positions within the Y zeolite's faujasite structure. Furthermore, zeolites may include a wide range of Cu species, including single Cu cations at ion-exchange locations, O-bridge Cu dimers $[Cu\text{-}O\text{-}Cu]^{2+}$ or even chains, Cu^0 nanoclusters, and crystalline Cu, Cu_2O, and CuO of various sizes [32]. The 5%Cu/Y-IE catalysts were showing the highest reduction temperature than other catalysts indicating that the 5%Cu/Y-IE catalysts not only strong interaction between Cu^{2+}/Cu^{+} species and Y zeolite [33]. But it was highly dispersion than other catalysts[34] are shown in **Table 4.1**. To estimate the dispersion and quantify the surface concentration of metallic Cu^0, reduced Cu/Y catalyst was subjected to adsorb N_2O followed by H_2-TPR testing to acquire amounts of consumed H_2. The Cu dispersion was 58.4%, 49.5 % and 39.2% for 5%Cu/Y-IE, 5%Cu/Y-IM and 10%Cu/Y-IM respectively.

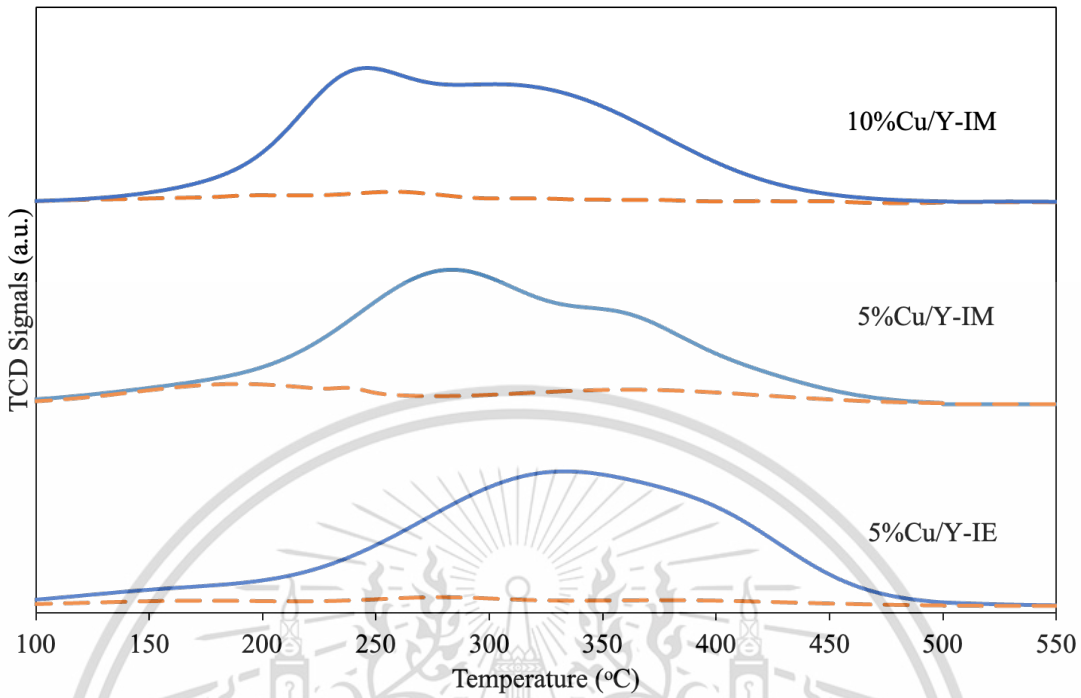

Figure 4.3. H_2-TPR of 5%Cu/Y-IE, 5%Cu/Y-IM and 10%Cu/Y-IM catalysts.

4.1.3 Physiochemical properties of Y zeolite and Cu/Y catalysts.

Table 4.1 summarized the amount of metal loading, BET surface area, pore volume, and average pore size diameter. The actual amount of Cu loading was 4.7 wt.%, 4.9 wt.%, and 8.2 wt.% for 5%Cu/Y-IE, 5%Cu/Y-IM, and 10%Cu/Y-IM respectively. These Cu loading were consistent with the desired amount of Cu loading and corresponding well with Cu content calculated by H_2-TPR. The BET surface area of NH_4^+Y3.5 was 763 m^2/g, and total pore volume was 0.57cm^3/g with an average pore size of 30.3 nm. After Cu loading on NH_4^+Y3.5 by different methods, the BET surface area significantly decreased to 713 and 584 m^2/g for 5%Cu/Y-IE and 5%Cu/Y-IM, respectively. Remarkable, the BET surface area of 5%Cu/Y-IE is higher than 5%Cu/Y-IM due to the ion exchange method give more Cu highly dispersed on surface of NH_4^+Y3.5 than impregnation method [35]. Furthermore, when increase the Cu loading from 5 to 10 wt.% the BET surface area of 10%Cu/Y-IM

significantly decreased. **Figure 4.4** shows adsorption-desorption isotherm of all catalysts. These catalysts show type IV isotherm indicating that they were mesopores structure[37].

Table 4.1 The amount of metal loading, surface area, average pore volume, and pore size diameter of catalysts

Catalyst	Cu loading [a] (%)	N_2 adsorption-desorption			H_2-TPR		
		S_{BET} (m^2/g)	V_p (cm^3/g)	D_p (nm)	H_2 consumption	Cu content (wt%)	Dcu (%)
NH_4^+Y	0	763	0.57	30.3	-	-	-
5%Cu/Y-IE	4.7	713	0.53	29.6	0.73	4.64	58.4
5%Cu/Y-IM	4.9	584	0.34	29.4	0.75	4.81	49.5
10%Cu/Y-IM	8.2	500	0.36	29.1	1.27	8.11	39.2

[a] Determined from XRF.

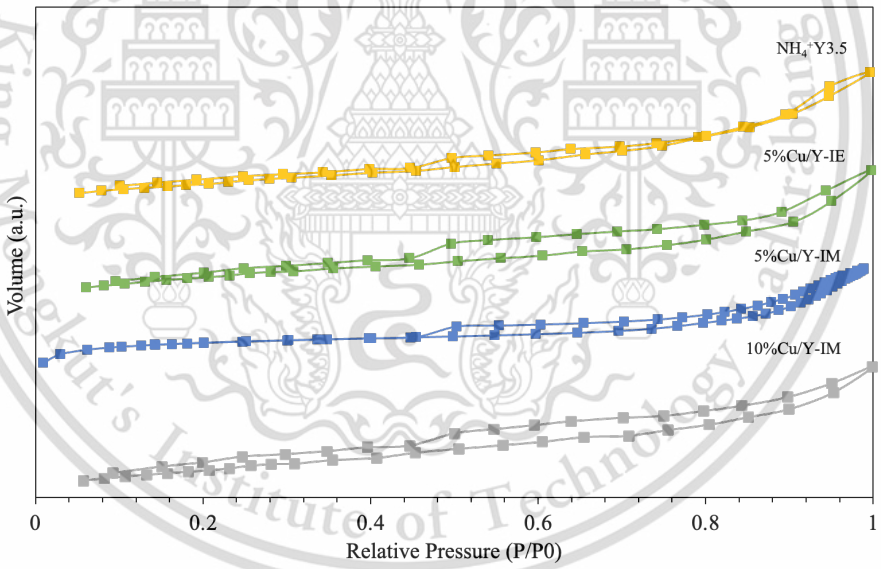

Figure 4.4 N_2-adsorption-desorption isotherm of NH_4^+Y3.5 5%Cu/Y-IE, 5%Cu/Y-IM and 10%Cu/Y-IM catalysts.

4.1.4 Transmission Electron microscope (TEM)

The morphology of HY zeolite and Cu/Y catalysts with particle size distribution of Cu were determined by TEM technique as the results show in **Figure 4.5**. The HY 3.5 zeolite shows the cylindrical mesopores connecting[38]. After immobilized with Cu on Y zeolite with different method. It was found that the Cu nanoparticles can be observed on all catalysts. Nevertheless, 5%Cu/Y-IE not only highly dispersed on Y zeolite but also the particles size distribution (3.53 nm) was smaller than 5%Cu/Y-IM (5.20 nm), indicating that the ion exchange method that exhibit for Cu high dispersion on Y zeolite[39]. Furthermore, 10%Cu/Y-IM was show the largest particle size (5.69 nm) and lowest dispersion corresponding with surface area **(Table 4.1)**

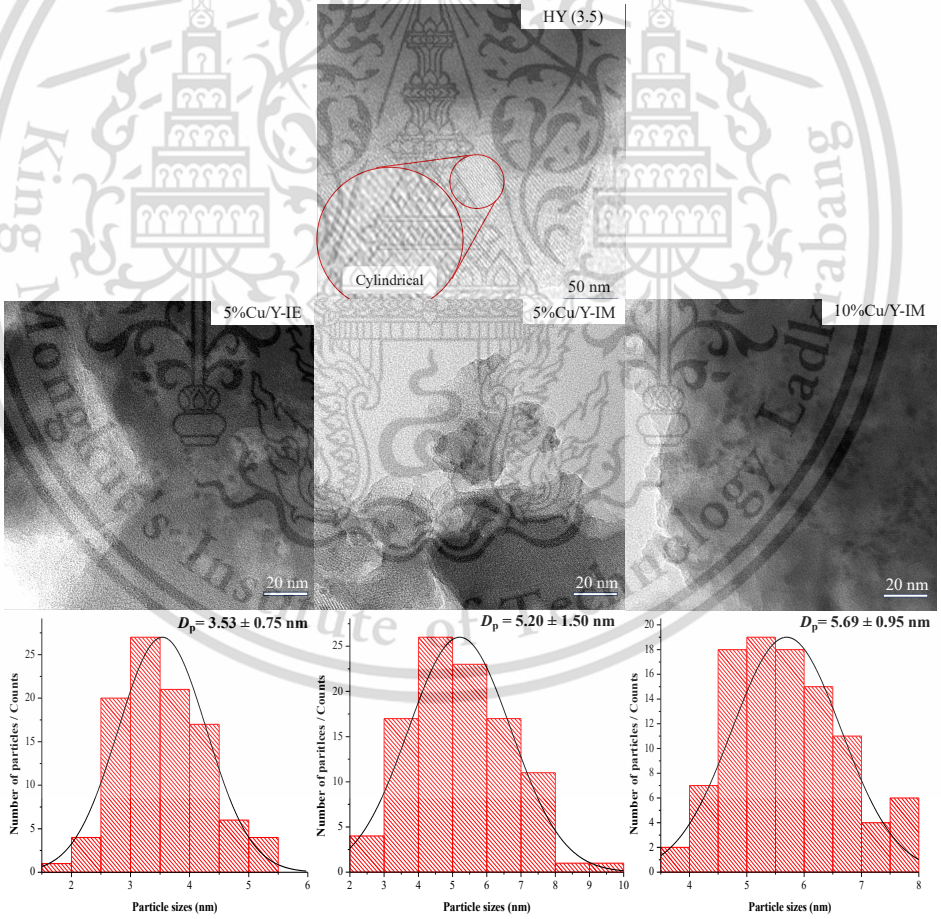

Figure 4.5. TEM image of HY3.5, 10%Cu/Y-IE and 10%Cu/Y-IM catalysts after reduction at 500 °C (Si/Al ratio= 3.5).

4.1.5 X-ray Photoelectron Spectroscopy (XPS)

The electronic state of 5%Cu/Y-IE, 5%Cu/Y-IM and 10%Cu/Y-IM catalyst was investigated by XPS analysis. The results of XPS spectra of 5%Cu/Y-IE, 5%Cu/Y-IM and 10%Cu/Y-IM catalysts are shown in **Figure 4.5.** It can be observed that for 5%Cu/Y-IE, 5%Cu/Y-IM and 10%Cu/Y-IM catalysts show peaks at 932.3 eV and 953.2 eV can be attributed to Cu^{+} species [40]. In the mean while the small peaks at 935.1 eV can be assigned to Cu^{2+} species, it suggests that most of Cu^{2+} was reduced to Cu^{+} species. Moreover, all these peaks shifted to lower binding energies, due to the electronic environment of the Cu have been changed. Hence, it could be transfer of electron from Y zeolite to Cu or Y zeolite act as an electron donor [41]. Furthermore, for the 5%Cu/Y-IE catalysts show the highest binding energy than the other catalysts. Because of it hardly to change from metallic Cu, it might be from the strong interaction between Cu and Y zeolite due to the nanoparticle of Cu are highly dispersed into the zeolite structure[42]. Corresponding with the H_2-TPR and dissociative N_2O adsorbed in **Figure 4.4**

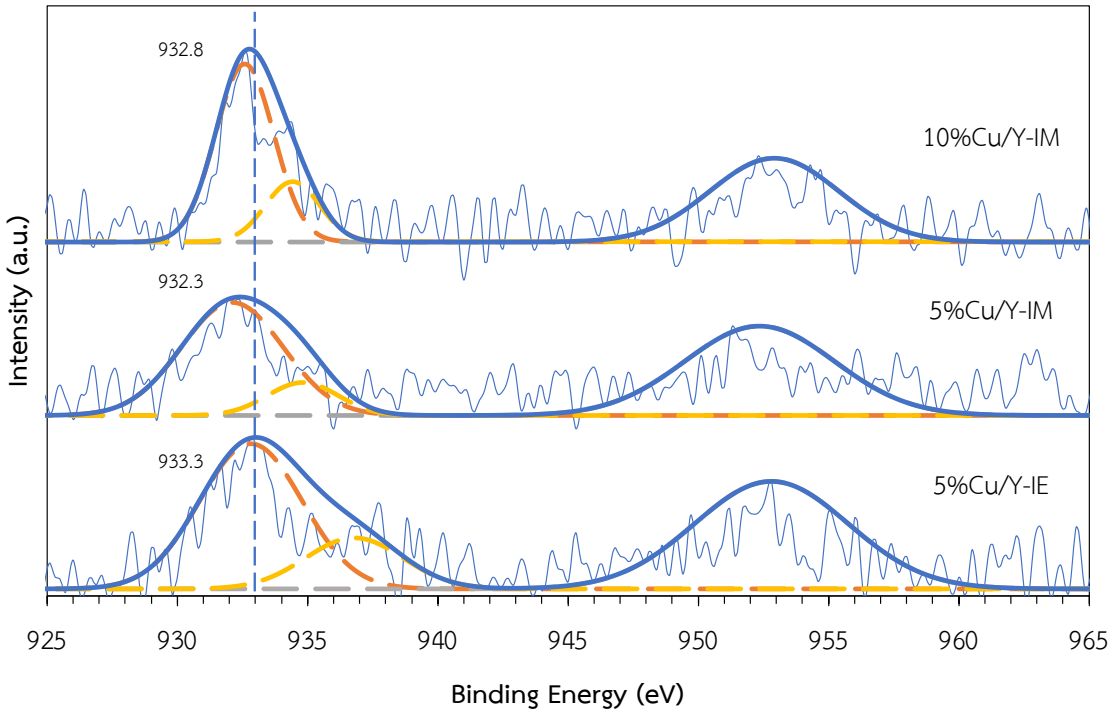

Figure 4.6. XPS spectra of Cu2p 5%Cu/Y-IE , 5%Cu/Y-IM and 10%Cu/Y-IM catalysts.

4.1.6 NH_3-Temperautre program desorption (NH_3-TPD)

The acidity and acid strength of catalysts were investigated by NH_3-TPD, and the results illustrated in **Figure 4.7.** The acidity deconvoluted from NH_3-TPD peaks of NH_4^+Y3.5 show ammonia desorption temperature lower than HY3.5, indicating that the HY3.5 not only stronger acid than the NH_4^+Y3.5 but present is more acidity as well [43] relating with in the **Table 4.2.** For the HY with different Si/Al ratio from 3.5 and 7.5 were produced three desorption peaks except HY100 was show two desorption peaks. According to, the low desorption temperature is derived from weakly adsorbed ammonia molecules via hydrogen while the higher desorption temperature is attributed to strong Brønsted acids acid sites [44]. Although, the Si/Al ratio of Y zeolites increased from 3.5 to 100, the total acidity remarkably decreases. Because of the higher number of aluminum atoms is attributed to the less unbalanced the network in zeolite structure and the lower strength of acid sites [45]. Due to when balanced by a proton as a contraction, also binds oxygen to the Si-O–Al bridge, forming hydroxyl groups that act as strong Brønsted acids. The interaction between the aluminum and oxygen atoms weakens the OH bond, increasing the acidic strength of the protons [-Al- (OH) -Si-] [46]. Hence, the results of acidity of HY with higher Si/Al ratio was show the total acidity will be decreased corresponding with **Table 4.2**. Moreover, when immobilized with Cu in NH_4^+Y3.5 zeolite and calcined the catalysts to form 5%Cu/Y-IE, 5%Cu/Y-IM and 10%Cu/Y-IM catalyst. The acidity of 5%Cu/Y-IE, 5%Cu/Y-IM and 10%Cu/Y-IM catalyst were the results illustrated in **Figure 4.8.** All of catalysts was show three desorption peaks, suggesting that the Cu can generated the total acidity and a strong acid site in Y zeolite. For 5%Cu/Y-IE by ion-exchanged was show the highest strong acid sites when compared with impregnation method (5%Cu/Y-IM and 10%Cu/Y-IM) because 5%Cu/Y-IE is higher surface area and dispersion **(Table 4.1)** of Cu than the catalyst prepared by impregnation method [47].

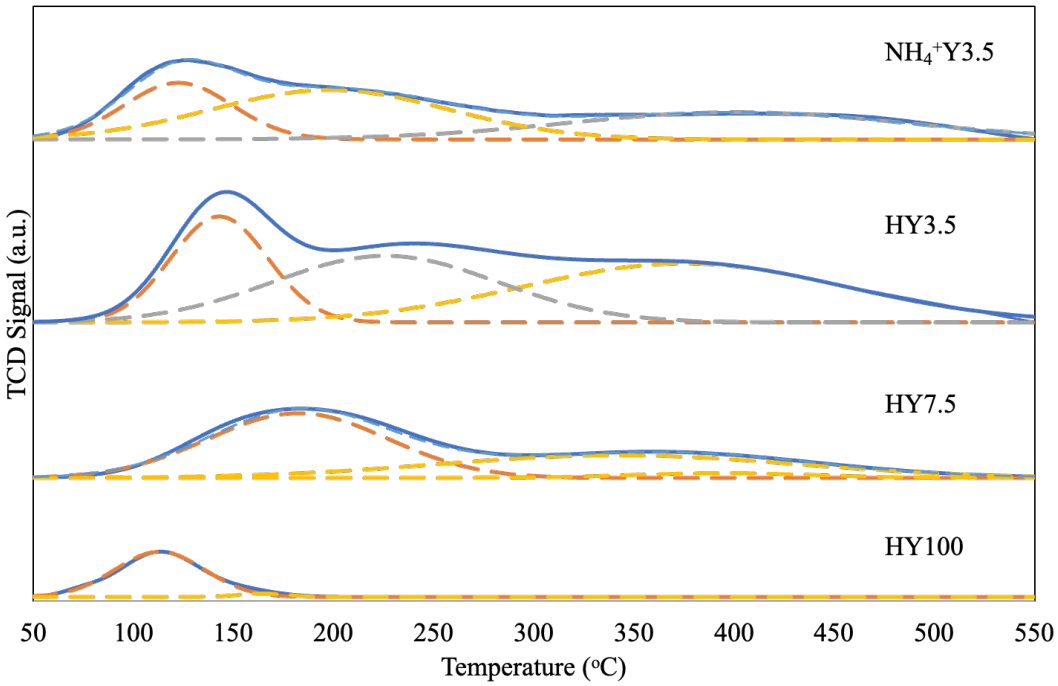

Figure 4.7. NH_3-TPD profiles of zeolite HY catalysts (Si/Al ratio 3.5,7.5, 100).

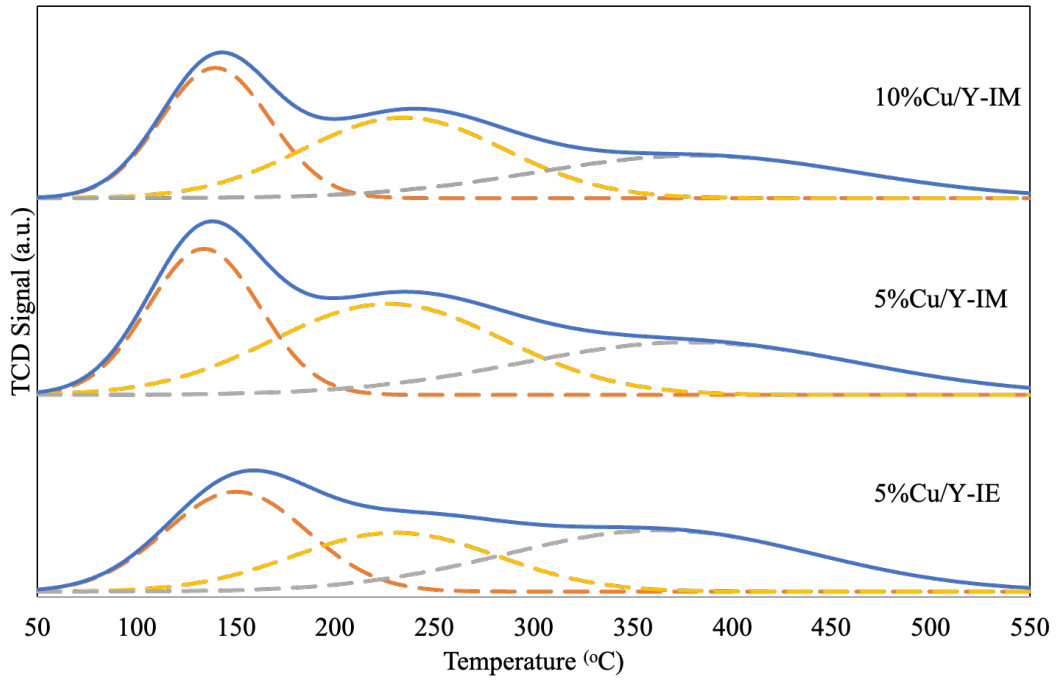

Figure 4.8. NH_3-TPD profiles of 5%Cu/Y-IE, 5%Cu/Y-IM and 10%Cu/Y-IM catalysts after reduction at 500 °C.

Table 4.2. Acidity of Y zeolite and Cu/Y catalysts

Catalysts	Acidity (μmol/g)[a]			
	Weak 120°C	Medium 250°C	Strong 350°C	Total (μmol/g)
NH_4^+Y	45.9	89.1	69.0	204.0
HY3.5	72.5	99.4	126.2	298.1
HY7.5	81.4	54.4	59.4	195.2
HY100	30.7	1.3	0.0	32.0
5%Cu/Y-IE	52.8	55.5	92.6	201.0
5%Cu/Y-IM	69.5	79.4	66.8	215.7
10%Cu/Y-IM	72.9	94.1	80.0	247.0

[a]Determined by NH_3-TPD

4.2 Catalytic activity of Y-zeolite catalyst in liquid phase catalytic transfer hydrogenation of furfuryl alcohol to GVL.

To understand the catalytic behavior of Y-zeolite catalyst in the liquid phase selective hydrogenation of furfuryl alcohol to GVL. The functional types (NH_4^+Y, HY) and Si/Al ratios of Y-zeolite have been verified. The reaction was carried out in 100ml of batch type stainless steel autoclave reactor at 160°C using 2-propanol as a hydrogen donor. **Table 4.3** summaries the catalytic performance of Y zeolite support in liquid phase hydrogenation of furfuryl alcohol (FOL) to GVL. The HY3.5 shows higher conversion of FOL (95%) than NH_4^+Y3.5 (45%). Because of HY occupied higher acidity than NH_4^+Y zeolite related with **Table 4.2** in NH_3-TPD**.** Moreover, the catalytic performance of HY zeolite with various Si/Al ratios was in the order of HY3.5 > HY7.5 > HY100. The highest conversion of FOL (95%) with highest selectivity to GVL (50%) can be obtained from HY3.5. This is presumably due to low Si/Al ratio has more negative framework charge generated more acidity site on zeolite that corresponding with the NH_3-TPD results.[48] However, NH_4^+

formed could be easier to exchange with the metal than HY zeolite. Therefore, NH_4^+Y was selected as a support of catalyst.

Table 4.3 Catalytic performance of zeolite support in liquid phase transfer hydrogenation of furfuryl alcohol to GVL[a]

Catalysts	Conversion (%)	Selectivity (%)			GVL Yield (%)
		GVL	IPL	FE	
NH_4^+Y 3.5	45	77	15	4	35
HY3.5	95	50	37	1	48
HY7.5	95	42	40	13	40
HY100	57	38	17	4	23

[a] Reaction condition**:** Furfuryl alcohol 200 µL (2.35 mmol), isopropanol 10 ml (130.8 mmol), catalyst 100 mg, temperature 160 ^oC, 1 h, N_2 pressure 10 bars.

To study catalytic performance of %Cu/Y-IE, 5%Cu/Y-IM and 10%Cu/Y-IM catalyst in liquid phase hydrogenation of furfuryl alcohol to GVL was performed in **Figure 4.9.** For 5%Cu/Y-IE show FOL conversion was 78% and 57% of GVL yield. While, for 5%Cu/Y-IM show the FOL conversion was dropped dramatically to 56.2% and 36.4% of GVL yield. It can be noted that the catalytic performance of 5%Cu/Y-IE was higher than 5%Cu/Y-IM. Because of 5%Cu/Y-IE has strong acidity than 5%Cu/Y-IM. Moreover, highly dispersed of Cu on 5%Cu/Y-IE can facilitate more H-transfer than 5%Cu/Y-IM. Although, when increase the amount of Cu loading to 10%Cu/Y-IM catalyst was shows furfuryl alcohol conversion was 69% and 47% of GVL yield. This might be from the agglomeration of Cu particle that blocking some pore of Y zeolite correlated with surface area was decreased **(Table 4.1)**.

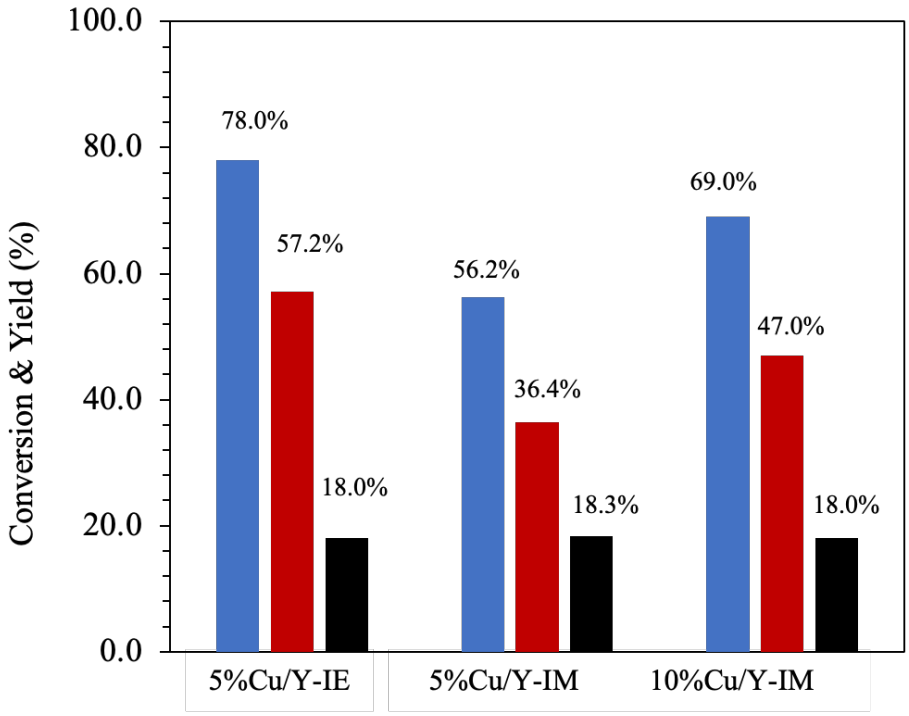

Figure 4.9. Catalytic performance of 5%Cu/Y-IE, 5%Cu/Y-IM and 10%Cu/Y-IM catalyst in liquid phase hydrogenation of furfuryl alcohol to GVL; (■) conversion (■) GVL yield (■) IPL yield Reaction condition**:** Furfuryl alcohol 200 µL, isopropanol 10 ml, catalyst 100 mg, 160 °C, 1 h, N_2 10 bars.

5%Cu/Y-IE, 5%Cu/Y-IM and 10%Cu/Y-IM catalyst was studied further as a catalyst on the production of GVL from furfuryl alcohol. For **Figure 4.10** was shows the change in product distribution with a reaction time from 60-480 min. At the beginning of reaction (1h) were show the catalytic activity of 5%Cu/Y-IE (**Figure 4.10a**, 78.0%) was higher than 5%Cu/Y-IM (**Figure 4.10b**, 60.0%) and 10%Cu/Y-IM (**Figure 4.10c**, 69%) catalyst and GVL yield in order of 5%Cu/Y-IE (57.2%) > 5%Cu/Y-IM (37.2%) and 10%Cu/Y-IM (47.0%). This suggest that the 5%Cu/Y-IE was higher initiate of reaction than others catalyst. Moreover, 5%Cu/Y-IE was show the highest catalytic activity at reaction time 4h (conversion 96%) when compared with 5%Cu/Y-IM (conversion 85%) and 10%Cu/Y-IM (conversion 75.9%) and GVL yield in order of 5%Cu/Y-IE (68.0%) > 5%Cu/Y-IM (58.0%) > 10%Cu/Y-IM (55.1%).

Although the amount of Cu loading increased to 10wt%, the catalytic activity and GVL yield were not increased when compared with 5wt% in the same preparation method. This might be from the lowest dispersion **(N_2O-TPR)** and surface area **(Table 4.1).**

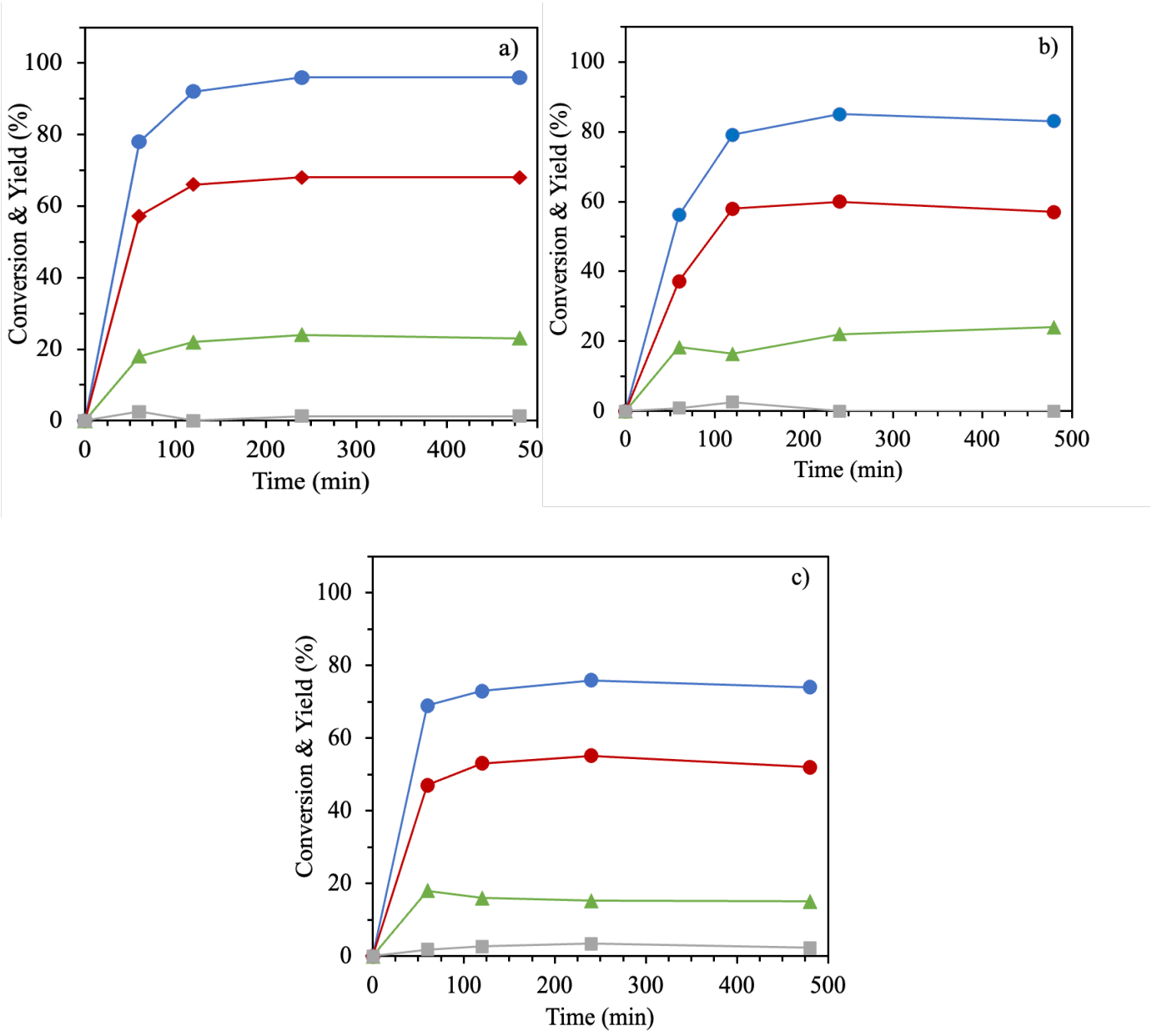

Figure 4.10. Time profiles of a) 5%Cu/Y-IE, b) 5%Cu/Y-IM and c) 10%Cu/Y-IM catalyst in liquid phase hydrogenation of furfuryl alcohol to GVL; (●) conversion, (●) GVL yield, (▲) IPL yield and (■) FE yield Reaction condition: Furfuryl alcohol 200 µL, isopropanol 10 ml, catalyst 100 mg, 160 °C, N_2 10 bars.

To assess catalyst deactivation in the batch reactor, the evolution of conversion with reaction time as a function of the product (weight x time) over 5%Cu/Y-IE was used to estimate the level of catalyst deactivation [49]. and plotted the variation of reactant concentration as a function of the catalyst mass x time product (w x t) using three different masses as show in **Figure 4.11.** The gap between the three curves of three different masses clearly apart as a function of w x t, indicating a rather large extent of catalyst deactivation [50]. Obviously, for 50mg show the conversion of furfuryl alcohol no longer changes after a relatively short reaction time. This result suggests that the 5Cu/Y-IE catalyst has generated coke deposited on surface of Y zeolite. That might be from the Y zeolite have more Brønsted acid site than Lewis acid site [51].

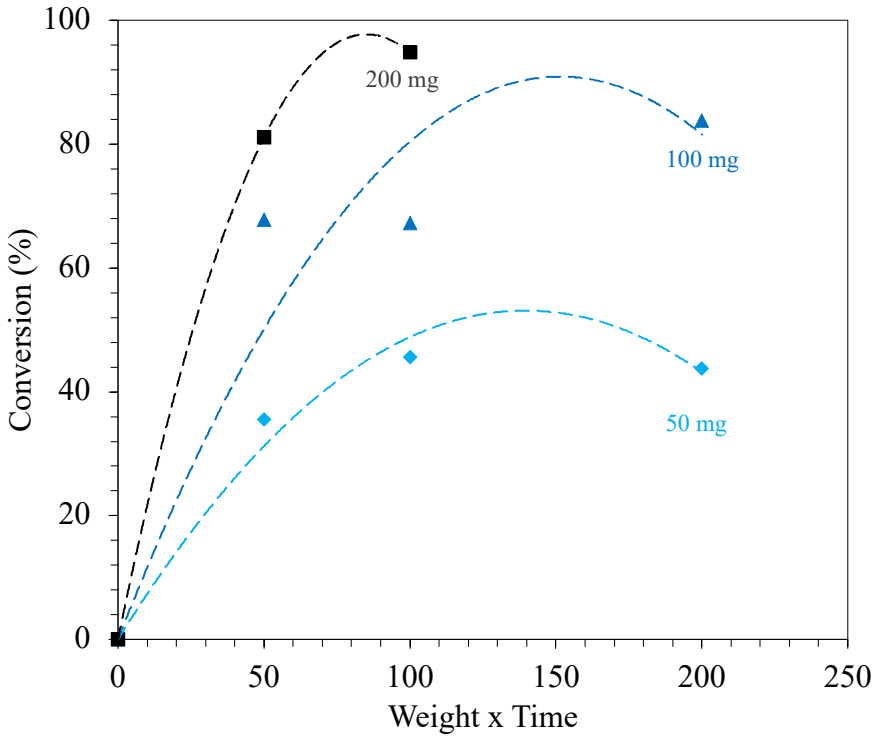

Figure 4.11. Evolution of conversion with reaction time as a function of the product (weight x time) over 5%Cu/Y-IE to asses catalyst deactivation catalyst in liquid phase hydrogenation of furfuryl alcohol to GVL. Reaction condition**:** Furfuryl alcohol 200 µL, isopropanol 10 ml, catalyst 100 mg, 160 °C, 1 h, N_2 10 bars.

4.21. Thermogravimetric analysis (TGA)

To evaluate carbon deposition on the catalyst surface, we used the thermogravimetry-derivative thermogravimetry (TG-DTG) approach, which involved heating the samples from ambient temperature to 900 °C in an air atmosphere. As illustrated in **Figure 4.12a**, the profiles of fresh 5%Cu/Y-IE reveals a weight loss of approximately 128°C, which corresponding to the removal of physically adsorbed water in pore of Y zeolite [52]. On the other hand, the three-weight loss staged were observed in spent 5%Cu/Y-IE **(Figure 4.12b)** at approximately 370, 535, and 795°C were observed in DTG profiles of the spent catalysts when compared with the fresh one. The weight loss at approximately 370°C to removal of absorb organic molecules, while the other two weight loss stages were attributed to different types of deposited carbon on surface for spent 5%Cu/Y-IE [53].

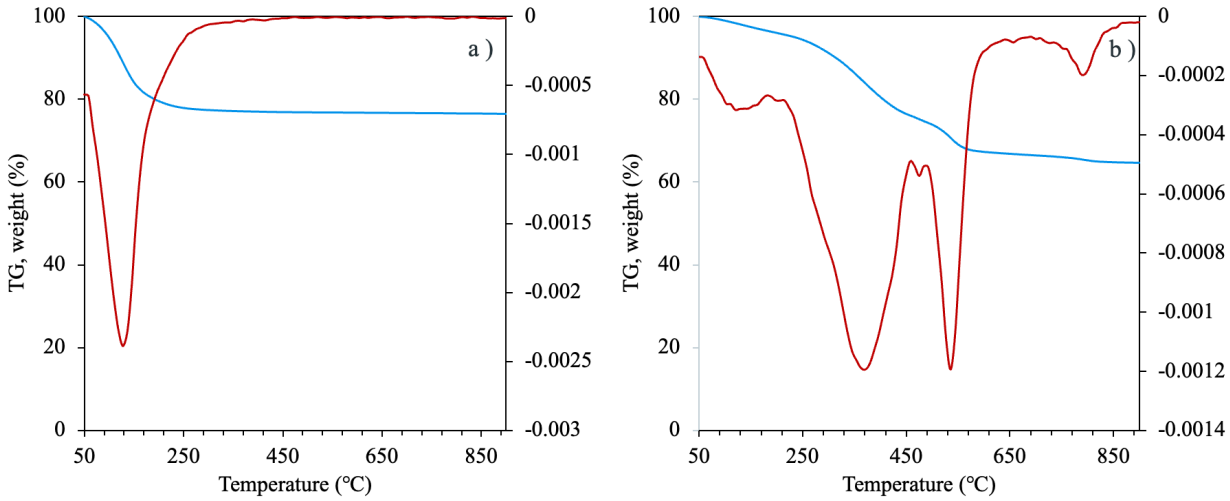

Figure 4.12. TG-DTG profiles for a) fresh 5%Cu/Y-IE catalyst b) spent 5%Cu/Y-IE for 8h catalyst.

PART 2 : To study catalytic performance of Cu phyllosilicate and secondary metal catalyst.

4.3. Catalysts Characterization

4.3.1 X-ray diffraction (XRD)

The crystalline structure and chemical phase composition of calcined catalysts were determined by X-ray diffraction technique (XRD). The measurement was carried out at the diffraction angles (2θ) between 20°and 80° and the results are shown in **Figure 4.13.** XRD patterns of catalysts, 30%CuPS, 1%NiCuPS ,1%AgCuPS, and 1%ZnCuPS, show weak and broad diffraction signals centered at 2θ = 31.2°, 35.8°, 57.3° and 63.2° which are characteristics for the chrysocolla [$Cu_2SiO_5(OH)_2$] structure of the copper phyllosilicate [54]. However, no diffraction peak of other metal oxides was observed when the secondary metals (Ni, Ag, Zn) were incorporated in the 30%CuPS. This is presumably due to small loading (∼1wt%, Table 1) of the metal oxides that could be highly dispersed on copper phyllosilicate structure. Nevertheless, a weak and broad peak at 2θ of 35.6, corresponding to CuO, was evidenced for 1%ZnCuPS. This suggests that the addition of ZnO could promote the decomposition of copper phyllosilicate, leading to the formation of the CuO crystallites as reported in literature [55].

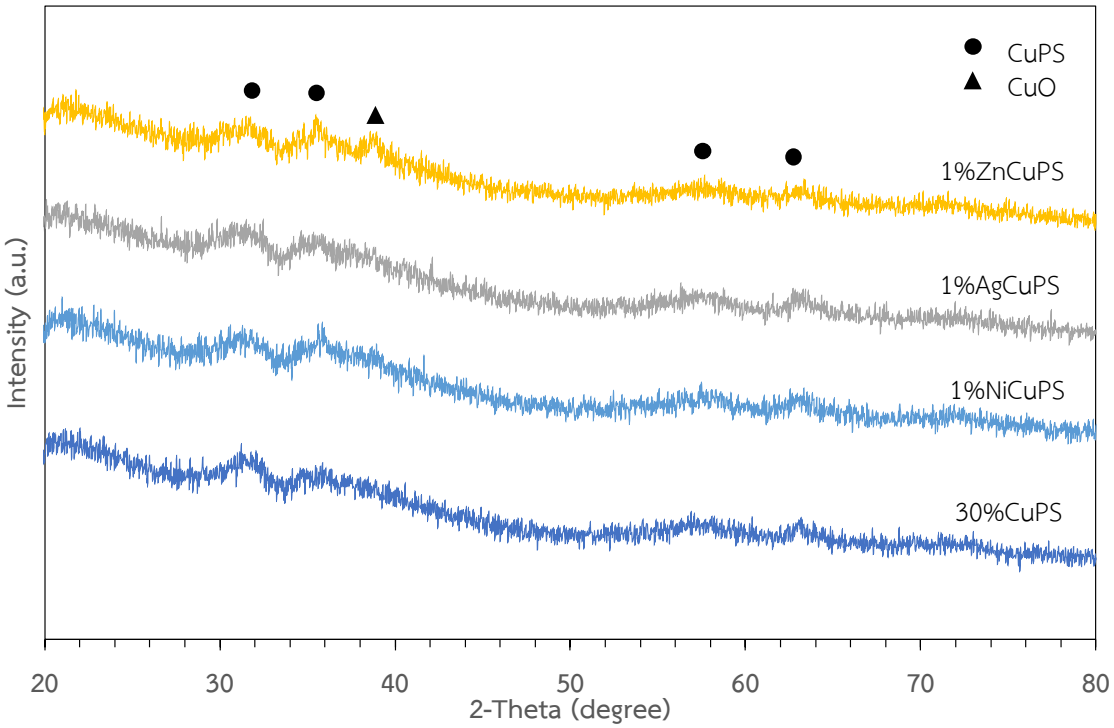

Figure 4.13. XRD pattern of a) 30%CuPS, b) 1%NiCuPS ,c) 1%AgCuPS, and d) 1%ZnCuPS catalyst.

4.3.2 Temperature program reduction of H_2 (H_2-TPR)

The reduction temperature and reduction behavior of 30%CuPS , 1%NiCuPS, 1%AgCuPS, and 1%ZnCuPS catalysts have been investigated by H_2-TPR technique and dissociative N_2O adsorbed resulting in illustrate in **Figure 4.14.** The 30%CuPS show one reduction board peak around 238.2°C with a correlated H_2 consumption to Cu content (**Table 4.4**) it could be from the strong interaction between Cu and Phyllosilicate structure as a supported [56]. Indicating that the Cu^{2+} species can be completely reduced to Cu^0. Obviously, the reduction peaks of 1%AgCuPS catalysts the reduction temperature (234.8 °C) were shifts to lower than 30%CuPS (238.2 °C), indicating that the decoration of Ag enhanced the reducibility of copper species [57]. On the other hand, for 1%NiCuPS catalyst was slightly shift to higher reduction temperature show a center peak around 238.7°C

when compare with 30%CuPS. According to the synergetic interaction between Ni and Cu. [10]. Nevertheless, the 1%ZnCuPS catalyst show a higher reduction temperature than other catalysts. which is probably due to the chemical interaction between Cu species and ZnO[58]. Moreover, 1%ZnCuPS can observed reduction peaks of CuO around at 270°C. According to from **Table 4.4** show 1%ZnCuPS is the lowest dispersion (61.6%) that might be from the ZnO can be generated Cu decompose out of structure. Also, the dissociative N_2O adsorbed on surface of 30%CuPS catalysts and react with metallic copper. The Cu^+ of all catalysts was form during N_2O oxidation can be easier to reduce at the low temperature around at 130-220°C. Because of the reduction peaks of Cu^+ oxidized by N_2O was revealed [59].

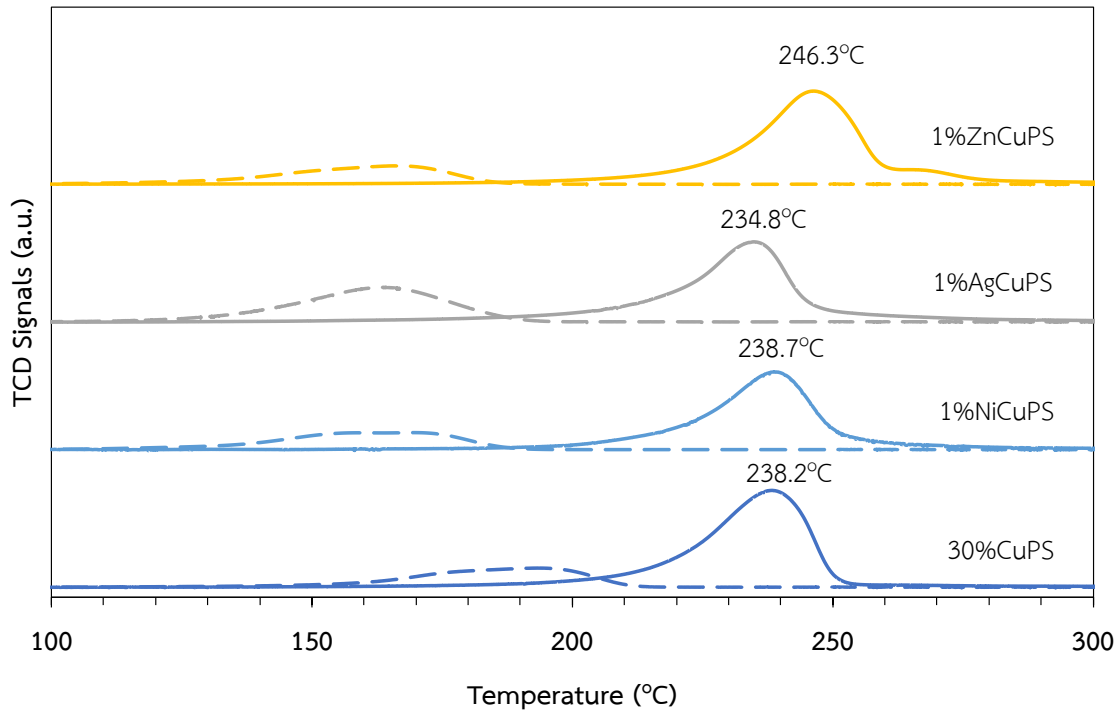

Figure 4.14. H_2-TPR of calcined and dissociative N_2O adsorbed CuPS catalysts

4.3.3 Physiochemical properties of CuPS and secondary metal catalysts

Table 4.4 Metal loading, surface area, pore size, pore volume, H_2 consumption, and Cu dispersion of CuPS and secondary metal on CuPS samples

Entry	Catalyst	Elemental composition (wt%)[a]				N_2 adsoption-desorption			H_2-TPR		
		Cu	Ag	Zn	Ni	S_{BET} (m^2/g)	D_{pore} (A)	V_{pore} (cm^3/g)	H_2 consumption	Cu content (wt%)[b]	Dcu (%)[b]
1	30%CuPS	28.0	-	-	-	409	159	0.87	4.39	27.9	71.5
2	1%NiCuPS	27.4	-	-	1.1	388	136	0.86	4.26	27.0	65.3
3	1%AgCuPS	28.8	1.0	-	-	380	147	0.73	4.51	28.6	66.7
4	1%ZnCuPS	27.3	-	1.1	-	371	147	0.65	4.27	27.1	61.6

[a] Determined by XRF.

The metal composition, BET surface area, pore size diameter of all catalysts were summarized in Table 1. Considering the amount actual amount of Cu loading on 30%CuPS , 1%NiCuPS, 1%AgCuPS, and 1%ZnCuPS catalysts were found to be 28.0, 27.4 ,28.8 and 27.3 wt% respectively. Also, the actual amount of Ni, Ag and Zn contents in either sample were consistency with the desired loading. Correlated with Cu content calculated by H_2-TPR technique. For the BET surface area decreased order of 30%CuPS > 1%NiCuPS > 1%AgCuPS > 1%ZnCuPS, this could be suggesting that the incorporated metal oxides may occupy in the mesopore of 30%CuPS [24]. Furthermore, all catalysts exhibited hysteresis loop in N_2 adsorption-desorption isotherm indicating that, mesoporous material [60]. Moreover, the secondary metal on 30%CuPS was show the bigger mesopores **(Figure 4.15a)**. Corresponding with the average pore sizes diameters were decreased after immobilized with secondary metal calculate by the Barrett-Joyner-Halenda (BJH) **(Figure 4.15b)** In addition, for 1%ZnCuPS show the lowest surface area related with dispersion of Cu show the lowest dispersion. According to the CuO covering on the surface area of copper phyllosilicate correlated with XRD and H_2-TPR show the CuO was formed.

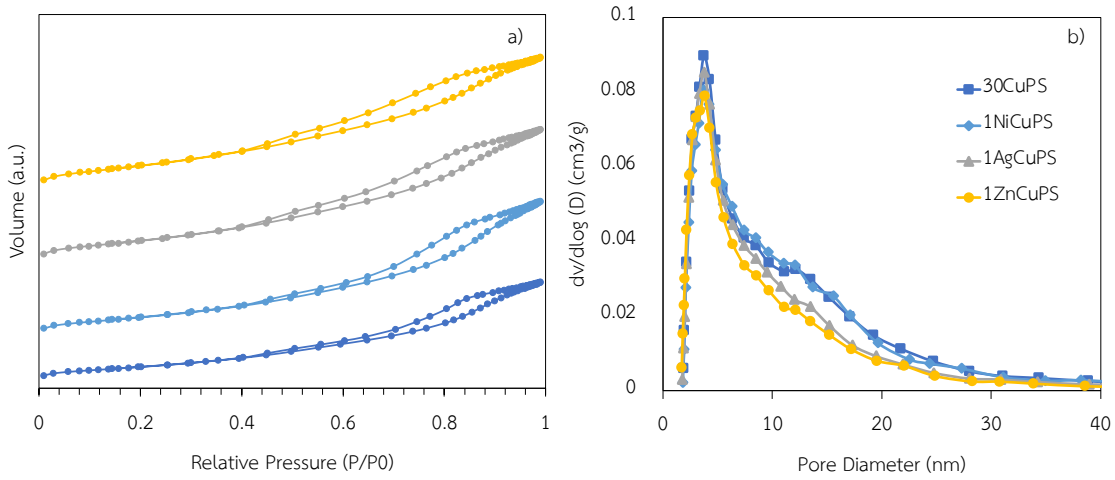

Figure 4.15 a) N_2-adsorption-desorption isotherm and b) pore diameter of CuPS and secondary metal catalyst

4.3.4 X-ray Photoelectron Spectroscopy (XPS)

The electronic state of 30%CuPS and secondary metal catalyst were investigated by XPS analysis. For the XPS spectra of 30%CuPS and secondary metal were showed in **Figure 4.16** For the Cu 2p XPS peaks of 30%CuPS corresponding to $Cu2p_{3/2}$ and $Cu2p_{1/2}$ appeared at 935.6 eV and 952.3 eV respectively attributed to Cu^{2+} species in the octahedral layers of copper phyllosilicate [61]. The 1%NICuPS show $Cu2p_{3/2}$ and $Cu2p_{1/2}$ were shifts to higher binding energy located at 935.9 and 955.5 eV, respectively[62]. The Ni2p3/2 and Ni2p1/2 peaks were deconvoluted into two peaks each at the binding energies of 857.0 and 863.0 e.V and 874.2 and 876.0 e.V. respectively. Moreover, The Ni2p3/2 was slightly shift to lower binding energies when compared as literature review, which were assign to the characteristic feature of Ni^{2+}[63] **(Figure 4.17a)**. As well as for the 1%AgCuPS catalyst were show the binding energy of $Cu2p_{3/2}$ slighlty migrates to higher at 935.9 eV for 1%AgCuPS [57]. The Ag 3d spectrum of 1%AgCuPS catalyst show a doublet

peak. For 1%AgCuPS show binding energies at 368.5 and 374.0 e.V. which are assigned to Ag $3d_{5/2}$ and Ag $3d_{3/2}$ respectively. Moreover, the 1%AgCuPS were showed slightly shift toward to lower binding energy than literature review, which were assign to the characteristic feature of Ag^{+}[64] **(Figure 4.17b)**. Furthermore, when addition of Zn on 30%CuPS show the $Cu2p_{3/2}$ binding energy of CuO is center around 934.0 eV [65]. Which indicated that the electron transfer from the Zn atoms to the Cu was enhanced for this catalyst. For the Zn 2p shows two peaks at binding energies of 1021.7 and 1045.4 which are assigned to Zn $2p_{1/2}$ and Zn $2p_{3/2}$ of tetrahedral Zn^{2+} respectively[66] **(Figure 4.17c)**. Therefore, the secondary metal secondary metal could be pulling electron form the copper [58].

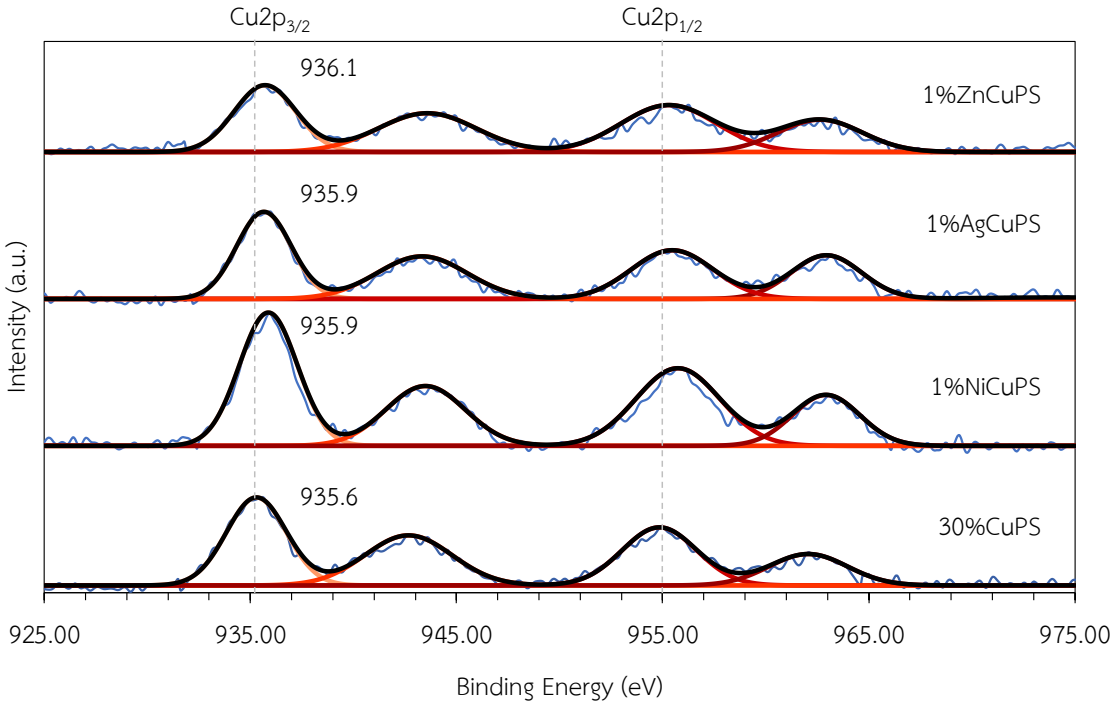

Figure 4.15. XPS spectra of Cu2p for CuPS catalysts

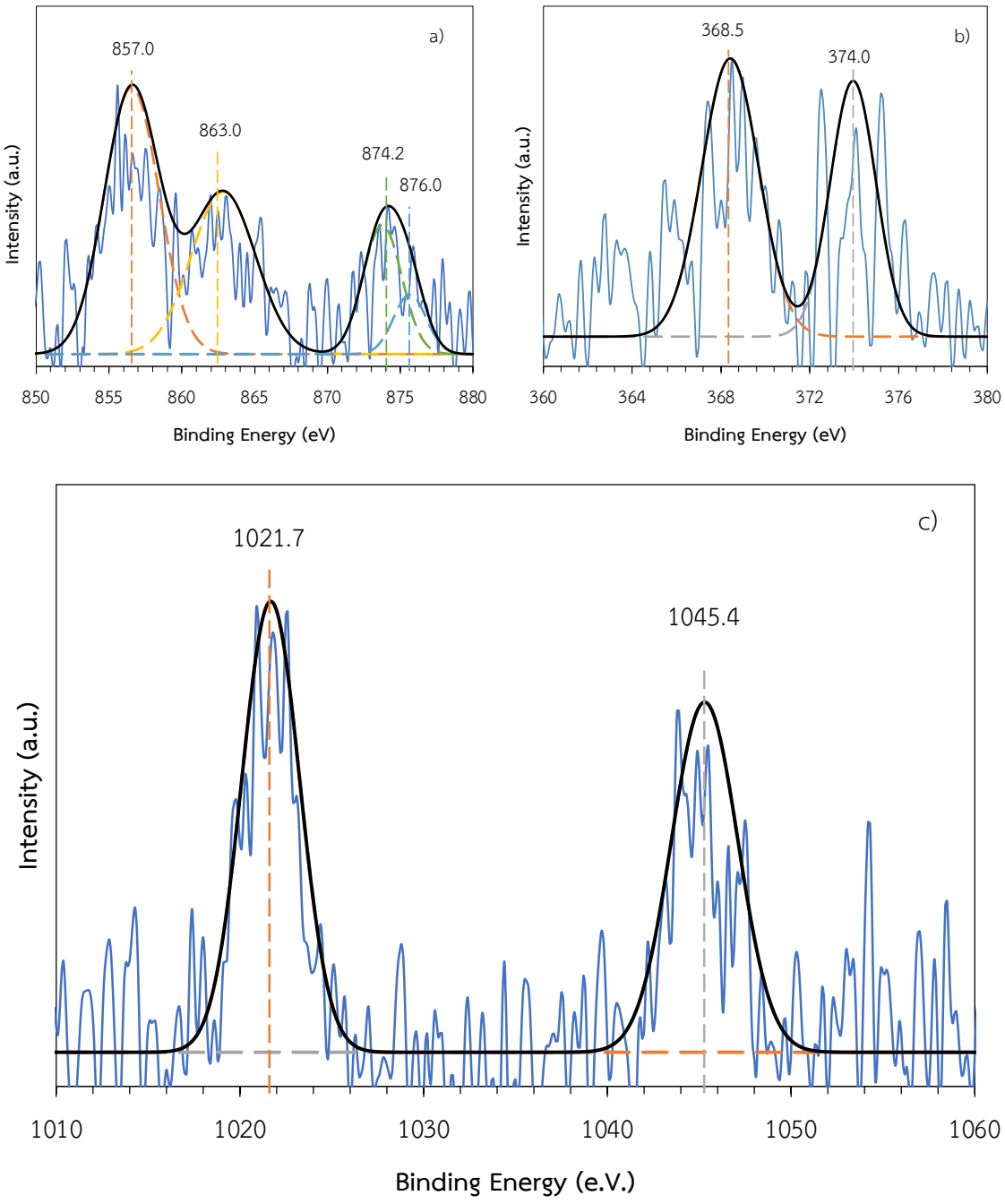

Figure 4.17. XPS spectra of a.) Ni 2p of 1%NiCuPS b.) Ag 3d of 1%AgCuPS and c.) Zn 2p of 1%ZnCuPS catalyst.

4.3.5 X-ray absorption near edge structure (XANES)

In order to verify the existence of octahedral and square planar Cu^{2+} species, 30%CuPS and 1%ZnCuPS have been investigated by the *in-situ* time-resolved X-ray absorption near edge spectroscopy (*in situ* TR-XANES) upon heating to 140°C as shown in **Figure 4.18.** The Cu edges energy for Cu foil (8979.1 eV.), Cu_2O (8980.0 eV.), CuO (8989.8 eV, square planar Cu^{2+} (Sq)) and $CuSO_4$ (8990.4 eV, octahedral Cu^{2+} (O_h)) were used as standard **(Figure 4.18a)** for linear combination fitting (LCF,[67]) 30%CuPS and 1%ZnCuPS exhibit characteristic edge energy adsorption at ~ 8991.1 eV **(Figure 4.18b)** that fall between the Cu edge energy of $CuSO_4$ (8990.4 eV) and CuO (8989.8 eV). This suggests that both catalysts are mixtures between octahedral Cu^{2+} (O_h) and square planar Cu^{2+} (Sq).

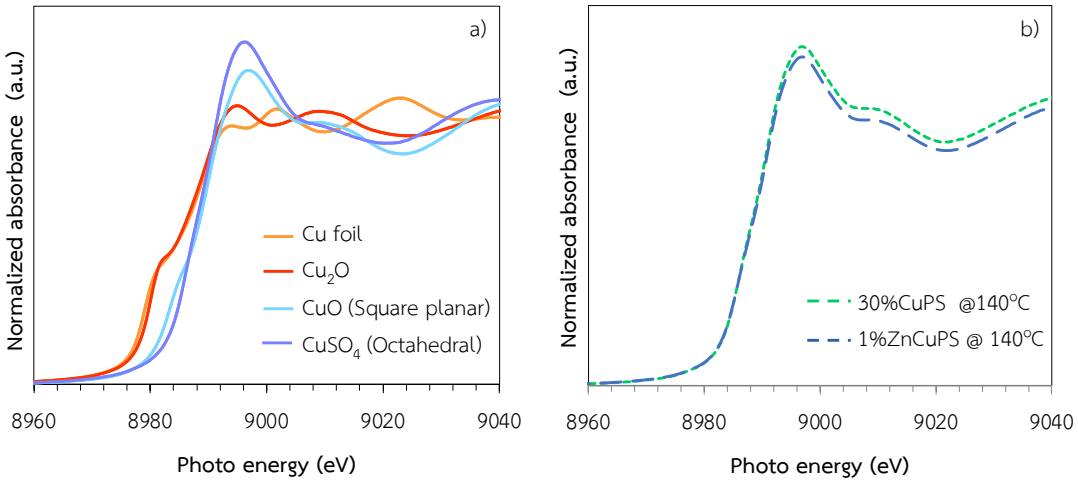

Figure 4.18. Cu K edge XANES spectra of a) Cu standards b.) 30%CuPS and 1%ZnCuPS under N_2 flow at 140 °C

The line-shape spectra of the 30%CuPS and 1%ZnCuPS are more resemble that to octahedral Cu^{2+} (O_h) species ($CuSO_4$), without a pre-edge feature at ~ 8984 eV that represents the square planar Cu^{2+} (Sq) species (CuO). This indicates that the majority of the Cu^{2+} species in both catalysts exist in the octahedral geometry, presumably within

the chrysocolla structure[68]. The linear combination fitting (LCF) clearly shows that 30%CuPS contain relatively more octahedral Cu^{2+} species (O_h) (67.5%) as compared to the square planar Cu^{2+} (Sq) (32.5%). In contrast, 1%ZnCuPS possesses more square planar Cu^{2+} (Sq) (55.6%) as compared to the octahedral Cu^{2+} species (O_h) (44.4%) were shown in **Table 4.5.** Because of Cu atom is bonded with six oxygen atoms in the octahedral layer with each phyllosilicate layer being linked by Vander der Waals interaction though the interlayer galleries. This is suggest that some of copper sheet can be easily substituted with a zinc atom [69].

Table 4.5. Fraction of Square planar Cu^{2+} species (CuO) and Octahedral Cu^{2+} species ($CuSO_4$) obtained from linear combination fitting (LCF) of 30%CuPS, and 1%ZnCuPS catalyst.

Catalyst	Temp (°C)	Square planar Cu^{2+} (%)	Octahedral Cu^{2+} (%)	Square planar/ Octahedral
30%CuPS	140	32.5	67.5	0.5
1%ZnCuPS	140	55.6	44.4	1.3

The Cu edges energy of both catalyst upon heating from 70-140 °C was show in **Figure 4.19.** The Cu edges energy of 30%CuPS was not significantly changed. However, in consistence with this finding, the Cu edge energy slightly shifts to a lower value for 1%ZnCuPS. That might be from the ZnO to gain more CuO spices. Related with the phase fraction of Square planar Cu^{2+} species (CuO) and Octahedral Cu^{2+} species ($CuSO_4$) obtained from linear combination fitting (LCF) for 30%CuPS and for 1%ZnCuPS at the beginning of both catalyst phase fraction of Octahedral Cu^{2+} species ($CuSO_4$) were 30%CuPS (70.5%) and 1%ZnCuPS (63.2%) Upon heating from 70-140 °C phase fraction of Octahedral Cu^{2+} species ($CuSO_4$) were 30%CuPS (67.5%) and 1%ZnCuPS (44.4%) changed to more Square planar Cu^{2+} species (CuO) **(Table 4.5).** This is presumably due to both catalysts were the

dehydration of adsorbed water at the edge of layer and the dehydroxylation of the interlayered Si-O-Cu-$(OH)_2$ [70] indicating that more defect of phyllosilicate structure resulting in more acidity. Thus, the 30%CuPS were not observed significant changed. While the 1%ZnCuPS was observed significant changed during heating to 140 °C. Suggesting that, Zn atoms was reduced interaction interlayer between phyllosilicate structure and Cu in octahedral layer [71]as shown the geometry of Cu in **Figure 4.20** indicating that during heating Zn^{2+} can promote decomposition some of Cu^{2+} out of phyllosilicate structure to CuO species corresponding with XRD results.

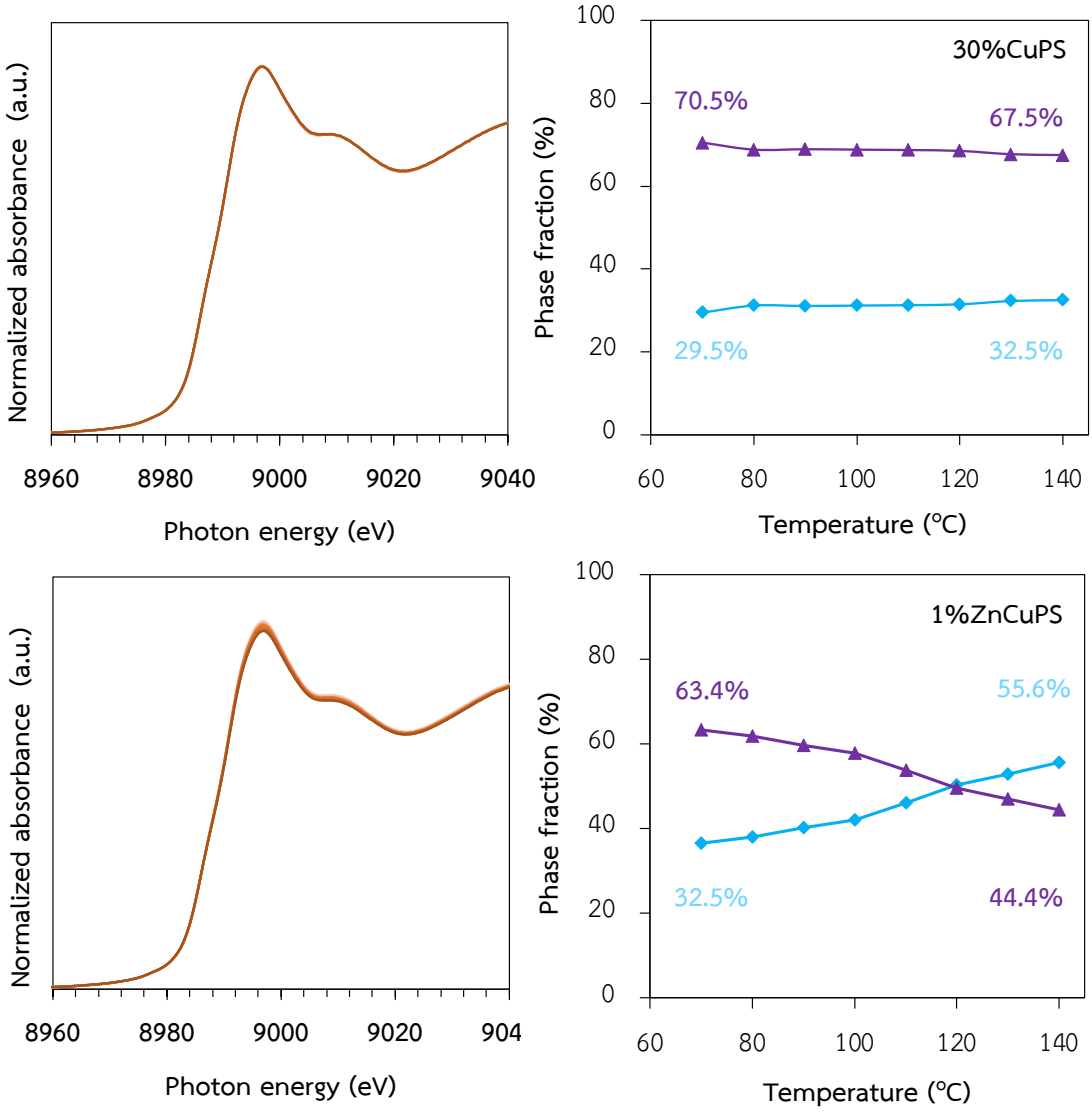

Figure 4.19. Cu K edge XANES spectra and phase fraction of Cu^{2+} species (◆) Square planar and (▲) Octahedral, obtained from linear combination fitting (LCF) of 30%CuPS, and 1%ZnCuPS upon heating from 70-140 °C.

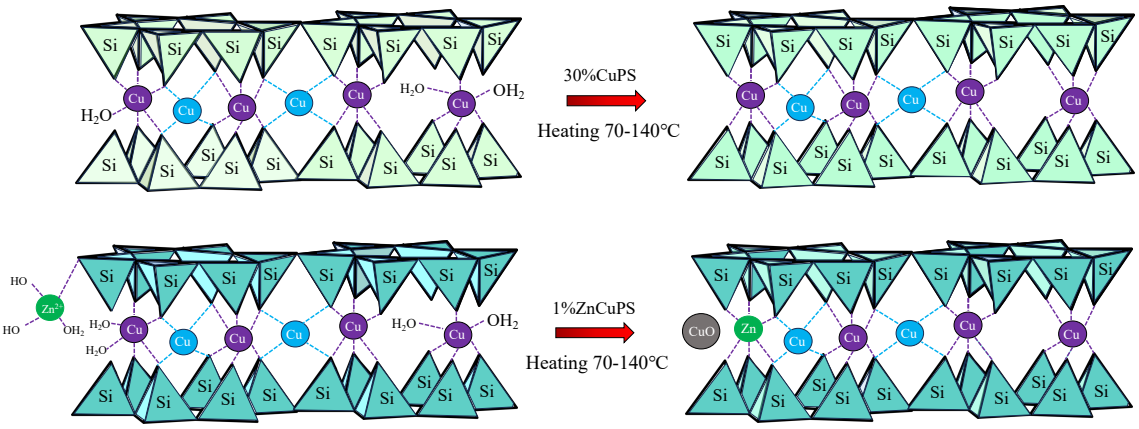

Figure 4.20. The demonstration of Cu^{2+} (Oh) transformation to Cu^{2+} (Sq) upon heating 70-140 °C.

To quantify the octahedral Cu^{2+} (O_h) and square planar Cu^{2+} (Sq) species, the linear combination fitting (LCF) of *in situ* TR-XANES spectra at temperature 140°C for 2h under isopropanol flow was performed on the 30%CuPS and 1%ZnCuPS catalyst the results was show in **Figure 4.21.** The Cu edges energy of both catalysts were not significantly changed during under isopropanol flow at temperature 140°C. In the meanwhile, linear combination fitting (LCF) of 30%CuPS was show octahedral Cu^{2+} species ($CuSO_4$) changed to more Square planar Cu^{2+} species (CuO) around ~ **4%**. Whereas 1%ZnCuPS were show Octahedral Cu^{2+} species ($CuSO_4$) changed to more Square planar Cu^{2+} species (CuO) around ~ **2%**. Nevertheless, the square planar of 1%ZnCuPS is more than 30%CuPS. This could be suggested that Zn atom is bonded with six oxygen atoms in the octahedral layer with some of phyllosilicate layer [72].

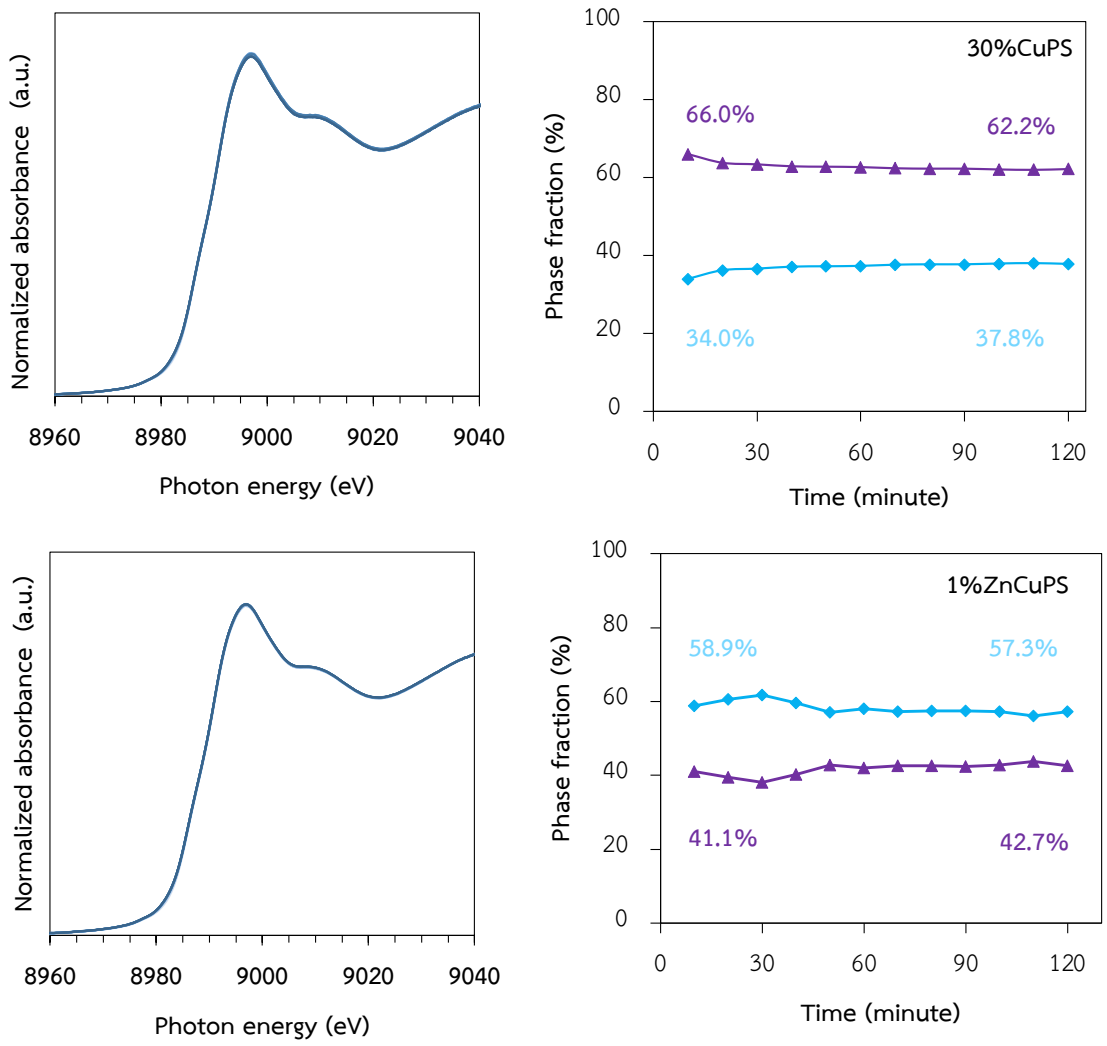

Figure 4.21. Cu K edge XANES spectra and phase fraction of Cu^{2+} species (◆) Square planar and (▲) Octahedral, obtained from linear combination fitting (LCF) of 30%CuPS, and 1%ZnCuPS at temperature 140°C for 2h under isopropanol flow.

4.3.6 Transmission Electron Microscope (TEM)

The morphology and EDX data to analyze the interaction between the Cu and ZnO was determined by TEM techniques. **Figure 4.22** 30%CuPS and 1%ZnCuPS catalysts, the prominent dark regions in the bright field TEM images (**Figure 4.22a and b**

respectively). 30%CuPS on the **Figure 4.22a** show the dark particles is a copper well highly dispersion more uniformly on SiO_2 layer and no black spot of CuO showed up [73]. Also, the rodlike copper phyllosilicate with typical filandrous structure was observed[74]. On other hand, when incorporated Zn on copper phyllosilicate to 1%ZnCuPS catalyst on the **Figure 4.22b** show the large particle of Cu cover on the surface of Cu phyllosilicate. In addition, some of Cu the agglomeration with Zn was show in elemental mapping, that could be related with the Cu species have a strong interaction with ZnO related with XPS results. Nevertheless, the remaining of lamellar structure of CuPS corresponding with XRD results and BET surface area. These results could be suggesting that the ZnO can promoted decomposition out of phyllosilicate and leads to the formation of the CuO crystallites.

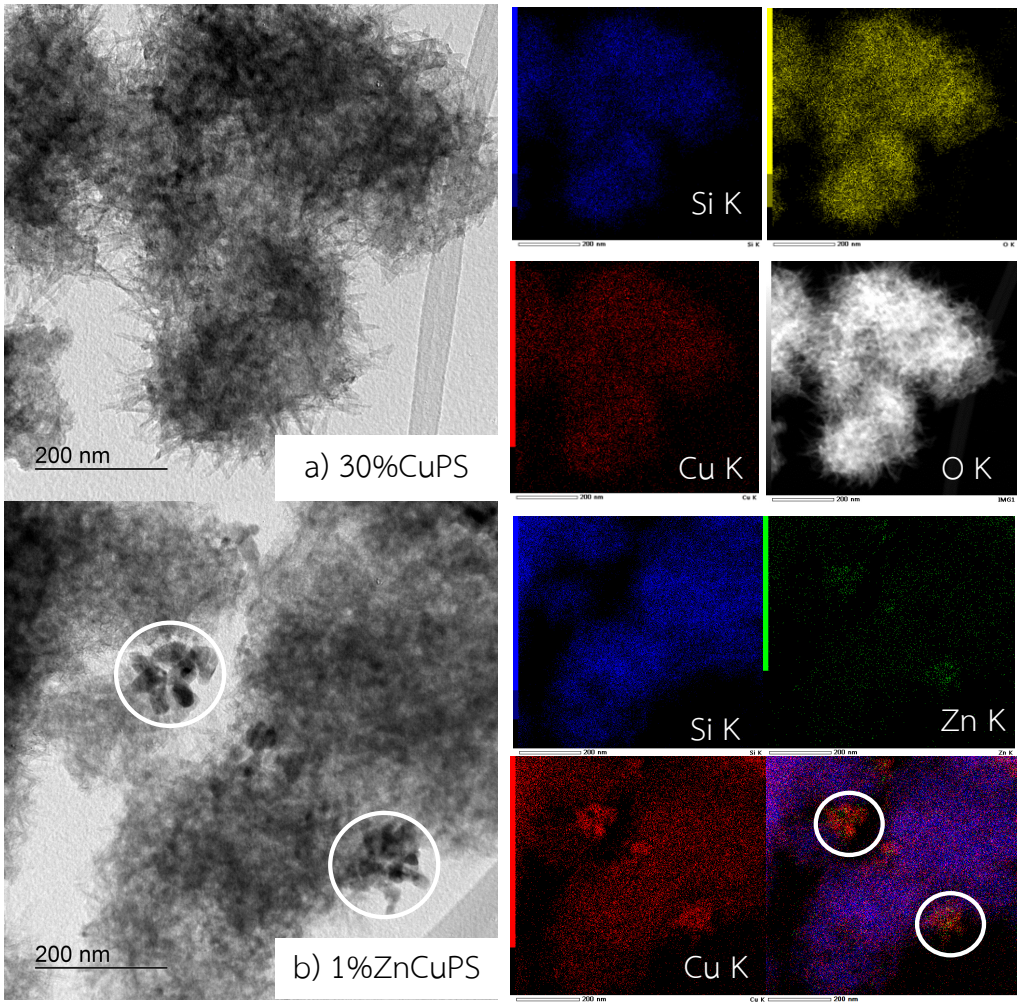

Figure 4.22. TEM-EDX of a.) 30%CuPS b.) 1%ZnCuPS catalyst.

4.3.7 NH_3-Temperature Program Desorption (NH_3-TPD)

The acidity and acid strength of all catalysts were investigated by NH_3-TPD, as show the results illustrate in **Figure 4.23.** The desorption peaks were deconvoluted into three peaks by the Gaussian deconvolution method. All catalysts contain three desorption peaks, generally the acid strength can be classified as a weak acid (< 120 °C) medium acid site (160 °C) and strong acid site (>250 °C)[75]. 30%CuPS were showing the main NH_3 desorption peak with a center around 134.0 °C and the most of weak acid site. Whereas, when addition of secondary metal on 30%CuPS the the shift of desorption peak towards higher temperature to medium and strong acid strength indicating that the presence of acid sites with different strength [76][77]. The amount of total acidity calculated from the deconvoluted peak compared with 1%NH_3 in He of catalysts were reported in **Table 4.6.** 30%CuPS catalysts show the most of weak acid site. Moreover, it show the highest total acidity indicating that the lamellar structure of copper phyllosilicate would result in the appearance of unsaturated/defective Si^{4+} and Cu^{2+} species in the catalysts surface[78]. When immobilized with secondary metal on 30%CuPS were show the total acidity decreased in the order 30%CuPS (35.9) > 1%AgCuPS (29.0) > 1%NiCuPS (27.5) and > 1%ZnCuPS (24.0 μmol). Corresponding with BET surface area of catalysts were decreased in **Table 4.4.** According to the acid site of copper phyllosilicate generated by edge of defect from Cu in lamellar structure [79]. Also, for the secondary metal could block some of the acid sites of copper phyllosilicate [80]. Thus, the acidity of catalysts depends on specific surface area. Furthermore, the secondary metal not only decreased the number of acid sites, but also decreased the strength of 30%CuPS sites [81]. However, the secondary metal can be improving a strong acid strength shift to higher desorption temperature. According to NH_3 adsorbed on strong Lewis acid associated with secondary metal sites [82] especially for 1%ZnCuPS the amount of acid sites with strong acid strength gradually increased [83].

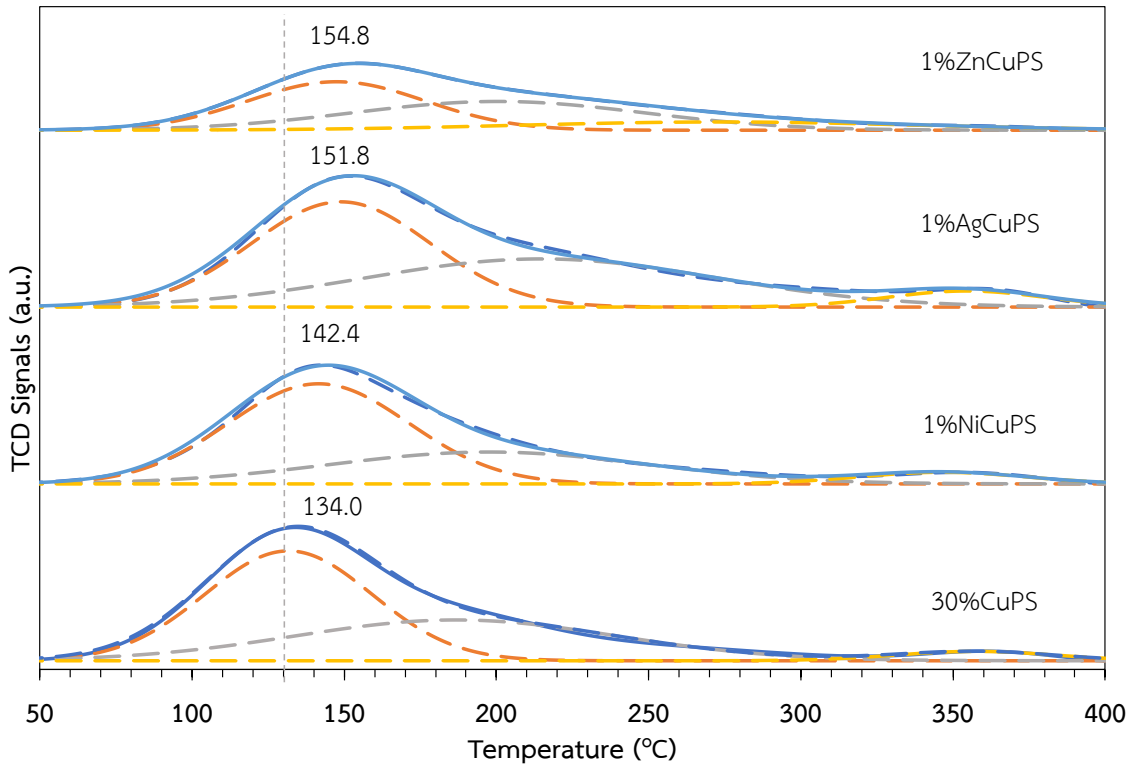

Figure 4.23. NH_3-TPD of CuPS catalysts

4.3.8. Pyridine-adsorbed infrared spectroscopy (Py-IR)

Py-FTIR was used to quantitative analyze the Lewis acid sites and Brønsted acid of catalysts As shown in **Figure 4.24.** The adsorption band at 1451 and 1608 cm^{-1} were attributed to the pyridine-adsorbed on Lewis's acid site (LA) on Cu^{2+} species of all catalysts. In the meanwhile, the adsorption band at 1548 and 1624 cm^{-1} were attributed to the pyridium ion formed after pyridine bonds with Brønsted acid site (BA) [84], and adsorption band at 1588 cm-1, hydrogen bonded pyridine[85]. The type of acid site was summarized in **Table 4.6.** The Lewis acid site of 30%CuPS was 17.7 μmol/g, while for 1%NiCuPS was not only reduce Lewis acid site from 17.7 to 12.9 μmol/g but the Ni can be induced Brønsted site (from 2.7 to 4.2 μmol/g) suggesting that the Ni could be gain more Brønsted acid site on copper phyllosilicate [86]. 1%AgCuPS was show not significantly changed from 30%CuPS. The highest ratio of LA/BA was show on 1%ZnCuPS,

indicating that Zn can improve the Lewis acid site on copper phyllosilicate [87]. Therefore, LA/BA ratio was extremely important for catalytic transfer hydrogenation to control the reaction pathway from furfuryl alcohol to GVL [88].

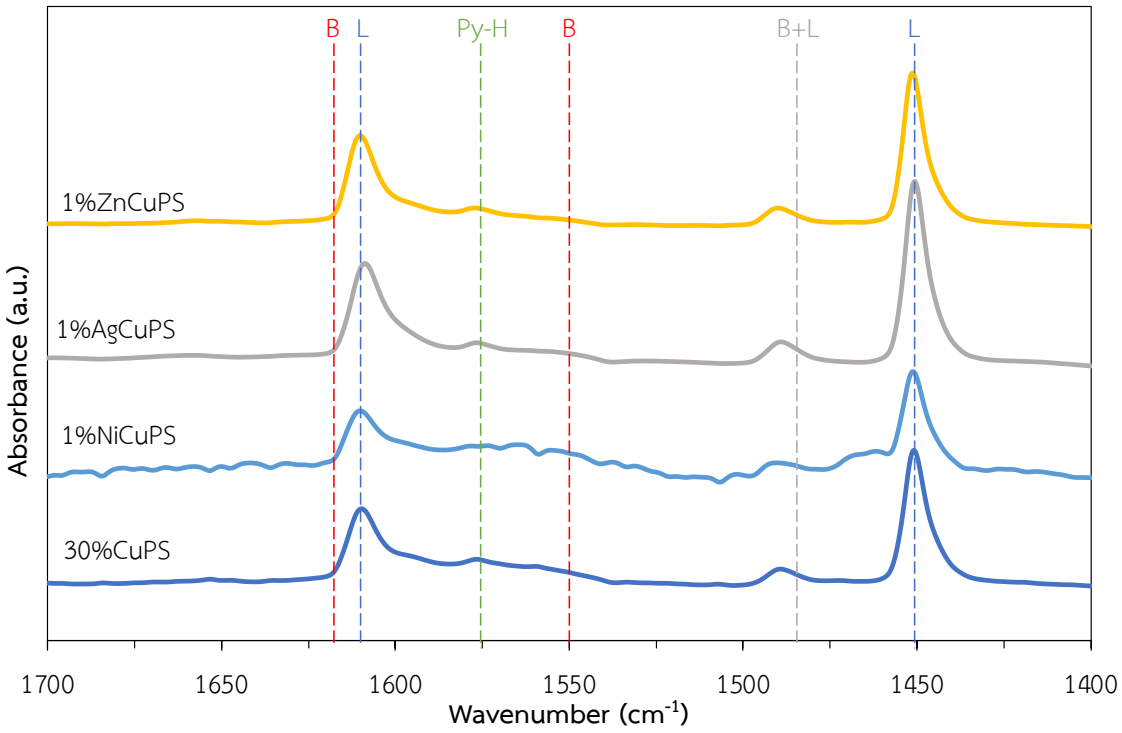

Figure 4.24. Pyridine-adsorbed IR spectra of CuPS catalysts.

Table 4.6. Acidity and Type of acid sites of 30%CuPS and secondary metal

Entry	Catalyst	Acidity (μmol/g)[a]				Type of acid site (μmol/g)[b]		
		Weak acid site (120°C)	Medium acid site (250°C)	Strong acid sites (350°C)	Total acidity (μmol/g)	Lewis acid (LA)	Brønsted acid (BA)	LA/BA
1	30%CuPS	18.5	15.1	2.2	35.9	17.7	2.7	6.6
2	1%NiCuPS	12.4	12.7	2.4	27.5	12.9	4.2	3.0
3	1%AgCuPS	13.0	13.4	2.6	29.0	17.2	2.2	7.7
4	1%ZnCuPS	10.0	9.8	4.2	24.0	13.8	1.43	9.6

[a]determined by NH_3-TPD [b] determined by Pyridine-IR

4.4 Catalytic activity of furfuryl alcohol to GVL in liquid-phase over Cu-phyllosilicate catalysts

To understand the catalytic activity of furfuryl alcohol to GVL catalysts in liquid phase over Cu-phyllosilicate catalysts. The reaction was carried out in 100 ml of batch type stainless steel autoclave reactor at reaction temperature 140 °C, reaction time 30min using 2-propanol as a hydrogen donor. **Table 4.7** summaries the catalytic performance of all catalysts. 30%CuPS catalyst shows catalytic performance (71.1%) and GVL yield 49.4%. 1%NiCuPS catalyst was show the catalytic activity (68.1%, GVL yield 49.4%) slightly dropped from 30%CuPS. However, Ni show the yield of IPL was slightly decreased because of the lowest of LA/BA ratio (3.0). it could be noted that after immobilized Ni on Cu phyllosilicate affect to Brønsted acid of Cu phyllosilicate was increased **(Table 4.6.** [89]**)**. 1%AgCuPS was show the catalytic activity (74.5%) GVL yield (54.5%) higher than 30%CuPS, indicating that Lewis acid of Ag has surplus on surface of 30%CuPS and it was increased in strong acid strength [90]related with NH_3-TPD and Pyridine-IR results. Moreover, 1%ZnCuPS show the highest activity (84%) and GVL yield (56.8%). That might be from the coexist with particle of Cu and Zn resulting in strong interaction between them as seen in XPS spectra results. In addition, 1%ZnCuPS has more defect in phyllosilicate structure resulting in the highest LA/BA ratio[92]. This could be noted that the strong acid strength and Lewis acid site from Zn can promoted the catalytic transfer hydrogenation [91]. Although, the total acidity was dramatically drop from 35.9 to 24.0 μmol/g **(Table 4.6).**

Table 4.7. Catalytic performance of furfuryl alcohol to GVL in liquid-phase over copper phyllosilicate catalysts.

Entry	Catalysts	Conversion (%)	Yield (%)			TON
			FE	GVL	IPL	
1	30%CuPS	71.1	2.0	49.4	19.1	2.1
2	1%NiCuPS	68.1	2.0	49.4	17.7	2.0
3	1%AgCuPS	74.2	1.7	54.5	17.7	2.2
4	1%ZnCuPS	84.0	5.4	56.8	22.6	2.5

Reaction condition: Furfuryl alcohol 200 µL (2.35 mmol), Isopropanol 10 mL (130.8 mmol) catalyst 200 mg , temperature 140°C , N_2 pressure 10 bar , 30 min

To be confirmed the reaction pathway have been investigated by time profiles and function of conversion and selectivity of 30%CuPS catalysts was show in **Figure 4.25.** The catalytic performance of furfuryl alcohol to GVL in liquid-phase for 30%CuPS catalyst at 140°C. The conversion of furfuryl alcohol increased rapidly to 72.3% at the beginning (1h) Also, the GVL yield increased rapidly in the first 1h. and then slightly increased to complete conversion 100% (8h) in **Figure 4.25a.** However, the GVL yield reached maximum of 60.8% after 4h while the IPL yield gradually increased. Moreover, further increasing the reaction time resulted in a slightly decreased in GVL yield and IPL yield was increased, related with **Figure 4.25b** was show the function of conversion and selectivity of 30%CuPS catalyst. From these results it could be said that the primary product is GVL and IPL is secondary product. Thus, it could be suggesting that the reaction is parallel reaction pathway to produced GVL. Because of after 4h the 30%CuPS when almost completely conversion of furfuryl alcohol, GVL can converted to gain more IPL yield and selectivity. Hence, these results presumably the catalytic transfer hydrogenation of furfuryl alcohol (FOL) to GVL

could be occurs through furfuryl ether (FE) and isopropyl levulinate (IPL) to produce GVL and FOL can convert directly to GVL product relating with propose mechanism in **Figure 4.26** [93].

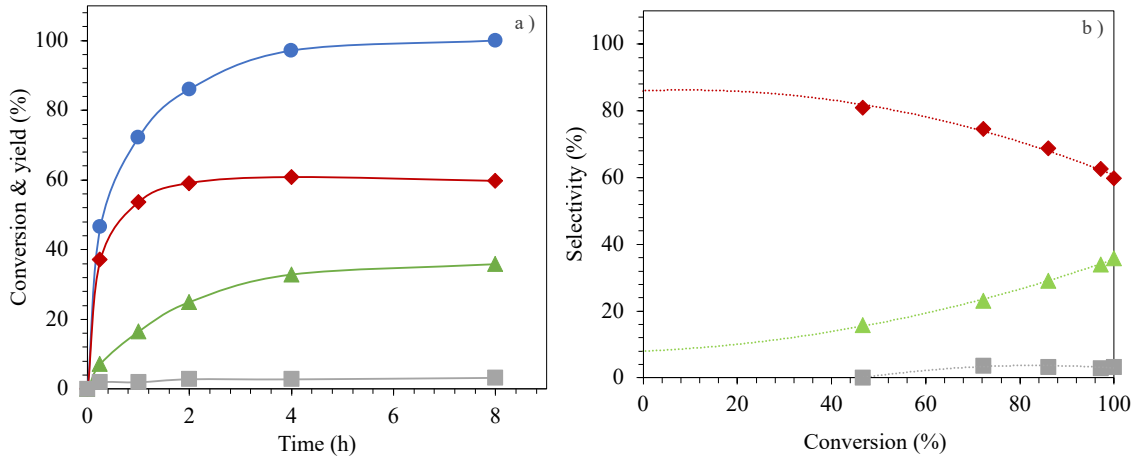

Figure 4.25. a) Time profiles between conversion and yield of 30%CuPS catalyst. b) Conversion and Selectivity of 30%CuPS catalyst; (●) conversion ,(◆) GVL, (▲) IPL, and (■) FE. Reaction condition: Furfuryl alcohol 200 µL (2.35 mmol), Isopropanol 10 mL (130.8 mmol) catalyst 200 mg , reaction temperature 140°C , N_2 pressure 10 bar.

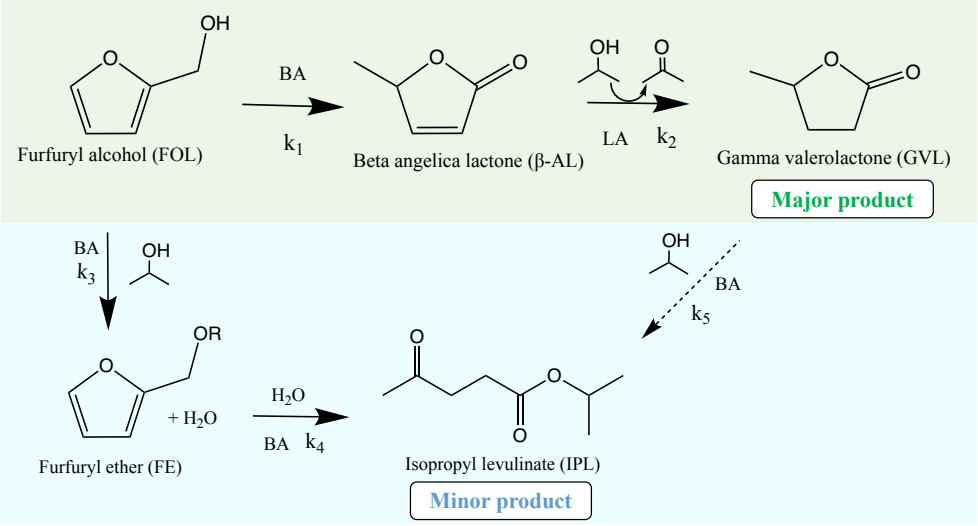

Figure 4.26. Propose mechanism of furfuryl alcohol to GVL via catalytic transfer hydrogenation.

To investigated initiate rate of the reaction by plot between weight (mg) and conversion of 30%CuPS and 1%ZnCuPS catalysts were show in **Figure 4.27a.** 30%CuPS were showing lower initiate rate of reaction, while 1%ZnCuPS catalyst was show higher than 30%CuPS indicating that Zn could be promoted the catalytic activity due to the strong interaction of Cu and Zn in 1%ZnCuPS catalysts and the highest ratio of LA/BA from Pyridine-IR results**.** To study the effect of water between 1%ZnCuPS and 1%ZnCuPS dried isopropanol at reaction temperature 140 °C, reaction time 1 hour using 2-propanol as a hydrogen donor was show in **Figure 4.27b.** Accordingly, from the reaction pathway in **Figure 4.26**, suggesting that furfuryl alcohol (FOL) can converted to be furfuryl ether and its can produce by product is a water in systems [22]1%ZnCuPS **(Figure 4.27b)** was show the catalytic activity 87.6% and 66.3% of (■)GVL selectivity. After using dried isopropanol with 1%ZnCuPS the catalytic activity was dropped dramatically to 72.2%. This is results should be suggesting that the water has affected lead to decreased activity. However, the GVL selectivity increased from 66.3 to 72.7% when compared with 1%ZnCuPS at normally condition. Because of reducing water from the system can promoted step transfer hydrogenation and rearrangement to gain more GVL selectivity. Consequently, the water has affect to be reduce esterification reaction in the systems [94]corresponding with **Figure 4.26.**

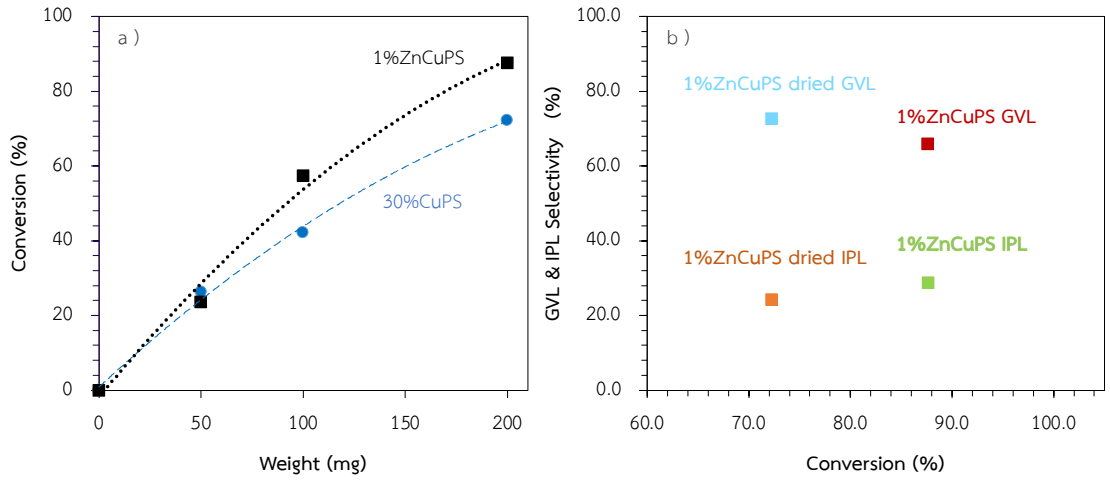

Figure 4.27. a) To study initiate rate of reaction. b) To study the effect of water between 1%ZnCuPS and 1%ZnCuPS dried isopropanol. Reaction condition: Furfuryl alcohol 200 µL (2.35 mmol), Isopropanol 10 mL (130.8 mmol) catalyst 200 mg, reaction temperature 140°C, reaction time 1h, N_2 pressure 10 bar

From the reaction pathway from furfuryl alcohol to produced GVL **(Figure 4.26)**. was show the step of furfuryl ether (FE) can be produced isopropyl levulinate (IPL) by esterification reaction. Due to more of hydrogen donor (H-donor) in their systems. This is presumably could be promoted to produce more IPL. To control the reaction pathway from FOL to produce GVL directly should be investigated the effect of hydrogen donor (H-donor) at reaction temperature 140 °C, reaction time 1h by using tetrahydrofuran (THF) to control volume 10mL was performed in **Table 4.8.** For the Entry 1 is normally conditioned to studied transfer hydrogenation in this work by using isopropanol as a H-donor (IPA/THF = 10:0) was show the catalytic activity to convert furfuryl alcohol (conversion 87.6%) and GVL yield (58.1%). Moreover, when decreased IPA/THF from 10:0 to 5:5 in entry 3 was not changed the activity of catalyst until decrease IPA/THF to 3:7 in entry 4 show the activity was dropped dramatically that could be from the H-donor in their system was not enough to transfer hydrogenation for convert furfuryl alcohol as well as IPA/THF to 1:9 in entry 5 show lowest the catalytic activity. Nevertheless, it was shows

the highest GVL selectivity than the other IPA/THF in **Figure 4.28.** It could be noted that the reaction pathway from furfuryl alcohol can be control by using a few of isopropanol as a hydrogen donor that could be controlled to increase GVL selectivity and decreased IPL. selectivity. Due to the reaction was reduced the esterification, even though, it was slow reaction rate to transfer hydrogenation corresponding with reaction pathway in **Figure 4.26**

Table 4.8. Effect of hydrogen donor in catalytic transfer hydrogenation of furfuryl alcohol to GVL

Entry	IPA/THF (mL)	Conversion %	Yield (%)			TON
			FE	GVL	IPL	
1	10 : 0	87.6	4.4	58.1	25.3	2.6
2	7 :3	87.7	2.2	61.0	24.7	2.6
3	5:5	88.3	2.3	62.3	23.2	2.6
4	3:7	74.3	2.0	61.2	11.0	2.2
5	1:9	55.9	0.0	49.5	7.6	1.7

Reaction condition: Furfuryl alcohol 200 µL (2.35 mmol), 1%ZnCuPS 200 mg, reaction temperature 140^{o}C, N_2 pressure 10 bar, reaction time 1h. Isopropanol 10 ml = 130.8 mmol

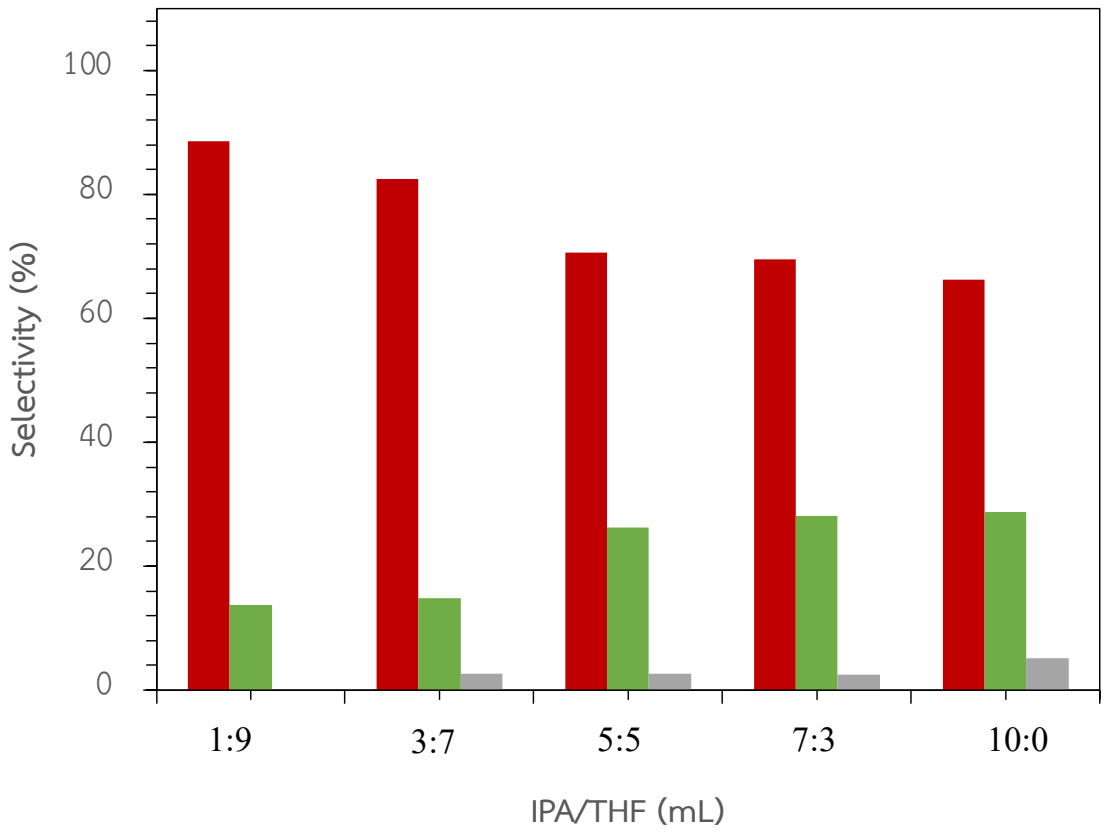

Figure 4.28. IPA/THF VS selectivity; (■) GVL, (■) IPL, (■) FE. Reaction condition: Furfuryl alcohol 200 µL (2.35 mmol) , Isopropanol 10 mL (130.8 mmol) 1%ZnCuPS as a catalyst 200 mg , temperature 140°C , N_2 pressure 10 bar, 1h

The IPA/THF = 1:9 was selected to studied because it was showing the highest GVL selectivity, further as a catalyst on the production of GVL from furfuryl alcohol. The change in product distribution with the reaction time from 0.5-24 hour was show in **Figure 4.29a**. According to these results, the conversion of furfuryl alcohol increased rapidly at the beginning (1h) was obtained conversion 55.8% and GVL yield 49.9%. At prolong time conversion was increased to 80.3% (24h) and GVL yield 70.9%. This result can be confirmed that the GVL is primary product and IPL is secondary product indicating that the parallel reaction related with reaction pathway **(Figure 4.26)** Moreover, the GVL selectivity (86.4%) still invariable also with IPL selectivity (13.9%) by without FE occurred

during in the reaction even though 24hour were show in **Figure 4.29b.** Indicating that the optimum reaction condition is IPA/THF = 1:9 for production of GVL with 1%ZnCuPS as a catalyst.

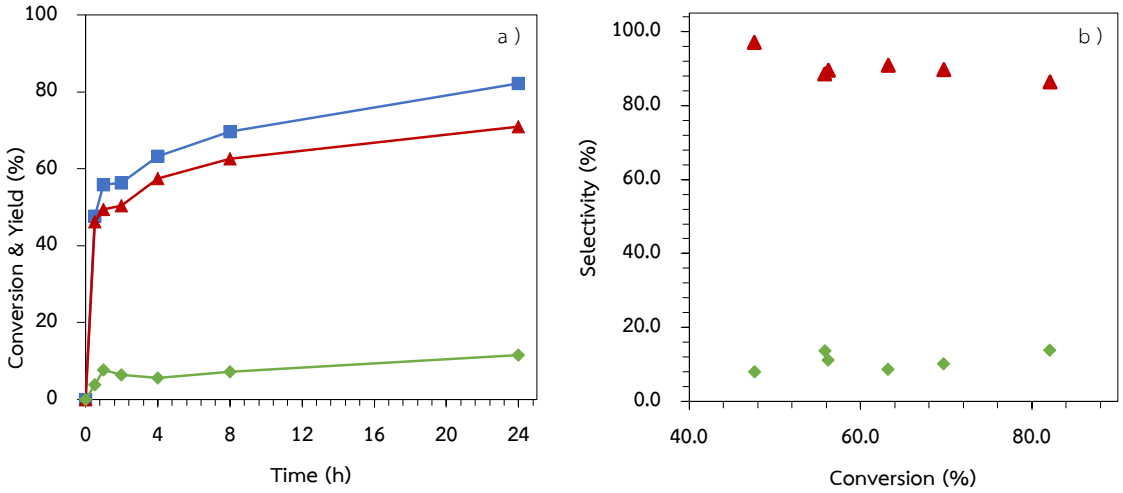

Figure 4.29. a) Time profiles of 1%ZnCuPS catalysts b) Conversion and Selectivity of 1%ZnCuPS catalysts; (■) conversion , (▲) GVL, (◆) IPL. Reaction condition: Furfuryl alcohol 200 µL (2.35 mmol), using IPA/THF = 1: 9 mL, catalyst 200 mg, reaction temperature 140°C, N_2 pressure 10 bar.

To study recyclability of 30%CuPS and 1%ZnCuPS catalysts at reaction temperature 140°C, reaction time 2h was performed in **Figure 4.30.** The fresh of 30%CuPS and 1%ZnCuPS catalyst was show the catalytic activity for 79.7% and 94.2% respectively also, with GVL yield for 57.4% and 60.8% for 30%CuPS and 1%ZnCuPS respectively. The seconds run and third runs the catalytic activity of 30%CuPS (78.7%, 63.2%) and 1%ZnCuPS (89.9% 77.9%) catalyst were decreased. Moreover, it was gradually decreased in third run from 94.2% to 77.9% and GVL yield from 60.8% to 54.8%. These might be from the Cu leaching during recyclability and which could be ascribed to carbon deposit on 1%ZnCuPS. However, GVL yield of 1%ZnCuPS (54.8%) was still higher than 30%CuPS (47.0%) even though run third times reaction.

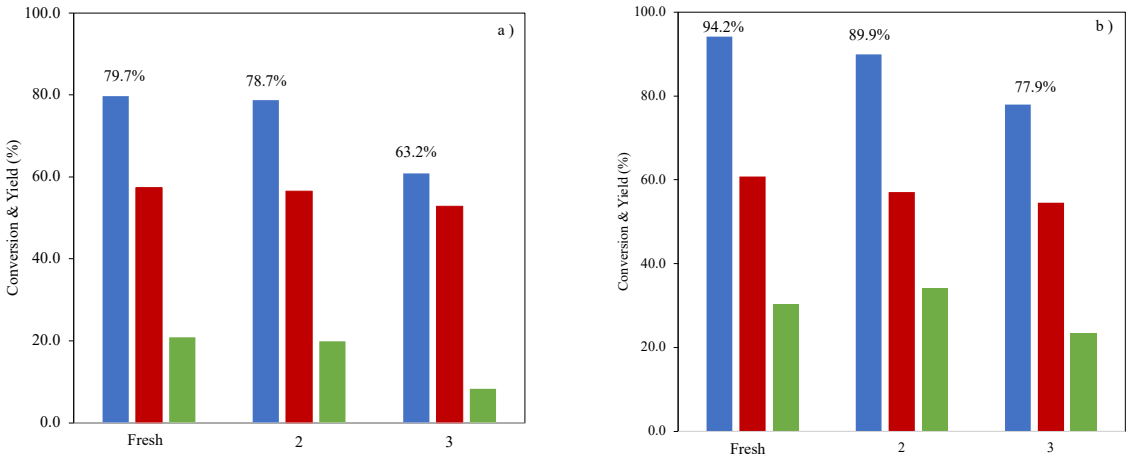

Figure 4.30. To study stability of a) 30%CuPS b) 1%ZnCuPS catalysts; (■) conversion , (■) GVL, (■) IPL. Reaction condition: Furfuryl alcohol 200 µL (2.35 mmol), Isopropanol 10 mL (130.8 mmol) catalyst 200 mg, reaction temperature 140°C, reaction time 2h, N_2 pressure 10 bars.

CHAPTER 5
CONCLUSION AND DISCUSSION

5.1 Conclusions

In this thesis, the study on conversion of furfuryl alcohol to GVL over Cu-based catalysts in liquid phase transfer hydrogenation has been investigated. The functional type (NH_4^+Y, HY) and Si/Al ratio of Y zeolite, for study the Cu/Y by ion exchanged and impregnation and to study the Cu phyllosilicate and secondary metal were investigated.

To comparative studied the functional type (NH_4^+Y, HY) and Si/Al ratio of Y zeolite and to design development of Cu-zeolite Y was successfully synthesized by ion exchange and impregnation method. The HY3.5 give the highest catalytic activity (95%). Due to high acidity and high surface area of Y zeolite. The 5%Cu/Y-IE gives almost completed catalytic activity (96%) and 5%Cu/Y-IE was the highest GVL yield (68%) at 4h indicating that the highest surface area, high dispersion, and the strong acid sites could be accelerator the catalytic activity. However, it was deactivation by coke deposit on surface area.

To investigate the 30%CuPS and secondary metal (Ni, Ag, Zn) in liquid phase transfer hydrogenation of furfuryl alcohol to GVL. 1%ZnCuPS was show the highest activity (84%) and GVL yield (56.8%) than the others candidate catalysts due to the interaction of Cu and Zn, also the highest ratio LA/BA was extremely important for catalytic transfer hydrogenation to control the reaction pathway from furfuryl alcohol to GVL

To study effect of hydrogen donor in catalytic transfer hydrogenation of furfuryl alcohol to GVL. The IPA/THF =1:9 was the best catalytic performance (82%) and GVL selectivity (86%) even though the reaction was further to 24 hour. Moreover, this result can be confirmed that the GVL is primary product and IPL is secondary product indicating that the parallel reaction.

5.2 Suggestions

5.2.1 Secondary alcohol (2-butanol, 2-pentanol, etc.) should be study the H-donor for catalytic transfer hydrogenation.

5.2.2 The reusability could be study for 5%Cu/Y-IE and 5%Cu/Y-IM catalysts should be investigated.

References

[1] F.H. Isikgor, C.R. Becer, Lignocellulosic biomass: a sustainable platform for the production of bio-based chemicals and polymers, Polym. Chem. 6 (2015) 4497–4559. https://doi.org/10.1039/C5PY00263J.

[2] S. Dutta, I.K.M. Yu, D.C.W. Tsang, Y.H. Ng, Y.S. Ok, J. Sherwood, J.H. Clark, Green synthesis of gamma-valerolactone (GVL) through hydrogenation of biomass-derived levulinic acid using non-noble metal catalysts: A critical review, Chemical Engineering Journal. 372 (2019) 992–1006. https://doi.org/10.1016/j.cej.2019.04.199.

[3] Y. Li, R. Zhang, L. Du, Q. Zhang, W. Wang, Catalytic mechanism of C–F bond cleavage: insights from QM/MM analysis of fluoroacetate dehalogenase, Catal. Sci. Technol. 6 (2016) 73–80. https://doi.org/10.1039/C5CY00777A.

[4] A. Prasertsab, Conversion of Furfural to Furfuryl Alcohol over Lewis Acid Zeolites: A Theoretical Study, (2018) 66.

[5] T.M. Lima, C.G.S. Lima, A.K. Rathi, M.B. Gawande, J. Tucek, E.A. Urquieta-González, R. Zboř il, M.W. Paixão, R.S. Varma, Magnetic ZSM-5 zeolite: a selective catalyst for the valorization of furfuryl alcohol to γ-valerolactone, alkyl levulinates or levulinic acid, Green Chem. 18 (2016) 5586–5593. https://doi.org/10.1039/C6GC01296E.

[6] Z. Fu, Z. Wang, W. Lin, W. Song, S. Li, High efficient conversion of furfural to 2-methylfuran over Ni-Cu/Al2O3 catalyst with formic acid as a hydrogen donor, Applied Catalysis A: General. 547 (2017) 248–255. https://doi.org/10.1016/j.apcata.2017.09.011.

[7] H. Du, X. Ma, P. Yan, M. Jiang, Z. Zhao, Z.C. Zhang, Catalytic furfural hydrogenation to furfuryl alcohol over Cu/SiO2 catalysts: A comparative study of the preparation methods, Fuel Processing Technology. 193 (2019) 221–231. https://doi.org/10.1016/j.fuproc.2019.05.003.

[8] S. Zhu, Y. Xue, J. Guo, Y. Cen, J. Wang, W. Fan, Integrated Conversion of Hemicellulose and Furfural into γ-Valerolactone over Au/ZrO_2 Catalyst Combined with ZSM-5, ACS Catal. 6 (2016) 2035–2042. https://doi.org/10.1021/acscatal.5b02882.

[9] H. Zhang, W. Yang, I.I. Roslan, S. Jaenicke, G.-K. Chuah, A combo Zr-HY and Al-HY zeolite catalysts for the one-pot cascade transformation of biomass-derived furfural to γ-valerolactone, Journal of Catalysis. 375 (2019) 56–67. https://doi.org/10.1016/j.jcat.2019.05.020.

[10] B. Cai, X.-C. Zhou, Y.-C. Miao, J.-Y. Luo, H. Pan, Y.-B. Huang, Enhanced Catalytic Transfer Hydrogenation of Ethyl Levulinate to γ-Valerolactone over a Robust Cu–Ni Bimetallic Catalyst, ACS Sustainable Chem. Eng. 5 (2017) 1322–1331. https://doi.org/10.1021/acssuschemeng.6b01677.

[11] G. Li, C. Liu, R. Rohling, E.J.M. Hensen, E.A. Pidko, Lewis Acid Catalysis by Zeolites * *These authors contributed equally., in: Modelling and Simulation in the Science of Micro- and Meso-Porous Materials, Elsevier, 2018: pp. 229–263. https://doi.org/10.1016/B978-0-12-805057-6.00007-7.

[12] G. Gómez Millán, H. Sixta, Towards the Green Synthesis of Furfuryl Alcohol in A One-Pot System from Xylose: A Review, Catalysts. 10 (2020) 1101. https://doi.org/10.3390/catal10101101.

[13] D.M. Alonso, S.G. Wettstein, J.A. Dumesic, Gamma-valerolactone, a sustainable platform molecule derived from lignocellulosic biomass, Green Chem. 15 (2013) 584. https://doi.org/10.1039/c3gc37065h.

[14] Y. Du, Z. Huang, J. Zhang, G. Jing, Fe_2O_3/HY Catalyst: A Microporous Material with Zeolite-Type Framework Achieving Highly Improved Alkali Poisoning-Resistant Performance for Selective Reduction of NO_x with NH_3, Environ. Sci. Technol. 54 (2020) 7078–7087. https://doi.org/10.1021/acs.est.0c00298.

[15] E. Schulman, W. Wu, D. Liu, Two-Dimensional Zeolite Materials: Structural and Acidity Properties, Materials. 13 (2020) 1822. https://doi.org/10.3390/ma13081822.

[16] B. Sun, F.-A. Khan, G. Süss-Fink, B. Therrien, Metal Catalysts Intercalated in Smectite Clays, in: Encapsulated Catalysts, Elsevier, 2017: pp. 387–441. https://doi.org/10.1016/B978-0-12-803836-9.00012-2.

[17] Z. Bian, S. Kawi, Preparation, characterization and catalytic application of phyllosilicate: A review, Catalysis Today. 339 (2020) 3–23. https://doi.org/10.1016/j.cattod.2018.12.030.

[18] H.P. Winoto, B.S. Ahn, J. Jae, Production of γ-valerolactone from furfural by a single-step process using Sn-Al-Beta zeolites: Optimizing the catalyst acid properties and process conditions, Journal of Industrial and Engineering Chemistry. 40 (2016) 62–71. https://doi.org/10.1016/j.jiec.2016.06.007.

[19] B. Tang, S. Li, W.-C. Song, Y. Li, E.-C. Yang, One-pot transformation of furfural into γ-valerolactone catalyzed by a hierarchical Hf-Al-USY zeolite with balanced Lewis and Brønsted acid sites, Sustainable Energy Fuels. 5 (2021) 4724–4735. https://doi.org/10.1039/D1SE00942G.

[20] T. Subramanian, K. Pitchumani, Transfer hydrogenation of carbonyl compounds and carbon–carbon multiple bonds by zeolite supported Cu nanoparticles, Catal. Sci. Technol. 2 (2012) 296–300. https://doi.org/10.1039/C1CY00383F.

[21] R. Shoja Razavi, M.R. Loghman-Estarki, Synthesis and Characterizations of Copper Oxide Nanoparticles Within Zeolite Y, J Clust Sci. 23 (2012) 1097–1106. https://doi.org/10.1007/s10876-012-0502-y.

[22] R. Behling, S. Valange, G. Chatel, Heterogeneous catalytic oxidation for lignin valorization into valuable chemicals: what results? What limitations? What trends?, Green Chem. 18 (2016) 1839–1854. https://doi.org/10.1039/C5GC03061G.

[23] W. Gong, C. Chen, R. Fan, H. Zhang, G. Wang, H. Zhao, Transfer-hydrogenation of furfural and levulinic acid over supported copper catalyst, Fuel. 231 (2018) 165–171. https://doi.org/10.1016/j.fuel.2018.05.075.

[24] K. Zhou, J. Chen, Y. Cheng, Z. Chen, S. Kang, Z. Cai, Y. Xu, J. Wei, Enhanced Catalytic Transfer Hydrogenation of Biomass-Based Furfural into 2-Methylfuran over Multifunctional Cu–Re Bimetallic Catalysts, ACS Sustainable Chem. Eng. 8 (2020) 16624–16636. https://doi.org/10.1021/acssuschemeng.0c06026.

[25] J. Xue, M. Wu, Y. Song, J. Zhao, J. Wu, Y. Quan, J. Ren, Study on performance of Ag-modified layered copper silicate catalyst for hydrogenation of dimethyl oxalate to methyl glycolate, Journal of Fuel Chemistry and Technology. 50 (2022) 1014–1022. https://doi.org/10.1016/S1872-5813(21)60011-2.

[26] S. Catillon-Mucherie, F. Ammari, J.-M. Krafft, H. Lauron-Pernot, R. Touroude, C. Louis, Preparation of Coimpregnated Cu–Zn/SiO_2 Catalysts: Influence of the Drying

Step on Metallic Particle Size and on Cu^{0} –Zn^{II} Interactions, J. Phys. Chem. C. 111 (2007) 11619–11626. https://doi.org/10.1021/jp0718956.

[27] X. Dong, X. Ma, H. Xu, Q. Ge, Comparative study of silica-supported copper catalysts prepared by different methods: formation and transition of copper phyllosilicate, Catal. Sci. Technol. 6 (2016) 4151–4158. https://doi.org/10.1039/C5CY01965F.

[28] A.M. Bahmanpour, F. Héroguel, M. Kılıç, C.J. Baranowski, L. Artiglia, U. Röthlisberger, J.S. Luterbacher, O. Kröcher, Cu–Al Spinel as a Highly Active and Stable Catalyst for the Reverse Water Gas Shift Reaction, ACS Catal. 9 (2019) 6243–6251. https://doi.org/10.1021/acscatal.9b01822.

[29] H. Mitta, P.K. Seelam, S. Ojala, R.L. Keiski, P. Balla, Tuning Y-zeolite based catalyst with copper for enhanced activity and selectivity in vapor phase hydrogenolysis of glycerol to 1,2-propanediol, Applied Catalysis A: General. 550 (2018) 308–319. https://doi.org/10.1016/j.apcata.2017.10.019.

[30] S. Elzey, J. Baltrusaitis, S. Bian, V.H. Grassian, Formation of paratacamite nanomaterials via the conversion of aged and oxidized copper nanoparticles in hydrochloric acidic media, J. Mater. Chem. 21 (2011) 3162. https://doi.org/10.1039/c0jm03705b.

[31] L. Liu, Z. Yao, B. Liu, L. Dong, Correlation of structural characteristics with catalytic performance of CuO/CexZr1−xO2 catalysts for NO reduction by CO, Journal of Catalysis. 275 (2010) 45–60. https://doi.org/10.1016/j.jcat.2010.07.024.

[32] D.L. Hoang, T.T.H. Dang, J. Engeldinger, M. Schneider, J. Radnik, M. Richter, A. Martin, TPR investigations on the reducibility of Cu supported on Al2O3, zeolite Y and SAPO-5, Journal of Solid State Chemistry. 184 (2011) 1915–1923. https://doi.org/10.1016/j.jssc.2011.05.042.

[33] F.P.G. Duatepe, O.Y. Orhan, E. Alper, Kinetics of Carbon Dioxide Absorption by Nonaqueous Solutions of Promoted Sterically Hindered Amines, Energy Procedia. 114 (2017) 57–65. https://doi.org/10.1016/j.egypro.2017.03.1147.

[34] L.I. van der Wal, K.P. de Jong, J. Zečević, The Origin of Metal Loading Heterogeneities in Pt/Zeolite Y Bifunctional Catalysts, ChemCatChem. 11 (2019) 4081–4088. https://doi.org/10.1002/cctc.201900441.

[35] C. Boruban, E. Nalbant Esenturk, Synthesis of CuO nanostructures on zeolite-Y and investigation of their CO2 adsorption properties, J. Mater. Res. 32 (2017) 3669–3678. https://doi.org/10.1557/jmr.2017.337.

[36] Z. Qin, B. Shen, X. Gao, F. Lin, B. Wang, C. Xu, Mesoporous Y zeolite with homogeneous aluminum distribution obtained by sequential desilication–dealumination and its performance in the catalytic cracking of cumene and 1,3,5-triisopropylbenzene, Journal of Catalysis. 278 (2011) 266–275. https://doi.org/10.1016/j.jcat.2010.12.013.

[37] Y. Huang, K. Wang, D. Dong, D. Li, M.R. Hill, A.J. Hill, H. Wang, Synthesis of hierarchical porous zeolite NaY particles with controllable particle sizes, Microporous and Mesoporous Materials. 127 (2010) 167–175. https://doi.org/10.1016/j.micromeso.2009.07.026.

[38] A.H. Janssen, A.J. Koster, K.P. de Jong, Three-Dimensional Transmission Electron Microscopic Observations of Mesopores in Dealuminated Zeolite Y, Angew. Chem. Int. Ed. 40 (2001) 1102–1104. https://doi.org/10.1002/1521-3773(20010316)40:6<1102::AID-ANIE11020>3.0.CO;2-6.

[39] the Department of Chemical Engineering, Faculty of Engineering, King Mongkut's University of Technology North Bangkok, 10800, Thailand, P. Worathanakul, N. Rakpasert, Influence of Different Preparation Methods of Copper Loading on Na-Y Zeolite for Green Gas Emission, IJESD. 7 (2016) 885–888. https://doi.org/10.18178/ijesd.2016.7.12.899.

[40] B.-L. Jiang, N. Jiang, Y.-X. Chang, Synthesis of highly active Cu(I)-Y(III)-Y zeolite and its selective adsorption desulfurization performance in presence of xylene isomers, Pet. Sci. 18 (2021) 295–306. https://doi.org/10.1007/s12182-020-00531-0.

[41] P. Wang, J. Zhang, C. Han, C. Yang, C. Li, Effect of modification methods on the surface properties and n-butane isomerization performance of La/Ni-promoted SO42−/ZrO2-Al2O3, Applied Surface Science. 378 (2016) 489–495. https://doi.org/10.1016/j.apsusc.2016.04.043.

[42] P. Munnik, P.E. De Jongh, K.P. De Jong, Recent Developments in the Synthesis of Supported Catalysts, Chem. Rev. 115 (2015) 6687–6718. https://doi.org/10.1021/cr500486u.

[43] S.P.D.S. Ribeiro, R.C. Martins, G.M. Barbosa, M.A.D.F. Rocha, A. Landesmann, M.A.C. Nascimento, R.S.V. Nascimento, Influence of the zeolite acidity on its synergistic action with a flame-retarding polymeric intumescent formulation, J Mater Sci. 55 (2020) 619–630. https://doi.org/10.1007/s10853-019-04047-w.

[44] J. Van Aelst, D. Verboekend, A. Philippaerts, N. Nuttens, M. Kurttepeli, E. Gobechiya, M. Haouas, S.P. Sree, J.F.M. Denayer, J.A. Martens, C.E.A. Kirschhock, F. Taulelle, S. Bals, G.V. Baron, P.A. Jacobs, B.F. Sels, Catalyst Design by NH_4OH Treatment of USY Zeolite, Adv. Funct. Mater. 25 (2015) 7130–7144. https://doi.org/10.1002/adfm.201502772.

[45] E.G. Derouane, J.C. Védrine, R.R. Pinto, P.M. Borges, L. Costa, M.A.N.D.A. Lemos, F. Lemos, F.R. Ribeiro, The Acidity of Zeolites: Concepts, Measurements and Relation to Catalysis: A Review on Experimental and Theoretical Methods for the Study of Zeolite Acidity, Catalysis Reviews. 55 (2013) 454–515. https://doi.org/10.1080/01614940.2013.822266.

[46] B.M. Weckhuysen, J. Yu, Recent advances in zeolite chemistry and catalysis, Chem. Soc. Rev. 44 (2015) 7022–7024. https://doi.org/10.1039/C5CS90100F.

[47] T. Ma, H. Imai, M. Yamawaki, K. Terasaka, X. Li, Selective Synthesis of Gasoline-Ranged Hydrocarbons from Syngas over Hybrid Catalyst Consisting of Metal-Loaded ZSM-5 Coupled with Copper-Zinc Oxide, Catalysts. 4 (2014) 116–128. https://doi.org/10.3390/catal4020116.

[48] I.S. Golubev, P.P. Dik, M.O. Kazakov, V.Yu. Pereyma, O.V. Klimov, M.Yu. Smirnova, I.P. Prosvirin, E.Yu. Gerasimov, D.O. Kondrashev, V.A. Golovachev, O.S. Vedernikov, A.V. Kleimenov, A.S. Noskov, The effect of Si/Al ratio of zeolite Y in NiW catalyst for second stage hydrocracking, Catalysis Today. 378 (2021) 65–74. https://doi.org/10.1016/j.cattod.2021.01.014.

[49] S. Wang, K. Goulas, E. Iglesia, Condensation and esterification reactions of alkanals, alkanones, and alkanols on TiO2: Elementary steps, site requirements, and

synergistic effects of bifunctional strategies, Journal of Catalysis. 340 (2016) 302–320. https://doi.org/10.1016/j.jcat.2016.05.026.

[50] D.T. Ngo, T. Sooknoi, D.E. Resasco, Improving stability of cyclopentanone aldol condensation MgO-based catalysts by surface hydrophobization with organosilanes, Applied Catalysis B: Environmental. 237 (2018) 835–843. https://doi.org/10.1016/j.apcatb.2018.06.044.

[51] C. Liu, G. Li, E.J.M. Hensen, E.A. Pidko, Relationship between acidity and catalytic reactivity of faujasite zeolite: A periodic DFT study, Journal of Catalysis. 344 (2016) 570–577. https://doi.org/10.1016/j.jcat.2016.10.027.

[52] J. Zhang, J. Chen, Selective transfer hydrogenation of biomass-based furfural and 5-hydroxymethylfurfural over hydrotalcite-derived copper catalysts using methanol as hydrogen donor, (n.d.).

[53] E.-M. Lems, S. Winklehner, C. Hansmann, W. Gindl-Altmutter, S. Veigel, Reinforcing effect of poly(furfuryl alcohol) in cellulose-based porous materials, Cellulose. 26 (2019) 4431–4444. https://doi.org/10.1007/s10570-019-02348-6.

[54] F. Dong, Y. Zhu, H. Zhao, Z. Tang, Ratio-controlled synthesis of phyllosilicate-like materials as precursors for highly efficient catalysis of the formyl group, Catal. Sci. Technol. 7 (2017) 1880–1891. https://doi.org/10.1039/C7CY00233E.

[55] X. Wang, K. Ma, L. Guo, Y. Tian, Q. Cheng, X. Bai, J. Huang, T. Ding, X. Li, Cu/ZnO/SiO 2 catalyst synthesized by reduction of ZnO-modified copper phyllosilicate for dimethyl ether steam reforming, Applied Catalysis A: General. 540 (2017) 37–46. https://doi.org/10.1016/j.apcata.2017.04.013.

[56] Y. Sun, F. Meng, Q. Ge, J. Sun, Importance of the Initial Oxidation State of Copper for the Catalytic Hydrogenation of Dimethyl Oxalate to Ethylene Glycol, ChemistryOpen. 7 (2018) 969–976. https://doi.org/10.1002/open.201800225.

[57] H. Li, Y. Cui, Y. Liu, L. Zhang, Q. Zhang, J. Zhang, W.-L. Dai, Highly efficient Ag-modified copper phyllosilicate nanotube: Preparation by co-ammonia evaporation hydrothermal method and application in the selective hydrogenation of carbonate, Journal of Materials Science & Technology. 47 (2020) 29–37. https://doi.org/10.1016/j.jmst.2020.02.020.

[58] D.-T. To, Y.-C. Lin, Copper Phyllosilicates-Derived Catalysts in the Production of Alcohols from Hydrogenation of Carboxylates, Carboxylic Acids, Carbonates, Formyls, and CO2: A Review, Catalysts. 11 (2021) 255. https://doi.org/10.3390/catal11020255.

[59] Y. Zhao, X. Kan, H. Yun, D. Wang, N. Li, G. Li, J. Shen, Synthesis of a high surface area and highly dispersed Cu-O-Si complex oxide used for the low-temperature hydrogenation of dimethyl oxalate to ethylene glycol, Catalysis Communications. 154 (2021) 106310. https://doi.org/10.1016/j.catcom.2021.106310.

[60] X. Du, N. Fu, S. Zhang, C. Chen, D. Wang, Y. Li, Au/CuSiO3 nanotubes: High-performance robust catalysts for selective oxidation of ethanol to acetaldehyde, Nano Res. 9 (2016) 2681–2686. https://doi.org/10.1007/s12274-016-1155-1.

[61] Z.-Q. Wang, Z.-N. Xu, S.-Y. Peng, M.-J. Zhang, G. Lu, Q.-S. Chen, Y. Chen, G.-C. Guo, High-Performance and Long-Lived Cu/SiO_2 Nanocatalyst for CO_2 Hydrogenation, ACS Catal. 5 (2015) 4255–4259. https://doi.org/10.1021/acscatal.5b00682.

[62] D. Mukherjee, R. Singuru, P. Venkataswamy, D. Damma, B.M. Reddy, Ceria Promoted Cu-Ni/SiO_2 Catalyst for Selective Hydrodeoxygenation of Vanillin, ACS Omega. 4 (2019) 4770–4778. https://doi.org/10.1021/acsomega.9b00039.

[63] R.-P. Ye, W. Gong, Z. Sun, Q. Sheng, X. Shi, T. Wang, Y. Yao, J.J. Razink, L. Lin, Z. Zhou, H. Adidharma, J. Tang, M. Fan, Y.-G. Yao, Enhanced stability of Ni/SiO2 catalyst for CO2 methanation: Derived from nickel phyllosilicate with strong metal-support interactions, Energy. 188 (2019) 116059. https://doi.org/10.1016/j.energy.2019.116059.

[64] S. Amokrane, A. Boualouache, P. Simon, M. Capron, G. Otmanine, D. Allam, S. Hocine, Effect of Adding Transition Metals to Copper on the Dehydrogenation Reaction of Ethanol, Catal Lett. 151 (2021) 2864–2883. https://doi.org/10.1007/s10562-020-03517-0.

[65] D. Xu, D. Fan, W. Shen, Catalyst-free direct vapor-phase growth of Zn1−xCu x O micro-cross structures and their optical properties, Nanoscale Res Lett. 8 (2013) 46. https://doi.org/10.1186/1556-276X-8-46.

[66] Z. Li, H. Chen, W. Liu, Full-Spectrum Photocatalytic Activity of ZnO/CuO/ZnFe2O4 Nanocomposite as a PhotoFenton-Like Catalyst, Catalysts. 8 (2018) 557. https://doi.org/10.3390/catal8110557.

[67] D. Mora-Fonz, T. Lazauskas, S.M. Woodley, S.T. Bromley, C.R.A. Catlow, A.A. Sokol, Development of Interatomic Potentials for Supported Nanoparticles: The Cu/ZnO Case, J. Phys. Chem. C. 121 (2017) 16831–16844. https://doi.org/10.1021/acs.jpcc.7b04502.

[68] Y.-J. Tsou, T.D. To, Y.-C. Chiang, J.-F. Lee, R. Kumar, P.-W. Chung, Y.-C. Lin, Hydrophobic Copper Catalysts Derived from Copper Phyllosilicates in the Hydrogenation of Levulinic Acid to **γ**-Valerolactone, ACS Appl. Mater. Interfaces. 12 (2020) 54851–54861. https://doi.org/10.1021/acsami.0c17612.

[69] H. Salam, Y. Dong, I. Davies, Development of biobased polymer/clay nanocomposites, in: Fillers and Reinforcements for Advanced Nanocomposites, Elsevier, 2015: pp. 101–132. https://doi.org/10.1016/B978-0-08-100079-3.00006-5.

[70] C.H. Lim, Expandable Phyllosilicate Reactions with Lithium on Heating, Clays and Clay Minerals. 34 (1986) 346–352. https://doi.org/10.1346/CCMN.1986.0340316.

[71] D. Grandjean, V. Pelipenko, E.D. Batyrev, J.C. Van Den Heuvel, A.A. Khassin, Tamara.M. Yurieva, B.M. Weckhuysen, Dynamic Cu/Zn Interaction in SiO_2 Supported Methanol Synthesis Catalysts Unraveled by in Situ XAFS, J. Phys. Chem. C. 115 (2011) 20175–20191. https://doi.org/10.1021/jp201839s.

[72] A. Manceau, Quantitative Zn speciation in smelter-contaminated soils by EXAFS spectroscopy, American Journal of Science. 300 (2000) 289–343. https://doi.org/10.2475/ajs.300.4.289.

[73] L. Chen, P. Guo, M. Qiao, S. Yan, H. Li, W. Shen, H. Xu, K. Fan, Cu/SiO2 catalysts prepared by the ammonia-evaporation method: Texture, structure, and catalytic performance in hydrogenation of dimethyl oxalate to ethylene glycol, Journal of Catalysis. 257 (2008) 172–180. https://doi.org/10.1016/j.jcat.2008.04.021.

[74] R.-P. Ye, Y. Chen, T.R. Reina, Z. Cao, T. Xu, X. Chen, Y. Jin, X.L. Zhang, J. Liu, Fabrication Method-Engineered Cu–ZnO/SiO_2 Catalysts with Highly Dispersed Metal

Nanoparticles toward Efficient Utilization of Methanol as a Hydrogen Carrier, Adv Energy Sustain Res. 2 (2021) 2100082. https://doi.org/10.1002/aesr.202100082.

[75] R. Ye, C. Zhang, P. Zhang, L. Lin, L. Huang, Y. Huang, T. Li, Z. Zhou, R. Zhang, G. Feng, Y.-G. Yao, Facile preparation of efficient Cu-SiO2 catalysts using a polyhydroxy molecular template to regulate surface copper species for dimethyl oxalate hydrogenation, Catalysis Communications. 174 (2023) 106586. https://doi.org/10.1016/j.catcom.2022.106586.

[76] F. Toledo, I.T. Ghampson, C. Sepúlveda, R. García, J.L.G. Fierro, A. Videla, R. Serpell, N. Escalona, Effect of Re content and support in the liquid phase conversion of furfural to furfuryl alcohol and 2-methyl furan over ReOx catalysts, Fuel. 242 (2019) 532–544. https://doi.org/10.1016/j.fuel.2019.01.090.

[77] O. Arbeláez, A. Orrego, F. Bustamante, A.L. Villa, Effect of Acidity, Basicity and ZrO2 Phases of Cu–Ni/ZrO2 Catalysts on the Direct Synthesis of Diethyl Carbonate from CO2 and Ethanol, Catal Lett. 146 (2016) 725–733. https://doi.org/10.1007/s10562-016-1699-4.

[78] F. Dong, G. Ding, H. Zheng, X. Xiang, L. Chen, catalyst for the synthesis of biofuel 2-methylfuran, (n.d.).

[79] W. Di, J. Cheng, S. Tian, J. Li, J. Chen, Q. Sun, Synthesis and characterization of supported copper phyllosilicate catalysts for acetic ester hydrogenation to ethanol, Applied Catalysis A: General. 510 (2016) 244–259. https://doi.org/10.1016/j.apcata.2015.10.026.

[80] N. Karanwal, M.G. Sibi, M.K. Khan, A.A. Myint, B. Chan Ryu, J.W. Kang, J. Kim, Trimetallic Cu–Ni–Zn/H-ZSM-5 Catalyst for the One-Pot Conversion of Levulinic Acid to High-Yield 1,4-Pentanediol under Mild Conditions in an Aqueous Medium, ACS Catal. 11 (2021) 2846–2864. https://doi.org/10.1021/acscatal.0c04216.

[81] Y. Wang, M. Craven, X. Yu, J. Ding, P. Bryant, J. Huang, X. Tu, Plasma-Enhanced Catalytic Synthesis of Ammonia over a Ni/Al $_2$ O $_3$ Catalyst at Near-Room Temperature: Insights into the Importance of the Catalyst Surface on the Reaction Mechanism, ACS Catal. 9 (2019) 10780–10793. https://doi.org/10.1021/acscatal.9b02538.

[82] S. Molina-Ramírez, M. Cortés-Reyes, C. Herrera, M.Á. Larrubia, L.J. Alemany, Comparison of Cu-CHA-Zeolites in the Hybrid NSR-SCR Catalytic System for NOx Abatement in Mobile Sources, Chemistry. 5 (2023) 602–615. https://doi.org/10.3390/chemistry5010043.

[83] L. Lin, X. Zhang, N. He, J. Liu, Q. Xin, H. Guo, Operando Dual Beam FTIR Study of Hydroxyl Groups and Zn Species over Defective HZSM-5 Zeolite Supported Zinc Catalysts, Catalysts. 9 (2019) 100. https://doi.org/10.3390/catal9010100.

[84] E. Parry, An infrared study of pyridine adsorbed on acidic solids. Characterization of surface acidity, Journal of Catalysis. 2 (1963) 371–379. https://doi.org/10.1016/0021-9517(63)90102-7.

[85] M.I. Zaki, M.A. Hasan, F.A. Al-Sagheer, L. Pasupulety, In situ FTIR spectra of pyridine adsorbed on SiO2–Al2O3, TiO2, ZrO2 and CeO2: general considerations for the identification of acid sites on surfaces of finely divided metal oxides, Colloids and Surfaces A: Physicochemical and Engineering Aspects. 190 (2001) 261–274. https://doi.org/10.1016/S0927-7757(01)00690-2.

[86] S.M. Kim, A. Armutlulu, W.-C. Liao, D. Hosseini, D. Stoian, Z. Chen, P.M. Abdala, C. Copéret, C. Müller, Structural insight into an atomic layer deposition (ALD) grown Al_2O_3 layer on Ni/SiO_2 : impact on catalytic activity and stability in dry reforming of methane, Catal. Sci. Technol. 11 (2021) 7563–7577. https://doi.org/10.1039/D1CY01149A.

[87] J. Zhang, E.C. Wegener, J.W. Harris, K.A. Unocic, L.F. Allard, S. Purdy, S. Adhikari, M.J. Cordon, J.T. Miller, T.R. Krause, S. Cheng, D. Liu, M. Li, X. Jiang, Z. Wu, Isolated metal sites in Cu-Zn-Y/Beta for direct and selective butene-rich C3+ olefins formation from ethanol, (n.d.).

[88] S. Pendem, I. Mondal, A. Shrotri, B.S. Rao, N. Lingaiah, J. Mondal, Unraveling the structural properties and reactivity trends of Cu–Ni bimetallic nanoalloy catalysts for biomass-derived levulinic acid hydrogenation, Sustainable Energy Fuels. 2 (2018) 1516–1529. https://doi.org/10.1039/C8SE00138C.

[89] W. Zhou, H. Xin, H. Yang, X. Du, R. Yang, D. Li, C. Hu, The Deoxygenation Pathways of Palmitic Acid into Hydrocarbons on Silica-Supported Ni12P5 and Ni2P Catalysts, Catalysts. 8 (2018) 153. https://doi.org/10.3390/catal8040153.

[90] V.L. Dagle, M.D. Flake, T.L. Lemmon, J.S. Lopez, L. Kovarik, R.A. Dagle, Effect of the SiO2 support on the catalytic performance of Ag/ZrO2/SiO2 catalysts for the single-bed production of butadiene from ethanol, Applied Catalysis B: Environmental. 236 (2018) 576–587. https://doi.org/10.1016/j.apcatb.2018.05.055.

[91] E. Lam, G. Noh, K. Larmier, O.V. Safonova, C. Copéret, CO2 hydrogenation on Cu-catalysts generated from ZnII single-sites: Enhanced CH3OH selectivity compared to Cu/ZnO/Al2O3, Journal of Catalysis. 394 (2021) 266–272. https://doi.org/10.1016/j.jcat.2020.04.028.

[92] A. Trasarti, A. Marchi, C. Apesteguia, Design of catalyst systems for the one-pot synthesis of menthols from citral, Journal of Catalysis. 247 (2007) 155–165. https://doi.org/10.1016/j.jcat.2007.01.016.

[93] A. Saotta, A. Allegri, F. Liuzzi, G. Fornasari, N. Dimitratos, S. Albonetti, Ti/Zr/O Mixed Oxides for the Catalytic Transfer Hydrogenation of Furfural to GVL in a Liquid-Phase Continuous-Flow Reactor, ChemEngineering. 7 (2023) 23. https://doi.org/10.3390/chemengineering7020023.

[94] H. Gómez Bernal, P. Benito, E. Rodríguez-Castellón, A.M. Raspolli Galletti, T. Funaioli, Synthesis of isopropyl levulinate from furfural: Insights on a cascade production perspective, Applied Catalysis A: General. 575 (2019) 111–119. https://doi.org/10.1016/j.apcata.2019.02.018.

APPENDICES

APPENDIX A

CALCULATION FOR CATALYST PREPARATION

Part 1

The calculation of 5%Cu/Y-IE catalysts prepared by ion-exchanged method with NH_4^+Y zeolite.

$$\frac{g}{\text{M.W. of Cu } (NO_3)_2 \cdot 3H_2O)} = \frac{MV}{1000}$$

For weight of metal for 5%Cu/Y-IE in 0.1 M and 400 mL of deionized water

$$\frac{g}{241.60\ g/mol} = \frac{(0.1M)\ (400mL)}{1000}$$

Weight of Cu = 9.664 g

The calculation of 5%Cu/Y-IM catalysts prepared by incipient wetness impregnation method on NH_4^+Y zeolite.

Calculation the weight of 5% copper loading of NH_4^+Y zeolite.

$$\text{\% metal loading} = \frac{\text{Weight of metal}}{\text{Weight of metal + weight of silica}}$$

For weight of metal for 5%Cu/Y-IM

$$5 = \frac{\text{Weight of Cu}}{\text{Weight of Cu + 5}} \times 100$$

Weight of Cu = 0.263 g

For weight of Cu complex for 5%Cu/Y-IM (M.W. of $Cu(NO_3)_2 \cdot 3H_2O$) = 241.6 g/mol)

Cu metal 63.546 g in $Cu(NO_3)_2 \cdot 3H_2O$) = 241.6 g

Cu metal 2.571 g in $Cu(NO_3)_2 \cdot 3H_2O$) = $\frac{0.263 \times 241.6}{63.546}$ = 1.005 g

Part 2

The calculation of 30%CuPS catalysts prepared by ammonia evaporation hydrothermal method.

Calculation the 40% colloidal silica solution for 6g

$$\text{Volume of colloidal silica} = \frac{\text{15 g of colloidal silica}}{\text{1.3 g/mL (density)}} = 11.6 \text{ mL}$$

Calculation the weight of 30% copper loading of phyllosilicate

$$\text{\% metal loading} = \frac{\text{Weight of metal}}{\text{Weight of metal + weight of silica}}$$

For weight of metal for 30%CuPS

$$30 = \frac{\text{Weight of Cu}}{\text{Weight of Cu + 6}} \times 100$$

Weight of Cu = 2.571 g

For weight of Cu complex for 30%CuPS (M.W. of $Cu(NO_3)_2 \cdot 3H_2O$) = 241.6 g/mol)

Cu metal 63.546 g in $Cu(NO_3)_2 \cdot 3H_2O$) = 241.6 g

Cu metal 2.571 g in $Cu(NO_3)_2 \cdot 3H_2O$) = $\frac{2.571 \times 241.6}{63.546}$ = 9.77 g

Calculation of 30% wt. ammonia solution (metal: NH_3= 1: 12) by mol for 30%CuPS

Mol Cu = $\frac{\text{2.571 g of Cu}}{\text{63.546 g/ mol}}$ = 0.0406 mol Cu x 12 = 0.4855 mol NH_3

Mol NH_3 = $\frac{\text{0.4855 mol } NH_3 \times \text{17 g} \times \text{100 g} \times \text{1mL}}{\text{1 mol} \times \text{30 g} \times \text{0.9 g}}$ = 30.23 mL

Calculation the secondary metal loading 1%Ni, 1%Ag, 1%Zn on 30%CuPS by incipient wetness impregnation method

% metal loading = $\frac{\text{Weight of metal}}{\text{Weight of metal + weight of 30\%CuPS}}$

For weight of metal for 1%NiCuPS

$$1 = \frac{\text{Weight of Ni}}{\text{Weight of Ni + 4g}} \times 100$$

Weight of Ni = 0.0404 g

For weight of Cu complex for 1%NiCuPS (M.W. of $Ni(NO_3)_2 \cdot 6H_2O$) = 290.81 g/mol)

Ni metal 58.690 g in $Ni(NO_3)_2 \cdot 6H_2O$) = 290.81 g

Ni metal 0.0404 g in $Ni(NO_3)_2 \cdot 6H_2O$) = $\frac{2.571 \times 241.6}{58.690}$ = 0.2001 g

Table A1 Summary of secondary metal on 30%CuPS

Catalyst	Metal complex	M.W. (g/mol)	Weight (g)	Solvent for dissolved
30%CuPS	$Cu(NO_3)_2 \cdot 3H_2O$)	241.60	9.7701	-
1%NiCuPS	$Ni(NO_3)_2 \cdot 6H_2O$)	290.81	0.2001	Acetone
1%AgCuPS	AgNO3	169.87	0.0646	Acetonitrile
1%ZnCuPS	$Zn(NO_3)_2 \cdot 6H_2O$)	297.46	0.1838	Acetone

APPENDIX B

CATALYST CHARACTERIZATION

Part 1

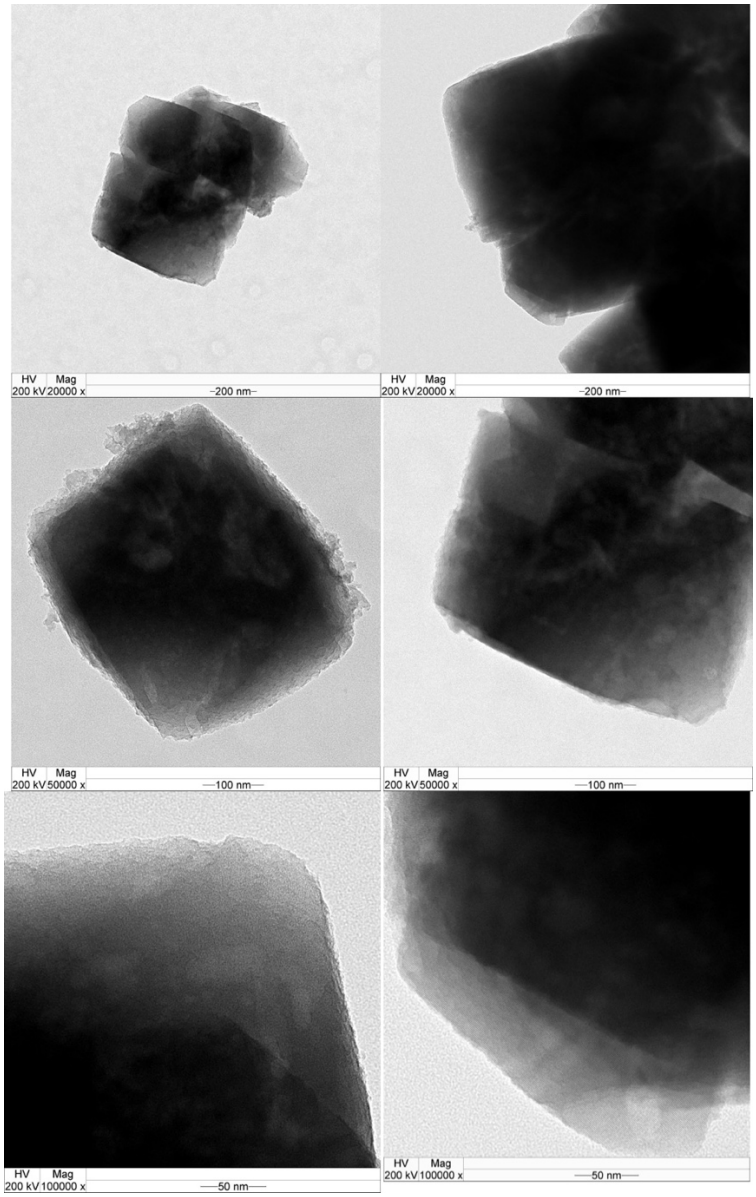

Figure B1. TEM image of HY3.5.

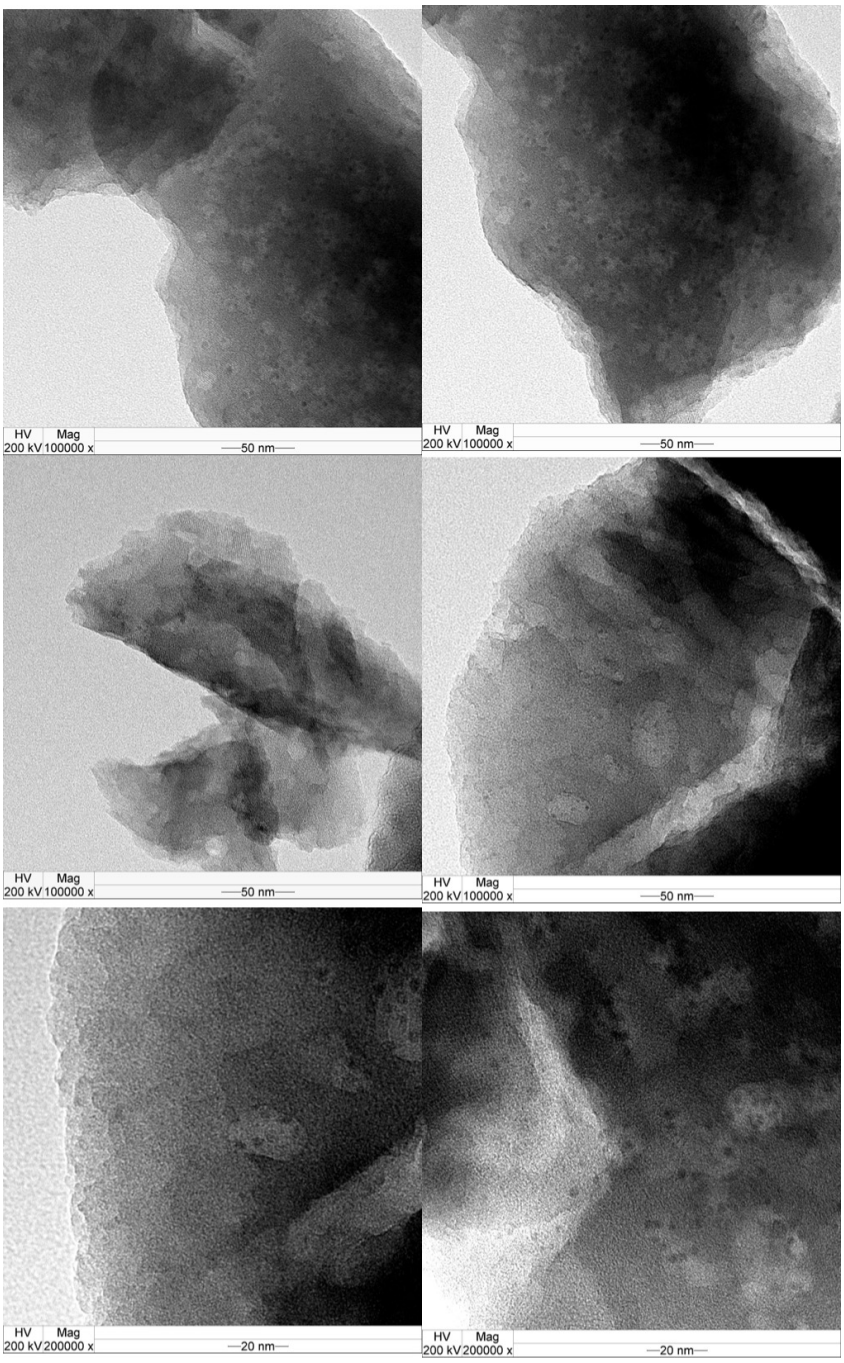

Figure B2. TEM image of 5%Cu/Y-IE.

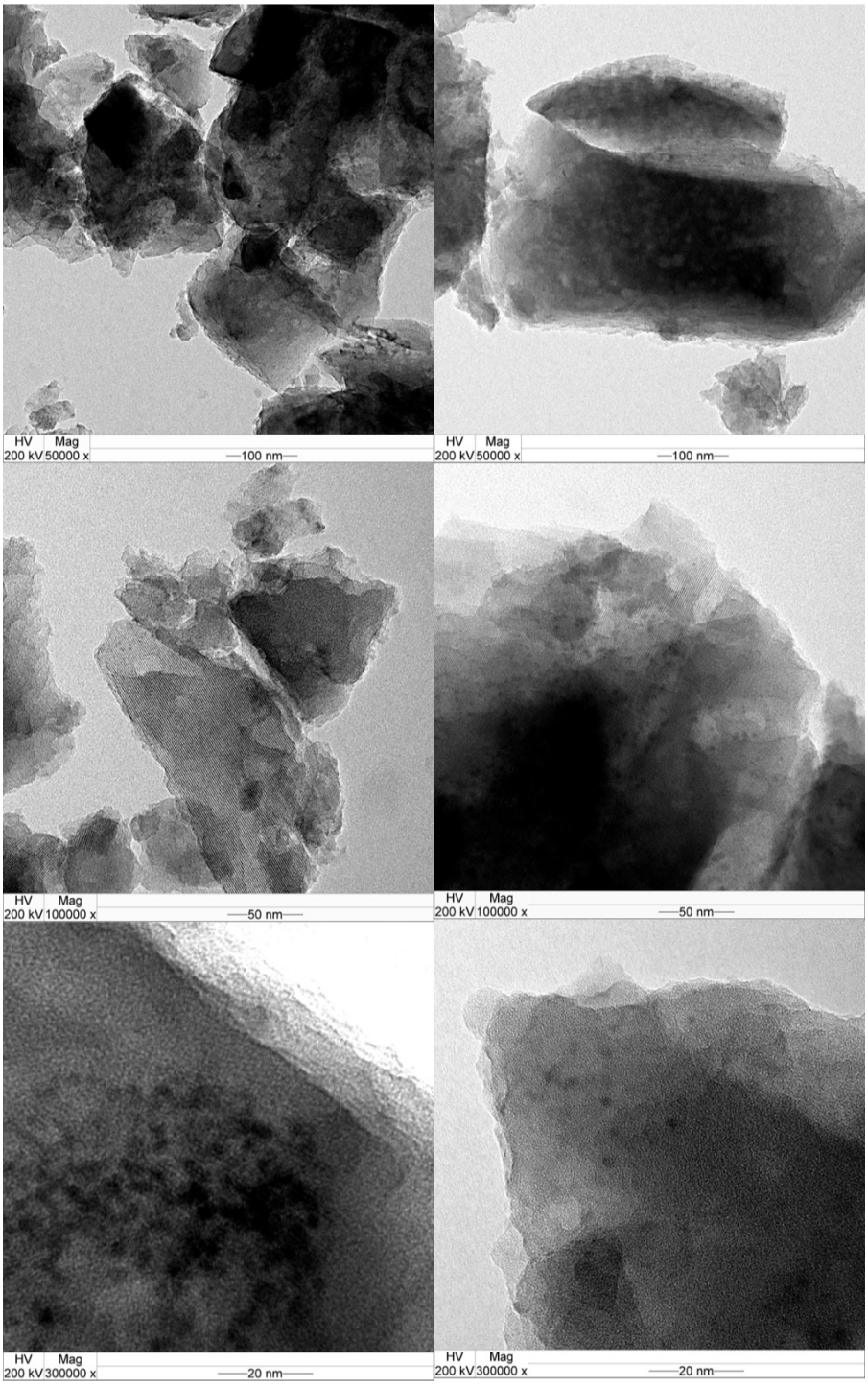

Figure B3. TEM image of 5%Cu/Y-IM.

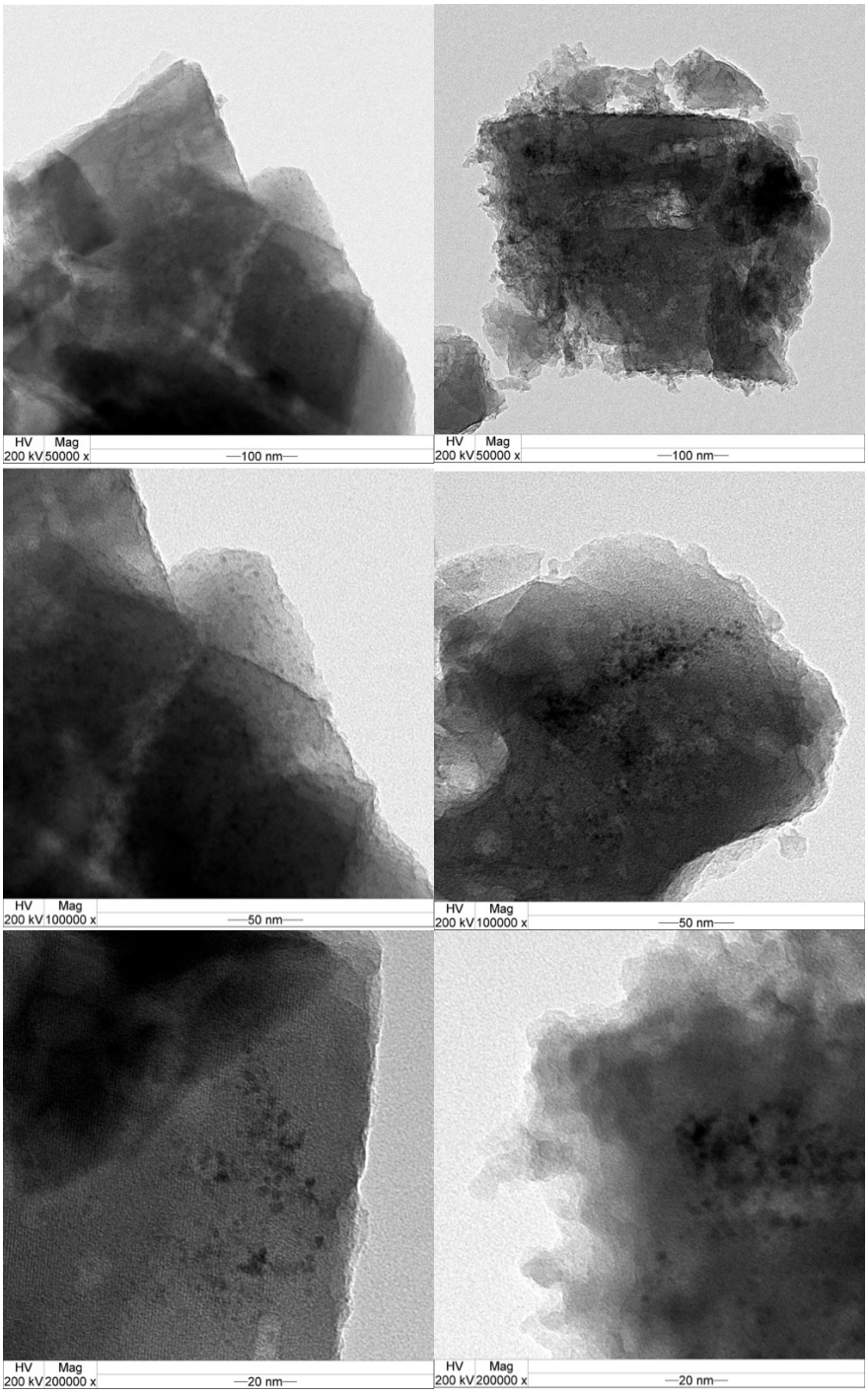

Figure B4. TEM image of 10%Cu/Y-IM.

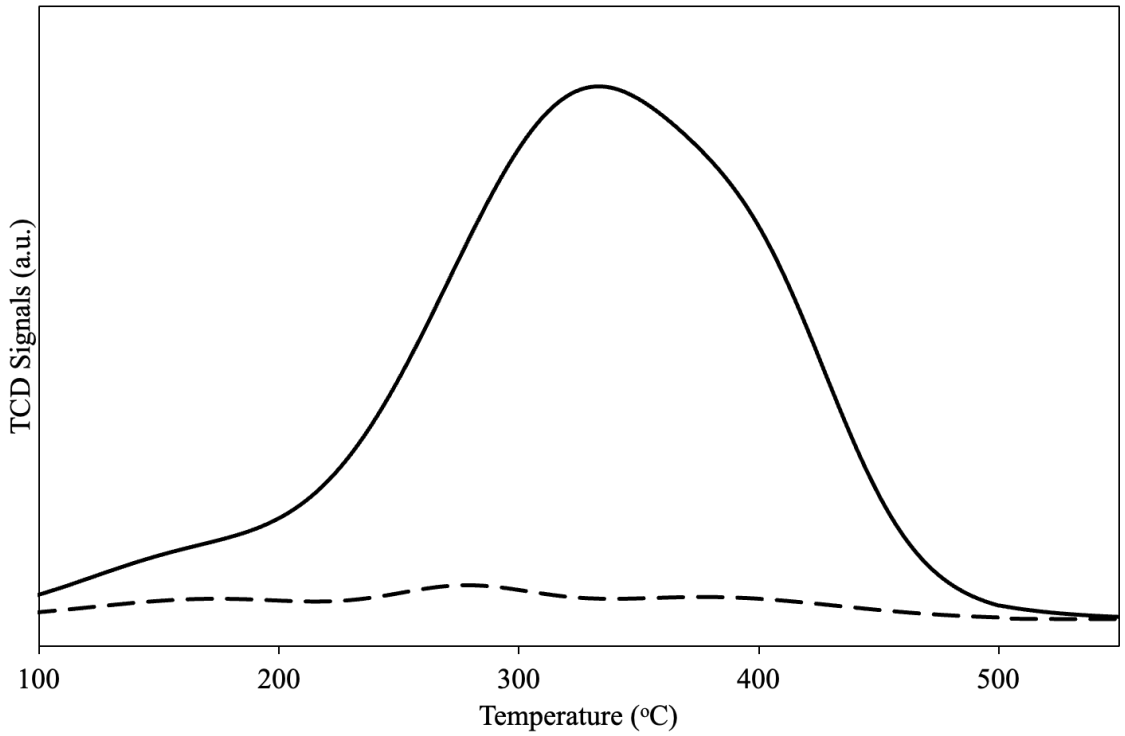

Figure B5. H_2-TPR and dissociative N_2O adsorbed of 5%Cu/Y-IE catalysts.

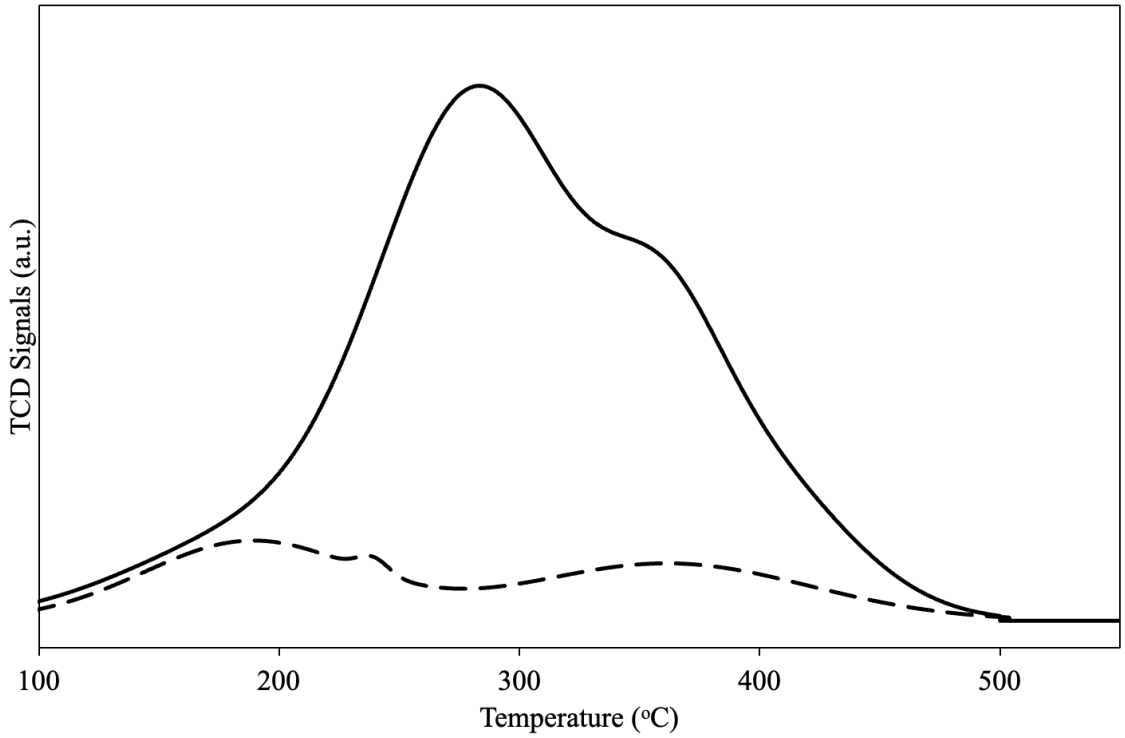

Figure B6. H_2-TPR and dissociative N_2O adsorbed of 5%Cu/Y-IM catalysts.

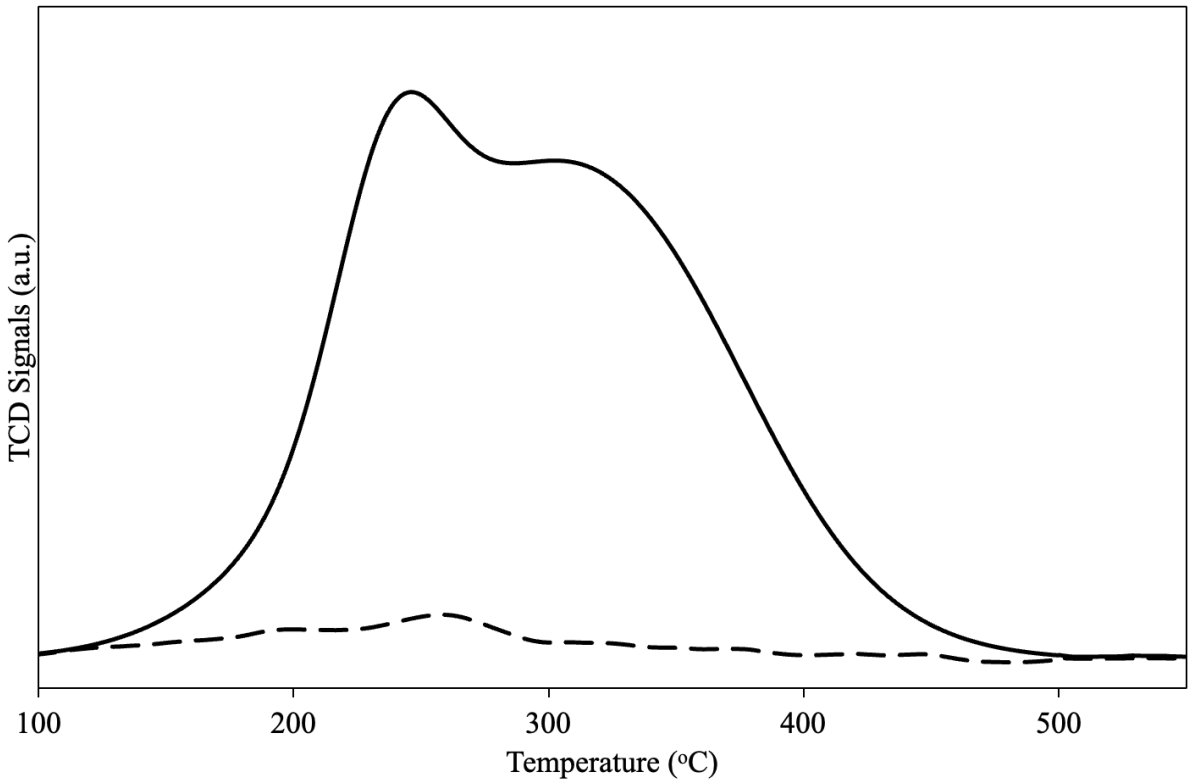

Figure B7. H_2-TPR and dissociative N_2O adsorbed of 10%Cu/Y-IM catalysts.

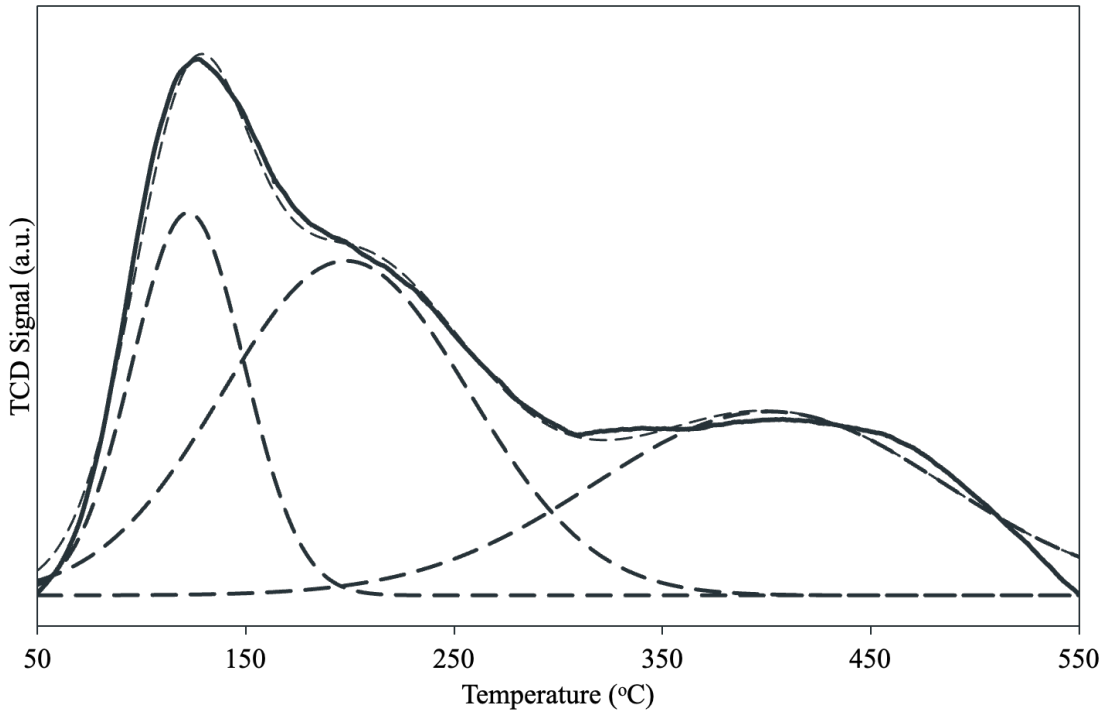

Figure B8. NH_3-TPD profiles of NH_4^+Y3.5 catalysts

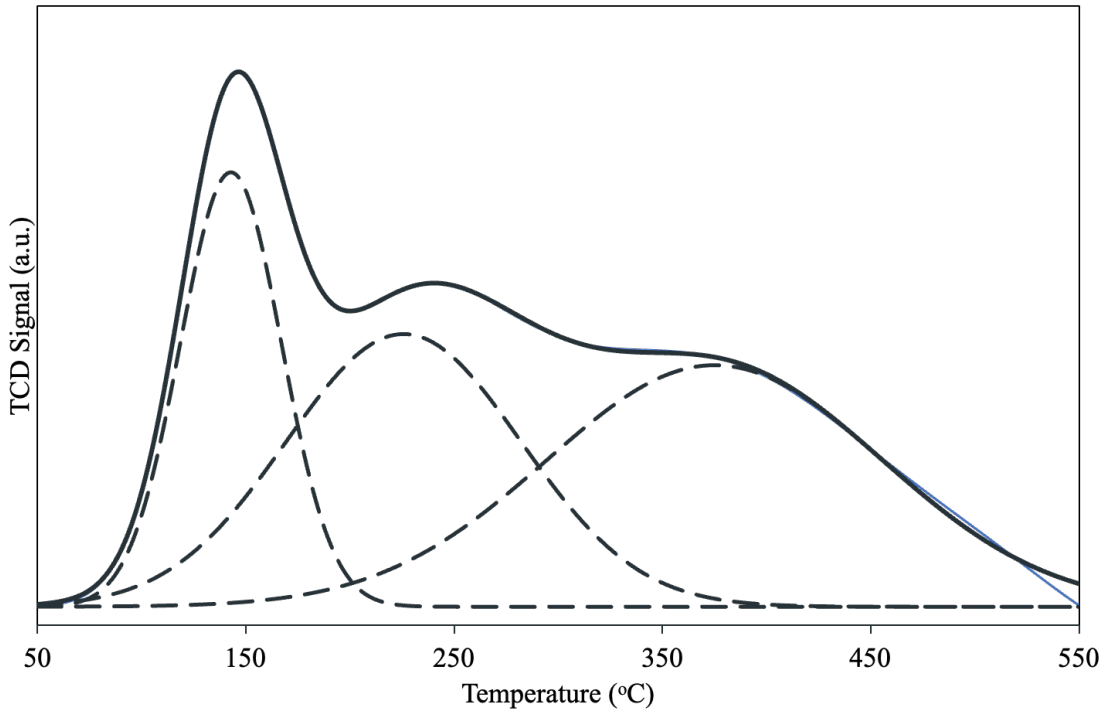

Figure B9. NH_3-TPD profiles of HY3.5 catalysts

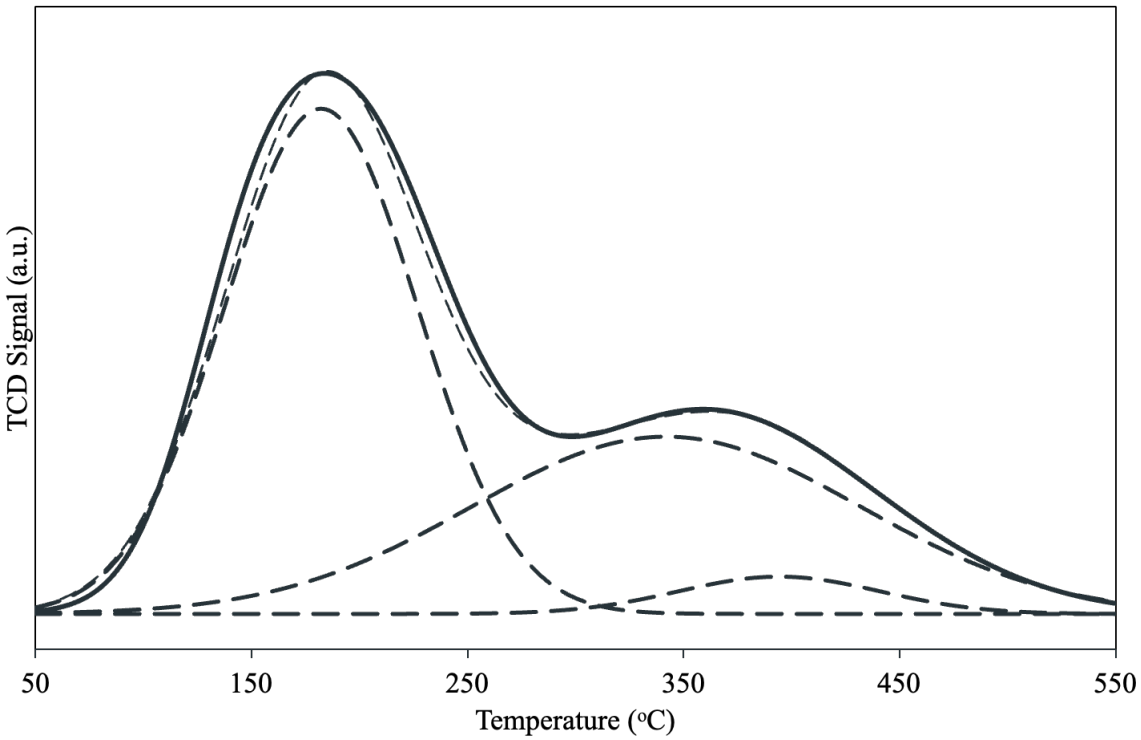

Figure B10. NH_3-TPD profiles of HY7.5 catalysts

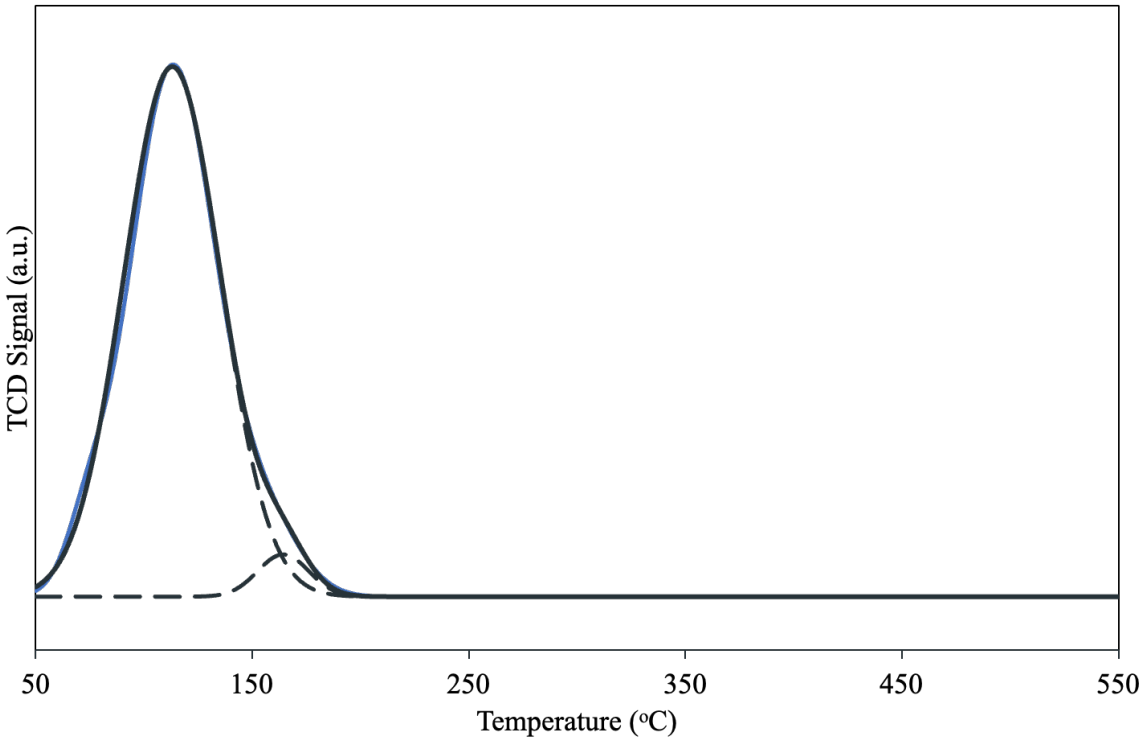

Figure B11. NH_3-TPD profiles of HY100 catalyst.

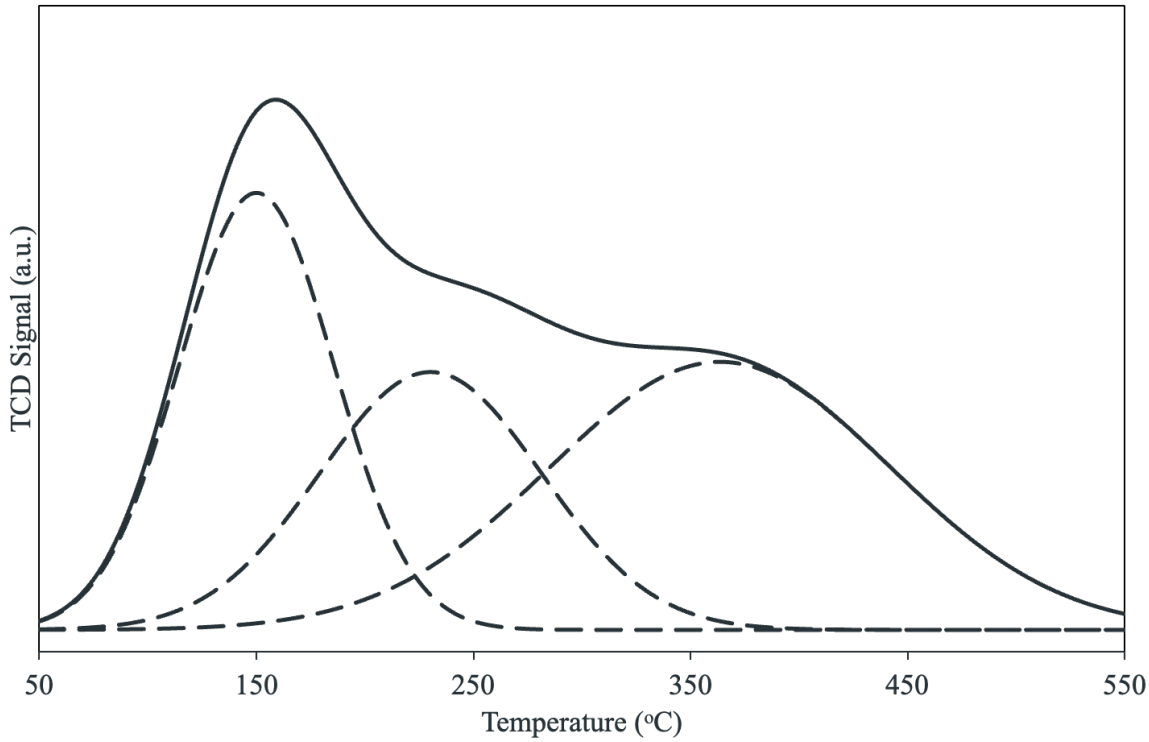

Figure B12. NH_3-TPD profiles of 5%Cu/Y-IE catalysts after reduction at 500 °C

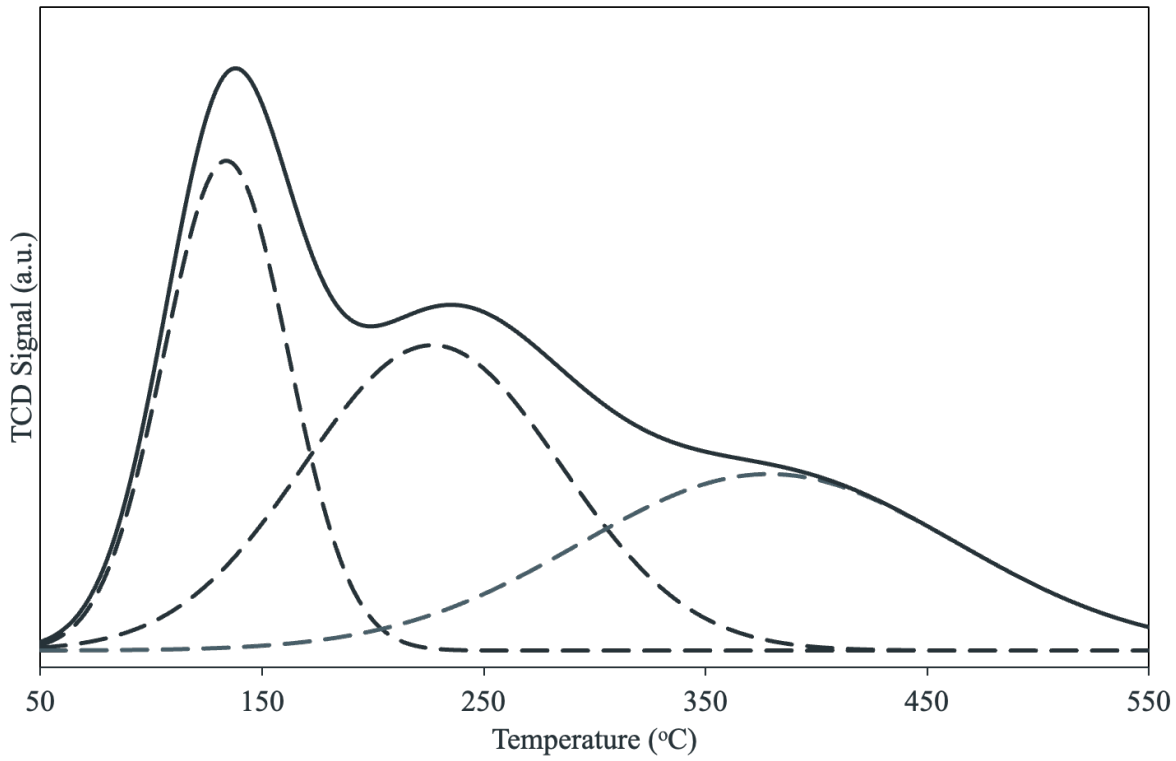

Figure B13. NH_3-TPD profiles of 5%Cu/Y-IM catalysts after reduction at 500 °C

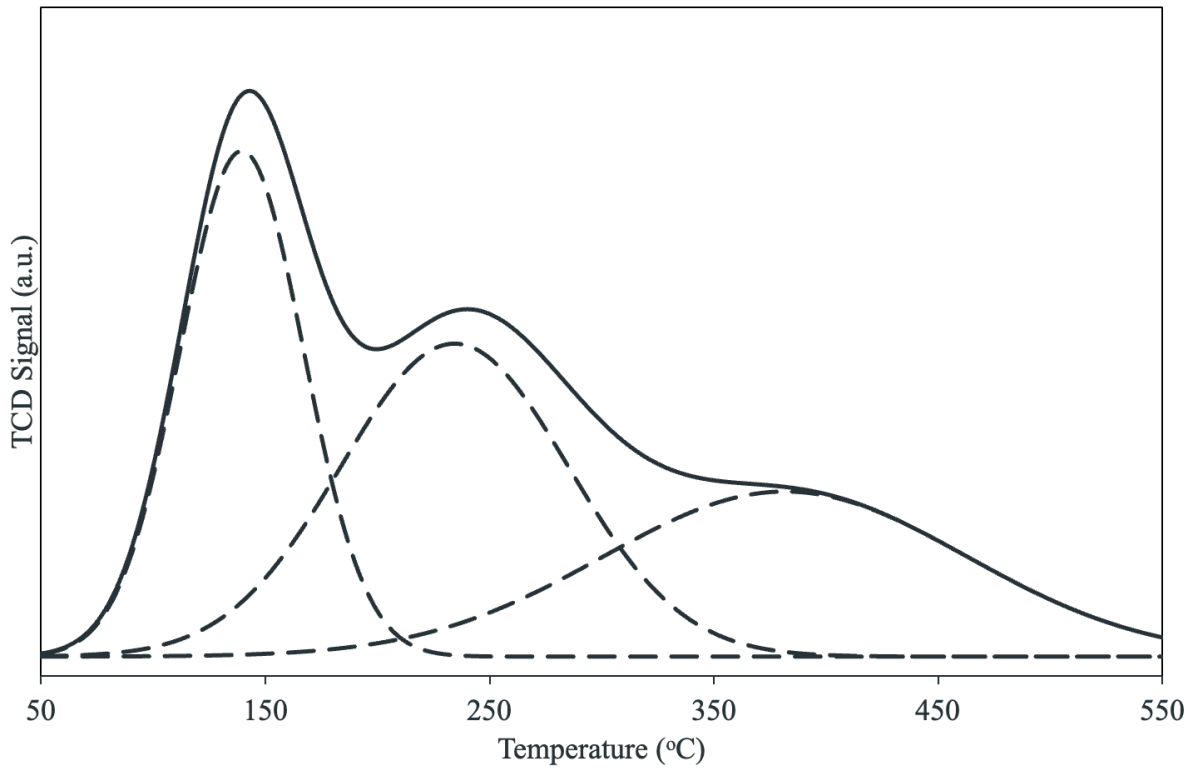

Figure B14. NH_3-TPD profiles of10%Cu/Y-IM catalysts after reduction at 500 °C

Part 2

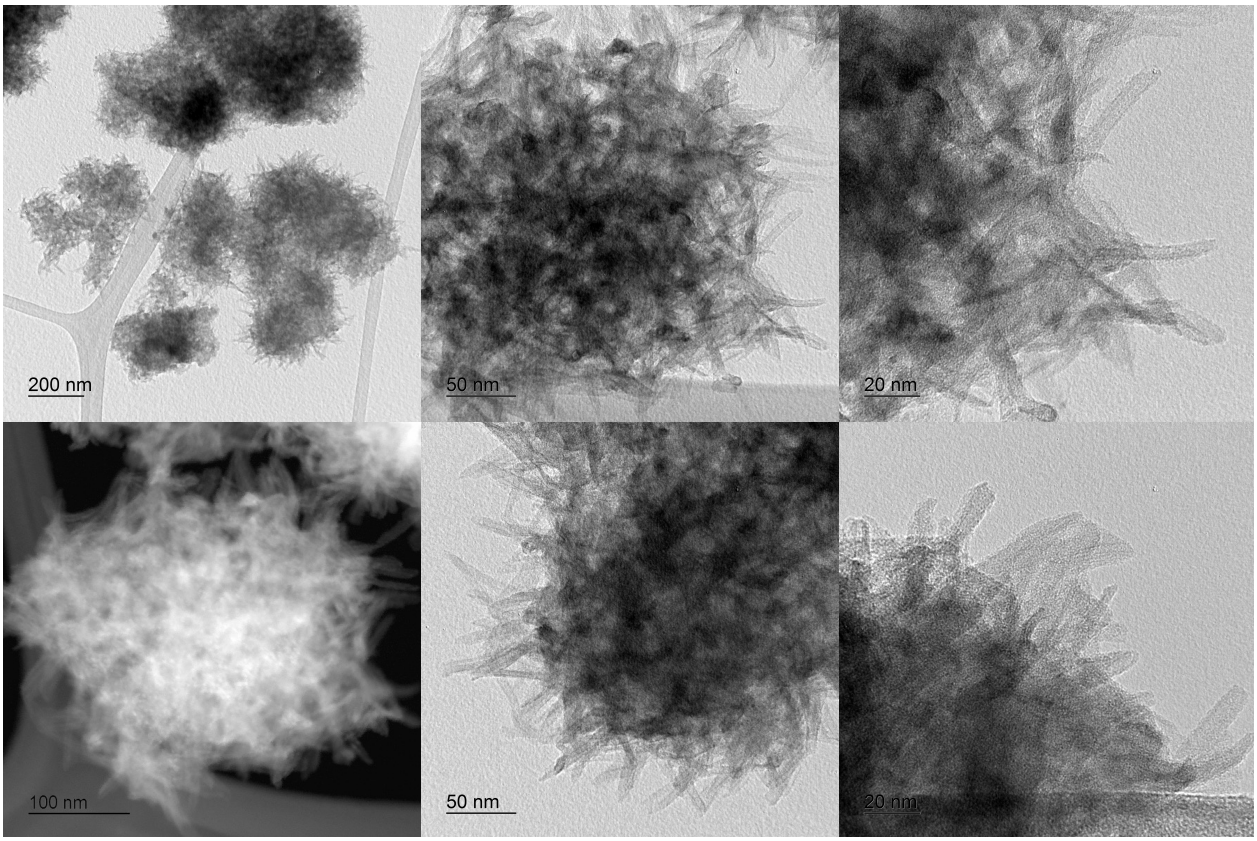

Figure B15 TEM image of 30%CuPS

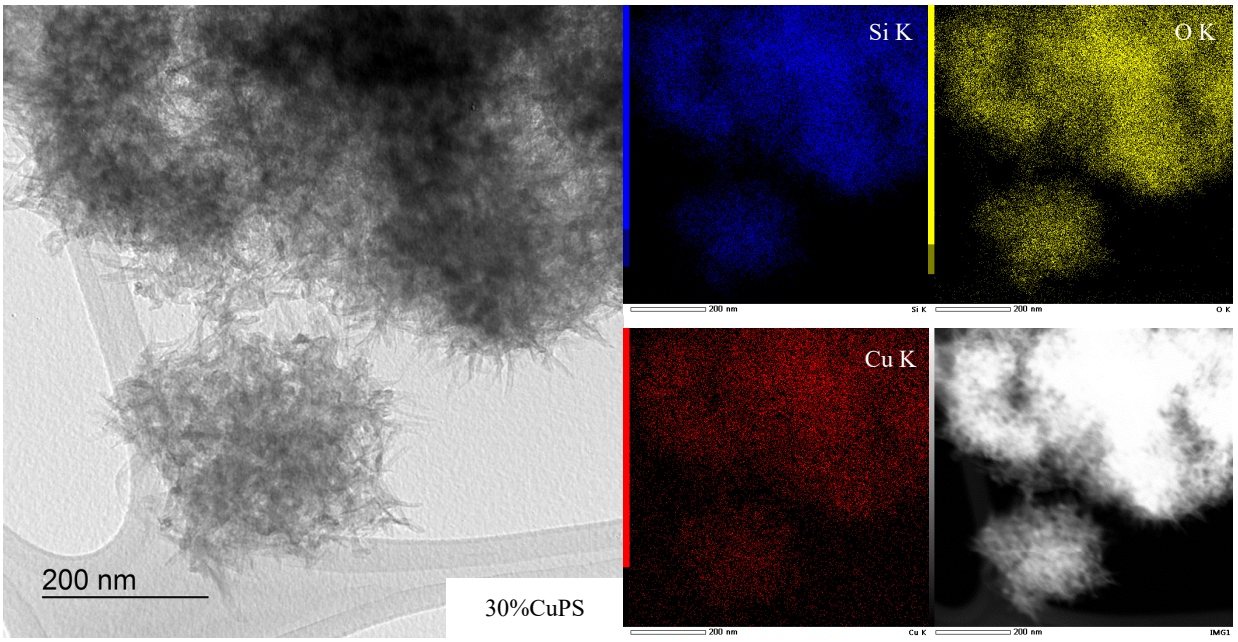

Figure B16 TEM image and elemental mapping of 30%CuPS

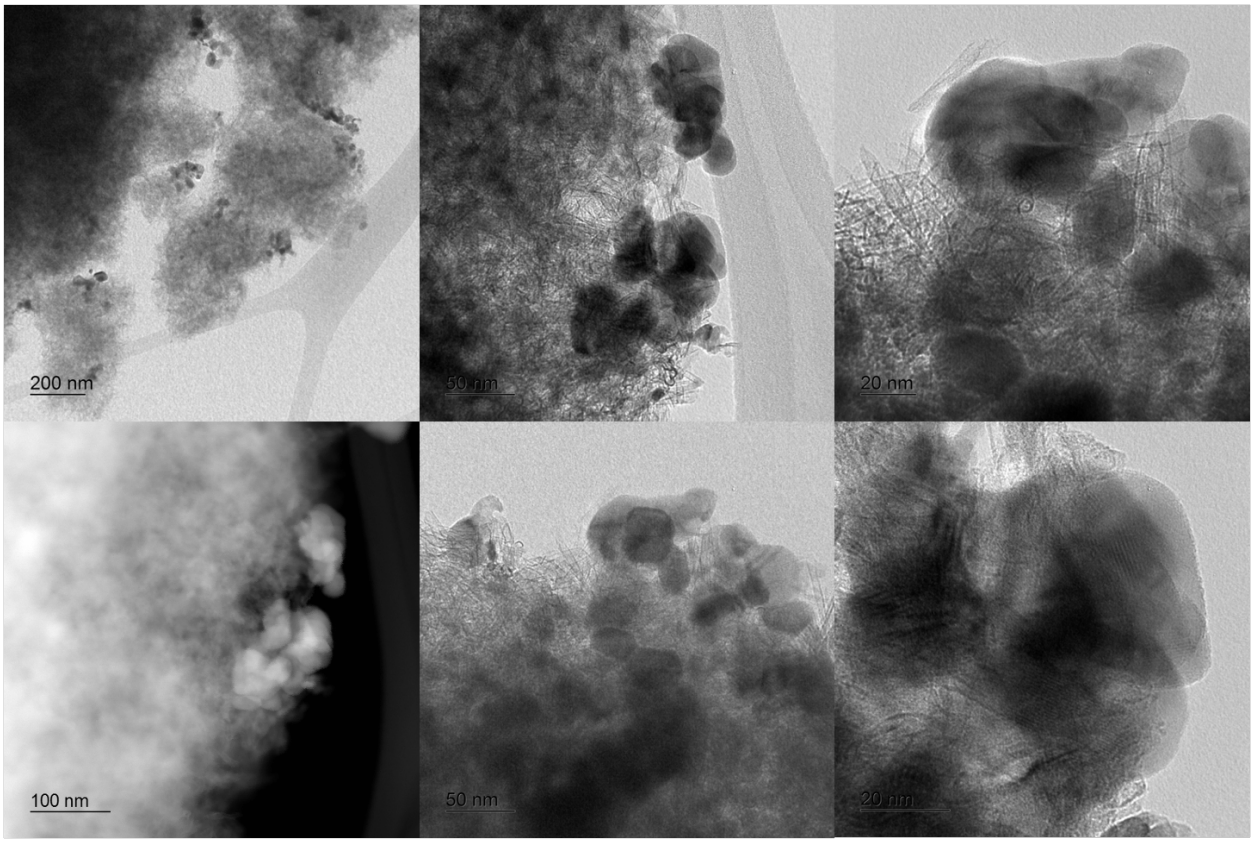

Figure B15 TEM image of 1%ZnCuPS

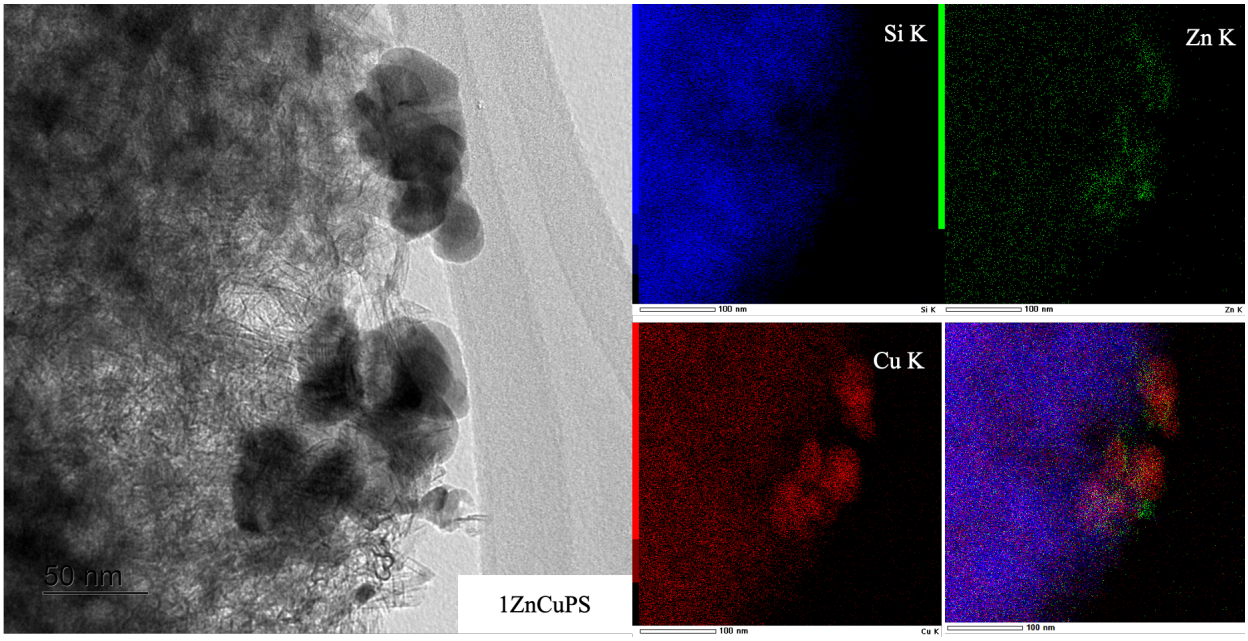

Figure B17 TEM image and elemental mapping of 1%ZnCuPS

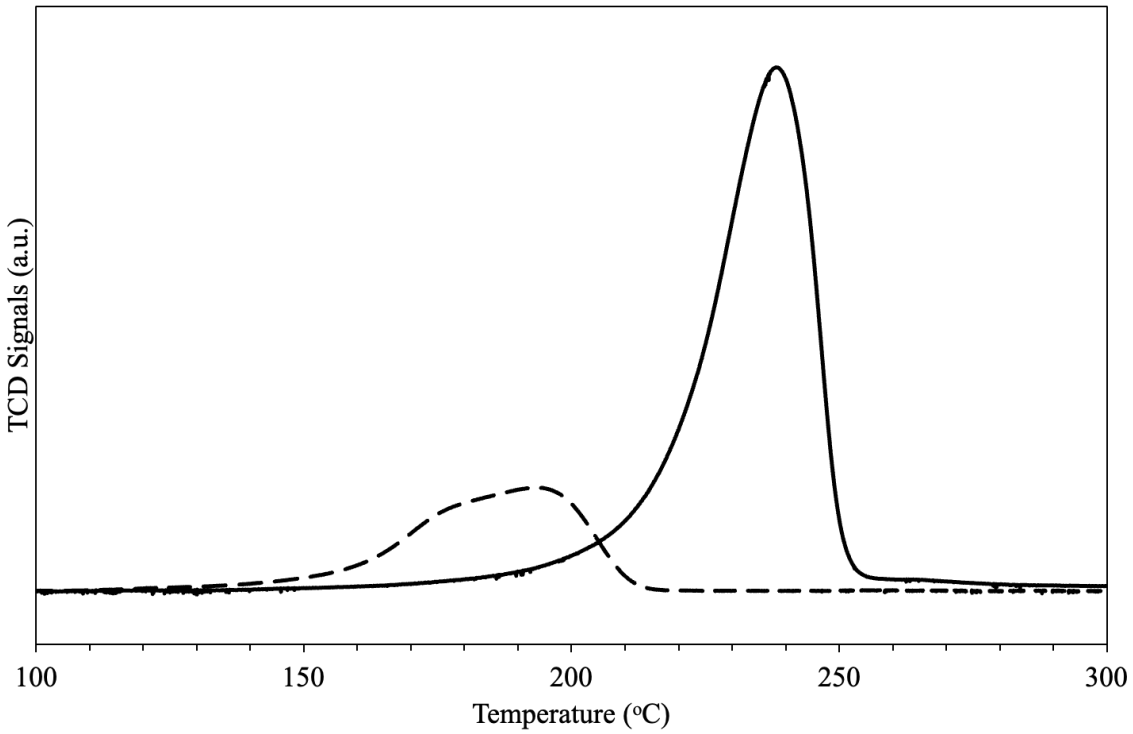

Figure B18 H_2-TPR of calcined and disscociative N_2O adsorbed 30%CuPS

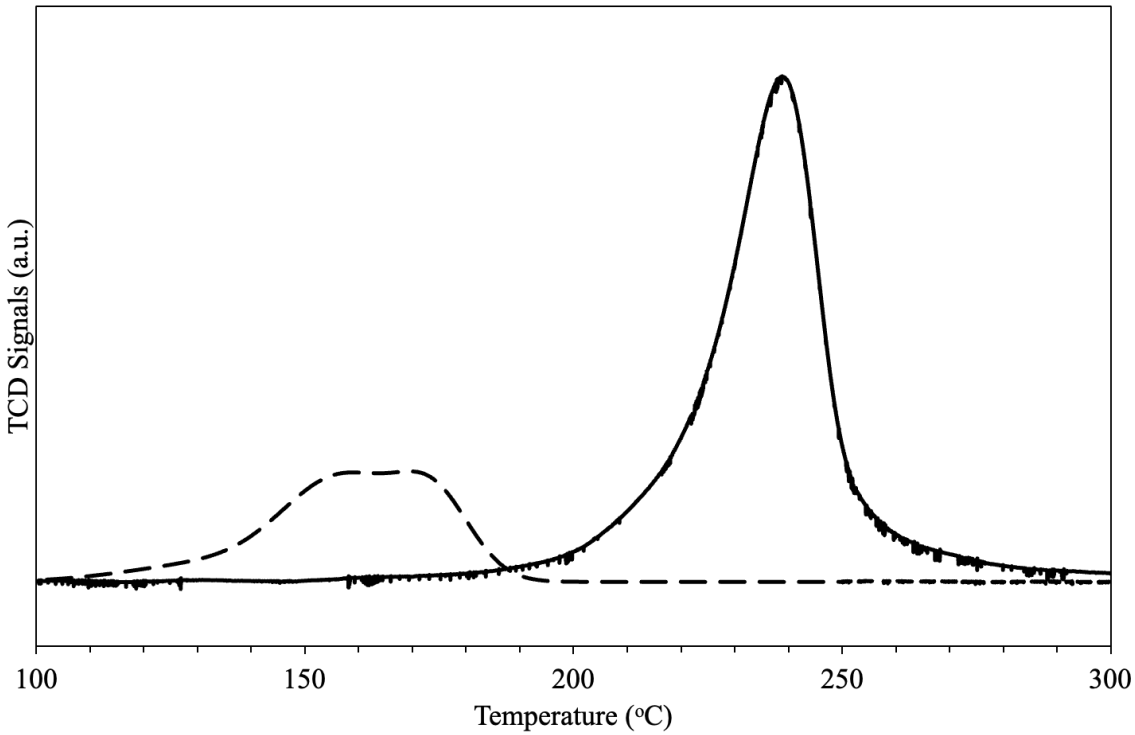

Figure B19 H_2-TPR of calcined and disscociative N_2O adsorbed 1%NiCuPS

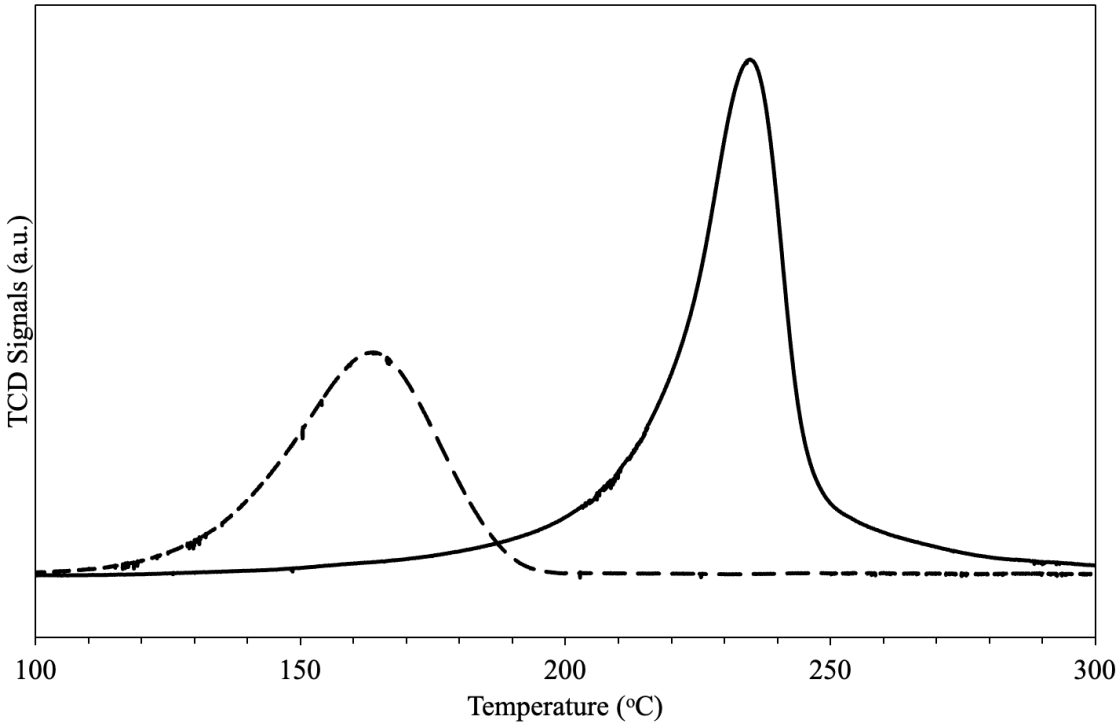

Figure B20 H_2-TPR of calcined and disscociative N_2O adsorbed 1%AgCuPS

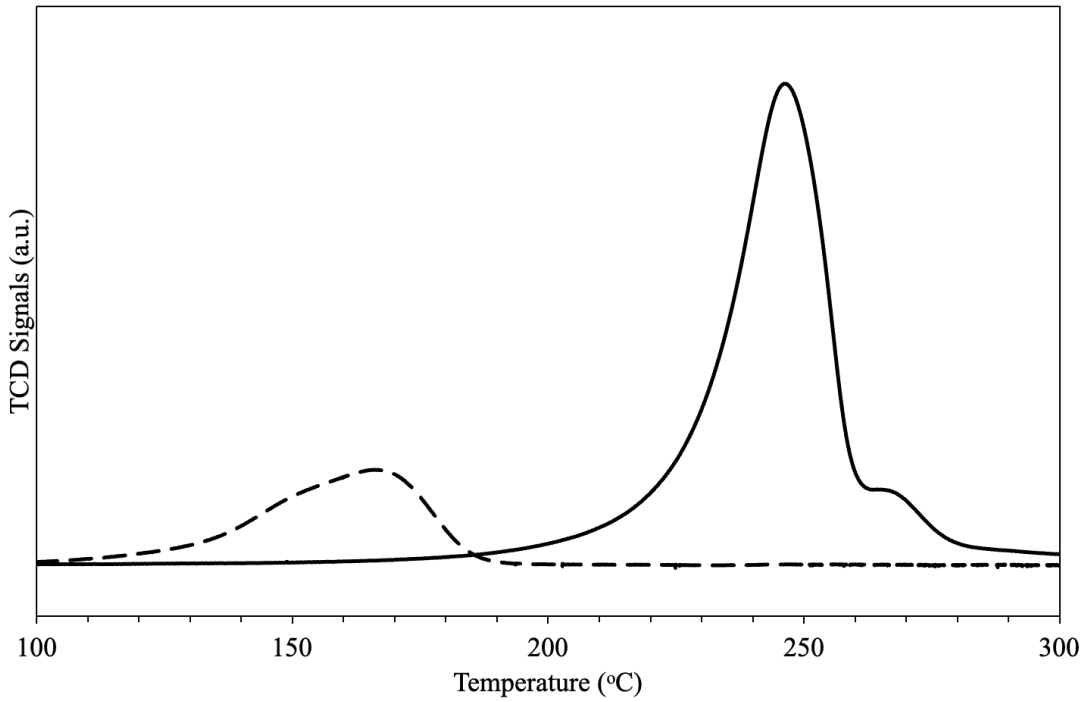

Figure B21 H_2-TPR of calcined and disscociative N_2O adsorbed 1%ZnCuPS

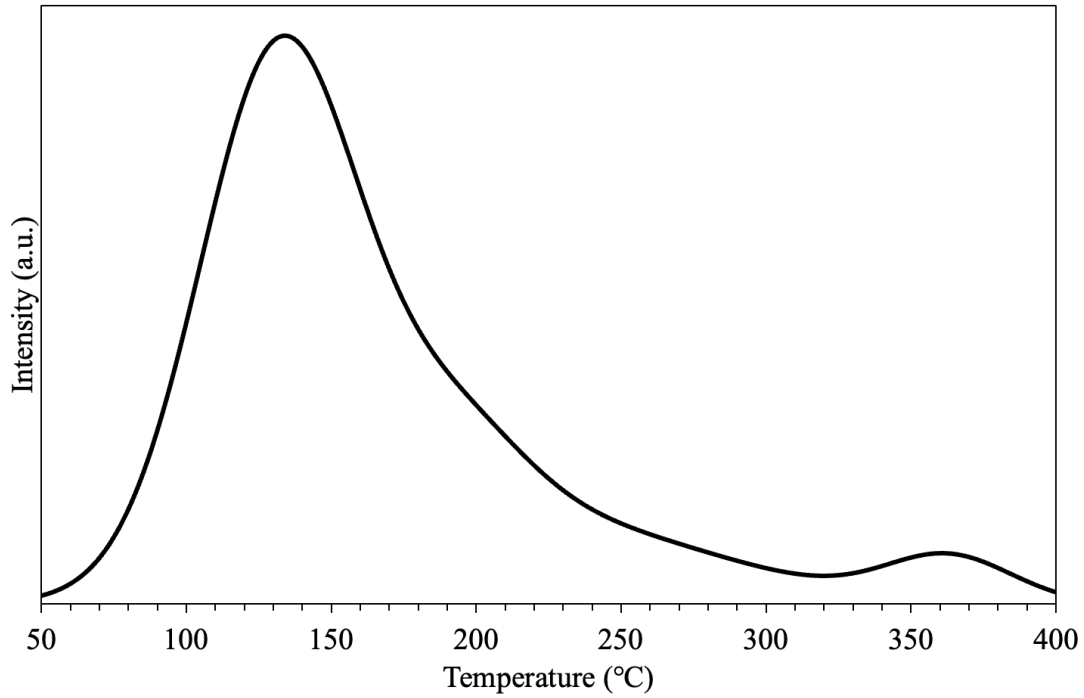

Figure B22 NH_3-TPD of 30%CuPS

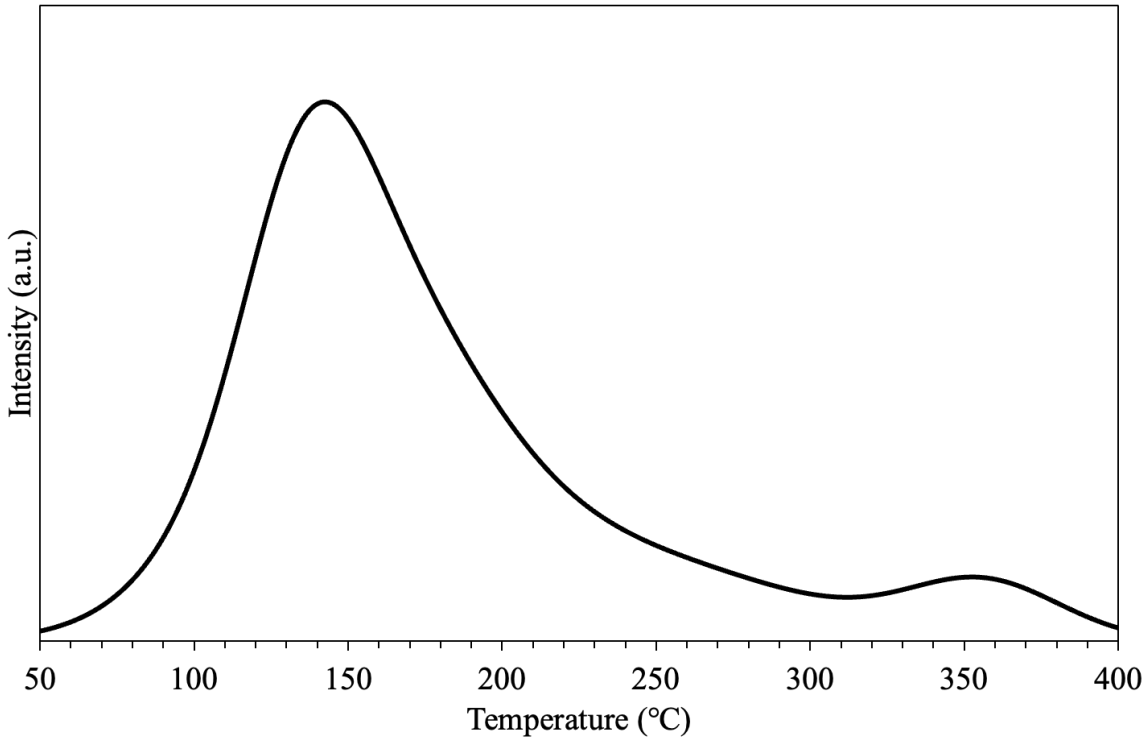

Figure B23 NH_3-TPD of 1%NiCuPS

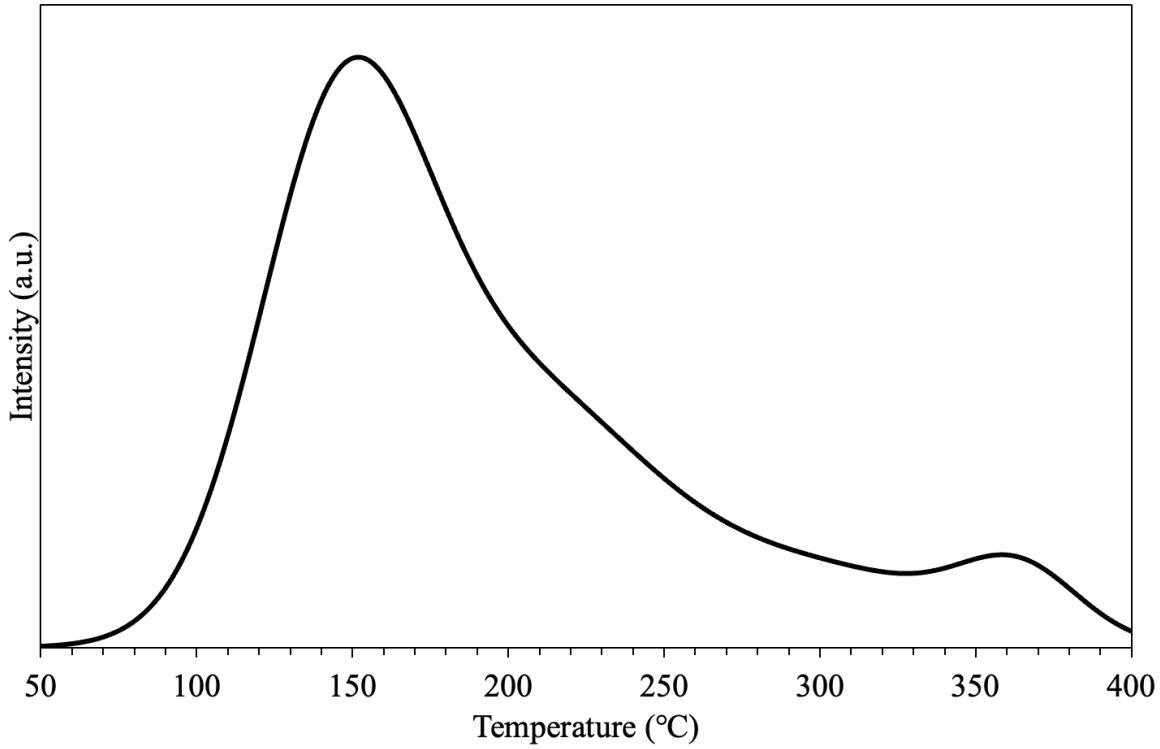

Figure B24 NH_3-TPD of 1%AgCuPS

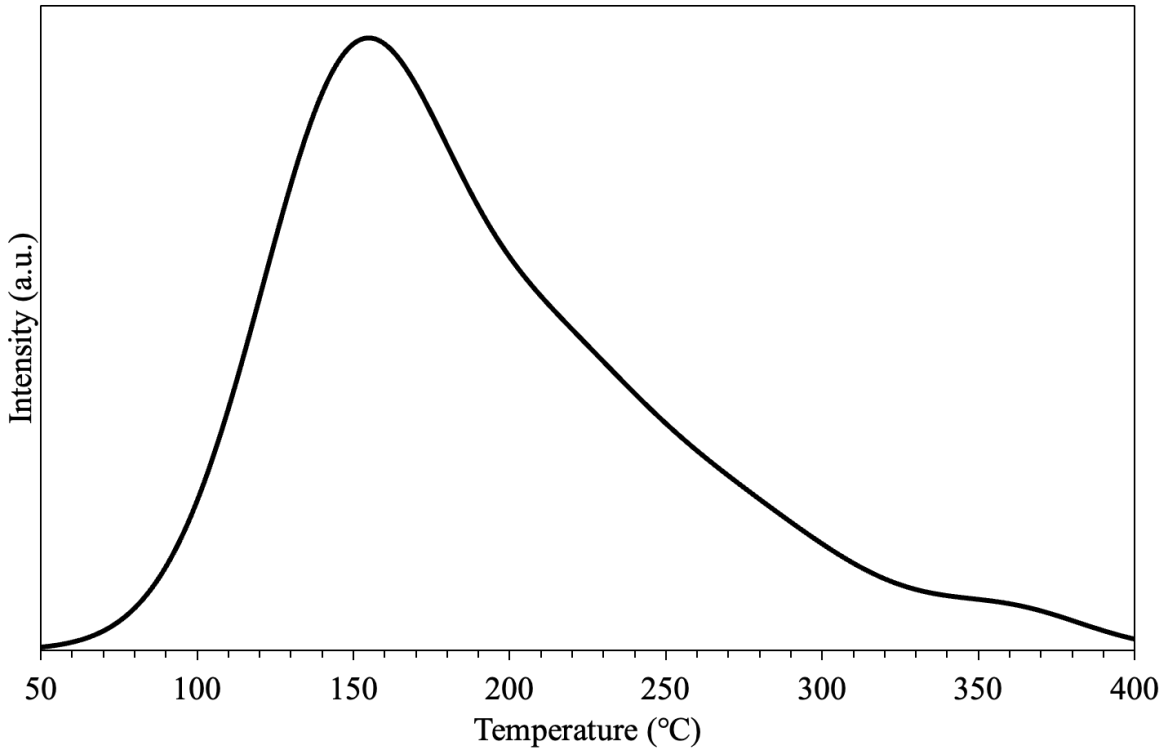

Figure B25 NH_3-TPD of 1%ZnCuPS

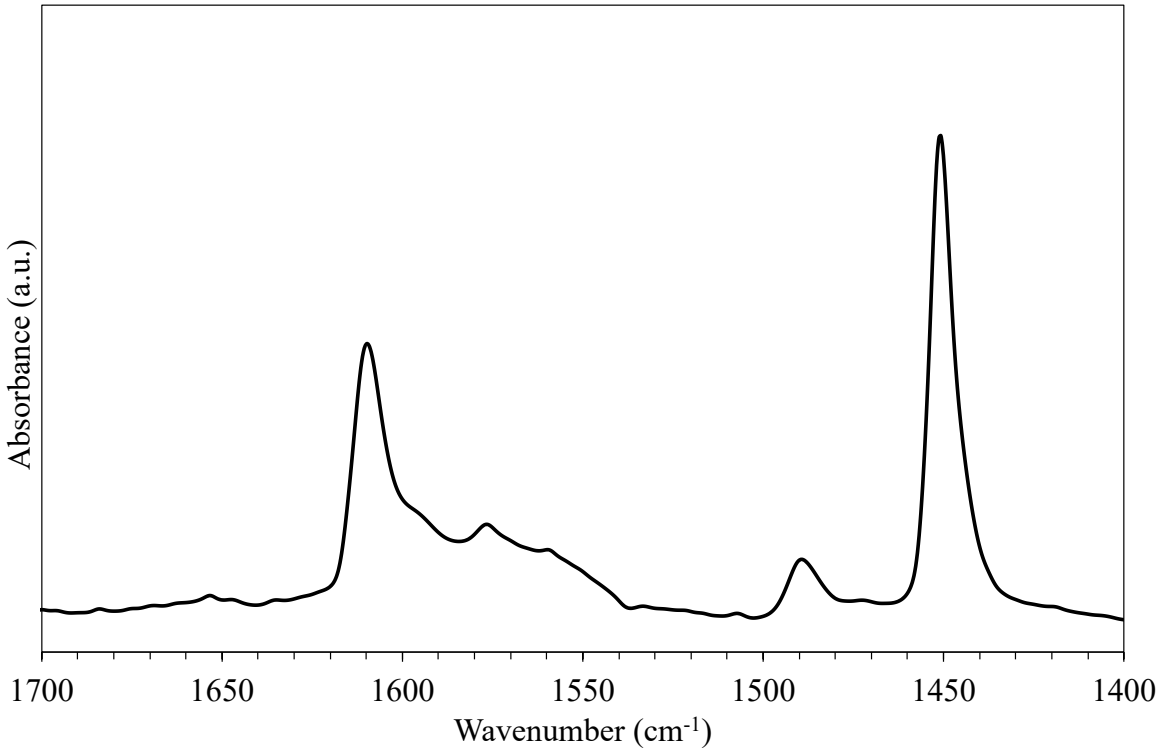

Figure B26 Pyridine IR of 30%CuPS

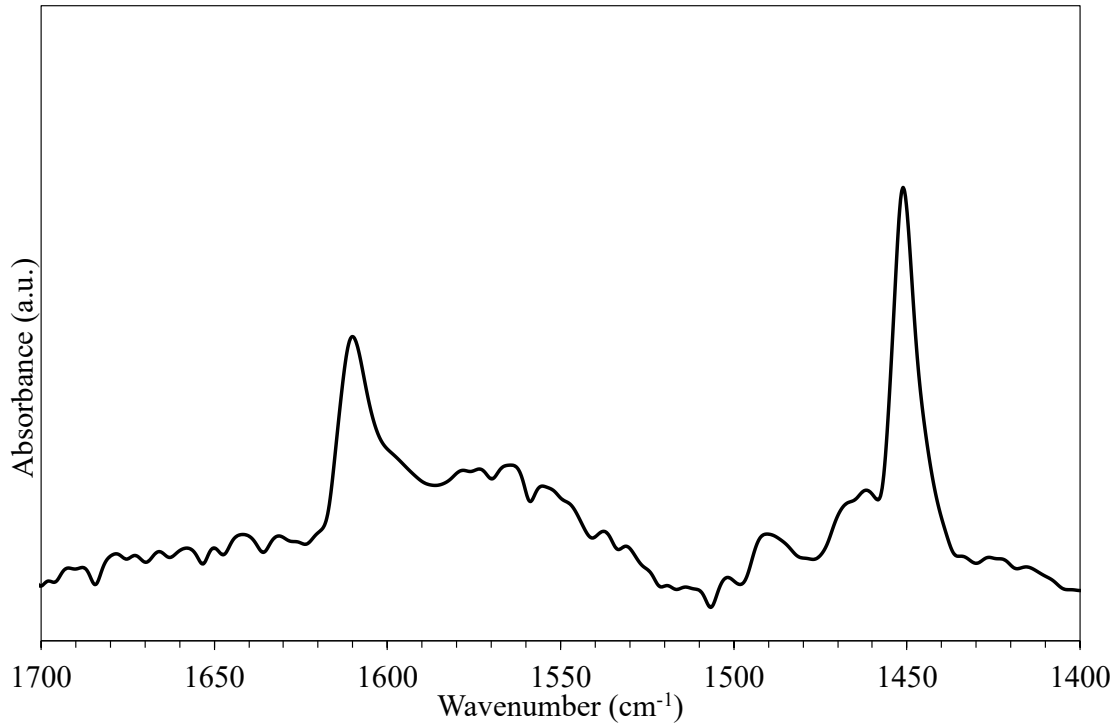

Figure B27 Pyridine IR of 1%NiCuPS

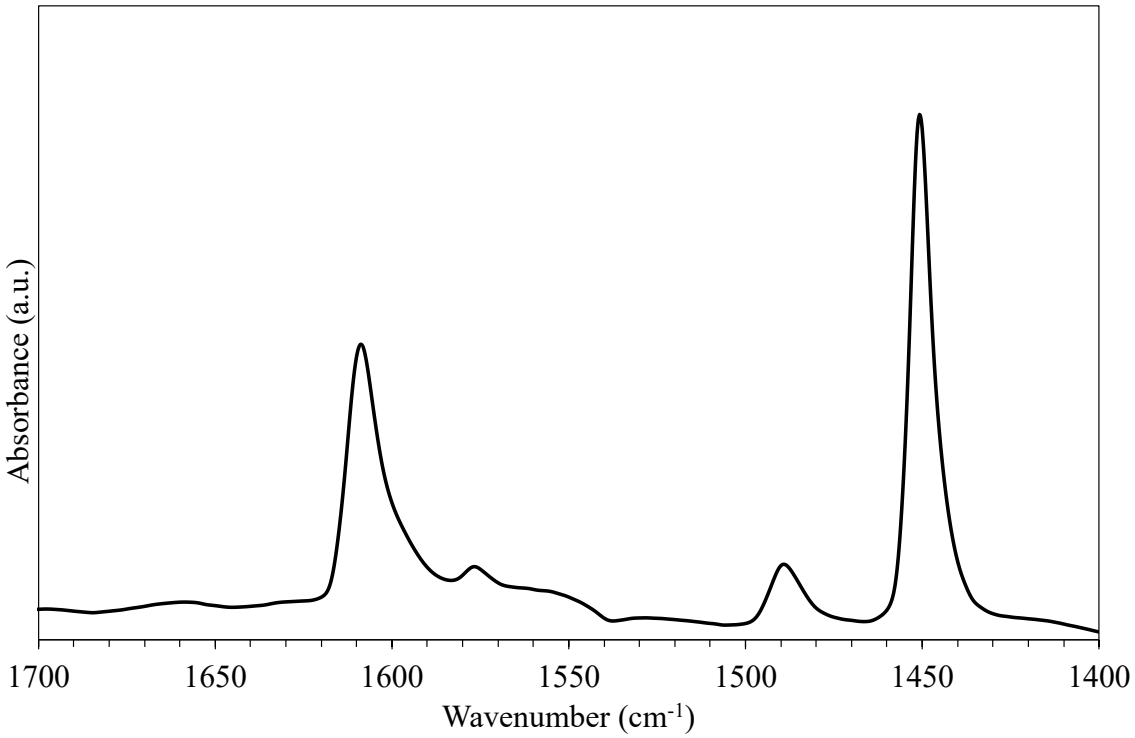

Figure B28 Pyridine IR of 1%AgCuPS

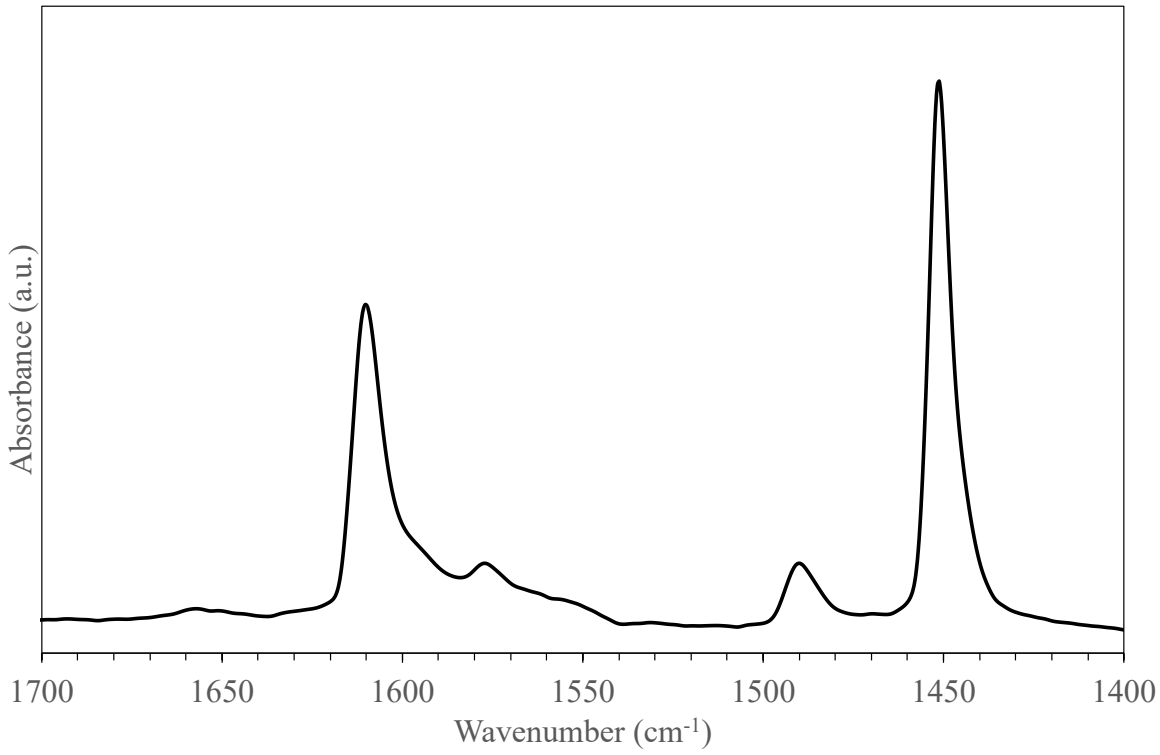

Figure B29 Pyridine IR of 1%ZnCuPS

APPENDIX C

REACTION DATA

TPR SIGNAL EVALUATION

The electronic signal from the TCD detector during TPR analysis is converted to mmol H_2, employing CuO as a standard. Here, CuO is used because it is a highly- reducible metal with clean and well-known reduction giving Cu metal as a final product following the equation:

$$CuO\ (s) + H_2\ (g) \longrightarrow Cu\ (s) + H_2O\ (g)$$

From TPR results of CuO standard

The peak area of CuO 6.658 give H2 consumption 0.724 mol.

5%CuY-IE give the peak area of 6.658

In-situ TRXANES Experimetal

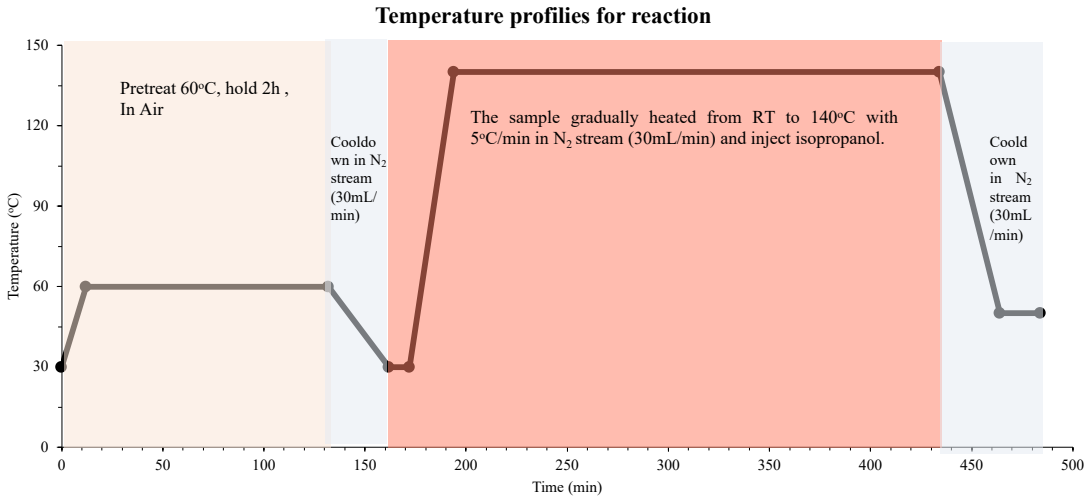

The phase fraction of Square planar Cu^{2+} species (CuO) and Octahedral Cu^{2+} species ($CuSO_4$) obtained from linear combination fitting (LCF) of 30%CuPS catalyst.

		R-factor	CuO	$CuSO_4$	$CuO/CuSO_4$
Temperature (°C)	70	0.0070	29.5	70.5	0.42
	80	0.0071	31.2	68.8	0.45
	90	0.0071	31.1	68.9	0.45
	100	0.0072	31.2	68.8	0.45
	110	0.0072	31.3	68.7	0.46
	120	0.0072	31.5	68.5	0.46
	130	0.0073	32.3	67.7	0.48
	140	0.0070	32.5	67.5	0.48
Time (min)	10	0.0080	34	66	0.52
	20	0.0069	36.2	63.8	0.57
	30	0.0070	36.6	63.4	0.58
	40	0.0069	37.1	62.9	0.59
	50	0.0080	37.2	62.8	0.59
	60	0.0077	37.3	62.7	0.59
	70	0.0068	37.6	62.4	0.60
	80	0.0067	37.7	62.3	0.61
	90	0.0067	37.7	62.3	0.61
	100	0.0078	37.9	62.1	0.61
	110	0.0067	38	62	0.61
	120	0.0066	37.8	62.2	0.61

The phase fraction of Square planar Cu^{2+} species (CuO) and Octahedral Cu^{2+} species ($CuSO_4$) obtained from linear combination fitting (LCF) of 1%ZnCuPS catalyst.

		R-factor	CuO	$CuSO_4$	$CuO/CuSO_4$
Temperature (°C)	70	0.0037	36.6	63.4	0.58
	80	0.0035	38.1	61.9	0.62
	90	0.0034	40.3	59.7	0.68
	100	0.0033	42.1	57.9	0.73
	110	0.0030	46.1	53.9	0.86
	120	0.0030	50.4	49.6	1.02
	130	0.0029	53	47	1.13
	140	0.0028	55.6	44.4	1.25
Time (min)	10	0.0025	58.9	41.1	1.43
	20	0.0024	60.6	39.4	1.54
	30	0.0023	61.8	38.2	1.62
	40	0.0022	59.7	40.3	1.48
	50	0.0021	57.1	42.9	1.33
	60	0.0020	58	42	1.38
	70	0.0019	57.3	42.7	1.34
	80	0.0019	57.4	42.6	1.35
	90	0.0020	57.5	42.5	1.35
	100	0.0019	57.2	42.8	1.34
	110	0.0019	56.2	43.8	1.28
	120	0.0019	57.3	42.7	1.34

Acidity

NH_3-TPD

$$\text{Calibration valve (CV)} = \frac{\text{(loop volume x \% analytical gas)}}{\text{Calibration area}}$$

Volume (μL) = CV x analytical area

$$\text{Amount adsorbed (μmol)} = \frac{\text{Pressure (atm) x V (μL)}}{\text{R (L x atm/K/mol) x (loop temperature (°C)+273.15}}$$

$$\text{Uptake (μmol/g)} = \frac{\text{Amount adsorbed (μmol)}}{\text{Catalyst weight (g)}}$$

GC CHROMATOGRAM

Prior to analysis, the products were identified by standard sample. Then, quantitative analysis was carried out with GC-FID (Gas chromatography equipped with Flame Ionization Detector). The analytical conditions of products from catalytic transfer hydrogenation of furfuryl alcohol to GVL are shown in Table C1 and Table C2 respectively.

Table C1 GC conditions for from catalytic transfer hydrogenation of furfuryl alcohol to GVL

Column	Rtx-5
Temperature program	45°C to 260 °C
Carrier gas	Nitrogen gas
Injection	260 °C
Detector	FID (260 °C)
Internal standard	10% Toluene/methanol

Table C1 Product distribution of 5%Cu/Y-IE catalyst from the measurement by GC-FID[a]

Product	Area	Response factor
FF	0	0.78
FE	5802	1.10
LA	0	0.65
IPL	39954	1.02
GVL	132482	1.04

[a] reaction condition: furfuryl alcohol 200μL (2.35 mmol), Isopropanol 10 mL, N_2 10 bar, 140°C ,1h

Calculation of furfuryl alcohol conversion, GVL selectivity and reaction yield

Calculation of conversion

Conversion can be calculated from the following equation:

Corrected area is a mathematic term where the area of interested is divided by the area of the standard. A

$$\text{Corrected area of A} = \text{Area of } \frac{\text{A}}{\text{Internal standard}}$$

$$\text{Conversion (\%)} = \frac{(\text{Corrected area of initial feed} - \text{Corrected of feed at any time}).\times 100}{\text{Corrected area of initial feed}}$$

For example, 5Cu/Y-IE catalyst

FOL conversion (%) of 5Cu/Y-IE catalysts

$$\text{FOL conversion (\%)} = \frac{(0.46) - (0.45)}{(0.46)} \times 100 = 78.4\%$$

Calculation of Yield

Calculate the precent yield of each component in sample as follow:

$$\text{\% Yield in each product} = \frac{(\text{Corrected area of product/ Response factor})}{(\text{Corrected area of FOL/ Response factor})} \times 100$$

For example, 5%Cu/Y-IE catalyst

GVL yield (%) of 5%Cu/Y-IE

$$\text{\% Yield of GVL} = \frac{(0.26/1.04)}{(0.46/1)} \times 100 = 58.0\ \%$$

Calculation of selectivity

% Selectivity can be obtained from the following equation:

$$\text{\% Selectivity in each product} = \frac{\text{Corrected area of product/ Response factor}}{\text{Total corrected area of product}} \times 100$$

For example, 5%Cu/Y-IE catalyst

GVL selectivity (%) of 5%Cu/Y-IE

$$\%.\ \text{Selectivity of GVL} = \frac{0.26}{(0.26 + 0.012 + 0.080)} \times 100 = 74.6\%$$

The catalytic activity of all catalysts

Table C2 Times profiles of 5%Cu/Y-IE catalyst

Time (min)	Conversion (%)	Yield (%)			Selectivity (%)			Mass balance
		FE	GVL	IPL	FE	GVL	IPL	
60	78.0	2.5	57.2	18.0	3.2	73.3	23.1	99
120	92.0	0.0	66.0	22.0	0.0	71.7	23.9	95
240	96.0	1.3	68.0	24.0	1.4	70.8	25.0	97
480	96.0	1.3	68.0	23.0	1.4	70.8	24.0	96

Reaction condition: Furfuryl alcohol 200 µL (2.35 mmol), Isopropanol 10 mL (130.8 mmol) 5%Cu/Y-IE 200 mg, reaction temperature 160°C, N_2 pressure 10 bars.

Table C3 Times profiles of 5%Cu/Y-IM catalyst

Time (min)	Conversion (%)	Yield (%)			Selectivity (%)			Mass balance
		FE	GVL	IPL	FE	GVL	IPL	
60	56.2	0.9	37.2	18.3	1.6	66.2	32.6	100
120	79.1	2.6	58.0	16.4	3.3	73.3	20.7	97
240	85.0	0.0	60.0	22.0	0.0	70.6	25.9	96
480	83.0	0.0	57.0	24.0	0.0	68.7	28.9	95

Reaction condition: Furfuryl alcohol 200 µL (2.35 mmol), Isopropanol 10 mL (130.8 mmol) 5%Cu/Y-IM 200 mg, reaction temperature 160°C, N_2 pressure 10 bar.

Table C3 Times profiles of 10%Cu/Y-IM catalyst

Time (min)	Conversion (%)	Yield (%)			Selectivity (%)			Mass balance
		FE	GVL	IPL	FE	GVL	IPL	
60	69.0	1.8	47.0	18.0	5.0	68.1	26.1	99.2
120	73.0	2.6	53.0	16.0	4.2	72.6	21.9	98.8
240	75.9	3.4	55.1	15.2	4.5	72.6	20.0	97.1
480	74.0	2.2	52.0	15.0	3.0	70.3	20.3	99.5

Reaction condition: Furfuryl alcohol 200 µL (2.35 mmol), Isopropanol 10 mL (130.8 mmol) 10%Cu/Y-IM 200 mg, reaction temperature 160°C, N_2 pressure 10 bar.

Table C4. Catalytic performance of 30%CuPS and secondary metal

Catalysts	Conversion %	Yield (%)			Selectivity (%)			GVL/IPL
		FE	GVL	IPL	FE	GVL	IPL	
30%CuPS	79.7	1.7	57.4	20.9	2.1	72.0	26.2	2.74
1%NiCuPS	91.9	3.4	56.7	32.6	3.7	61.7	35.5	1.70
1%AgCuPS	96.1	4.4	58.8	33.8	4.6	61.2	35.2	1.74
1%ZnCuPS	94.2	4.3	60.8	30.3	4.5	64.5	32.1	2.01

Reaction condition: Furfuryl alcohol 200 µL (2.35 mmol), Isopropanol 10 mL (130.8 mmol) catalyst 200 mg, reaction temperature 140°C, reaction time 2h N_2 pressure 10 bars.

Table C5. To study effect of water in 1%ZnCuPS catalyst

Catalysts	Conversion %	Yield (%)			Selectivity (%)			TON
		FE	GVL	IPL	FE	GVL	IPL	
1%ZnCuPS	87.6	4.4	58.1	25.3	5.1	66.3	28.8	2.6
1%ZnCuPS + iso dried (1)	72.2	2.5	52.5	17.5	3.5	72.7	24.2	2.2
1%ZnCuPS + iso dried (2)	80.4	3.1	54.4	23.6	3.8	67.7	29.3	2.4

Reaction condition: Furfuryl alcohol 200 µL (2.35 mmol), Isopropanol 10 mL (130.8 mmol) catalyst 200 mg, reaction temperature 140°C, reaction time 1h N_2 pressure 10 bars.

Table C6. Effect of hydrogen donor in catalytic transfer hydrogenation of furfuryl alcohol to GVL

Entry	IPA/THF (mL)	Conversion %	Yield (%)			TON
			FE	GVL	IPL	
1	10 : 0	87.6	4.4	58.1	25.3	2.6
2	7 :3	87.7	2.2	61.0	24.7	2.6
3	5:5	88.3	2.3	62.3	23.2	2.6
4	3:7	74.3	2.0	61.2	11.0	2.2
5	1:9	55.9	0.0	49.5	7.6	1.7

Reaction condition: Furfuryl alcohol 200 µL (2.35 mmol), catalyst 200 mg, reaction temperature 140°C, reaction time 1h N_2 pressure 10 bars.

Table C7. Time profiles of 1%ZnCuPS catalysts in IPA/THF = 1: 9 in catalytic transfer hydrogenation of furfuryl alcohol to GVL

Time (h)	Conversion (%)	Yield (%)		Selectivity (%)	
		GVL	IPL	GVL	IPL
0.5	47.6	46.3	3.9	97.1	8.1
1	55.9	49.5	7.6	88.6	13.7
2	56.3	50.4	6.3	89.6	11.3
4	63.2	57.4	5.6	90.8	8.8
8	69.7	62.5	7.1	89.7	10.2
24	82.1	71.0	11.4	86.4	13.9

Reaction condition: Furfuryl alcohol 200 µL (2.35 mmol), catalyst 200 mg, reaction temperature 140°C, N_2 pressure 10 bars.

AURTHER BIOGRAPHY

Name Mr. Thanisorn Rattanaphonchaiwat

Date of birth 29 June 1999

Address 934 Moo 2 Thephrarak Subdistrict, Thephrarak District , Samutprakarn Province 10270

Education (2020) Bachelor of Science in industrial chemistry GPA 3.01

International Conferences

Thanisorn Rattanaphonchaiwat, Tanyarat Shoosri, Tawan Sooknoi, Thapong Teerawatananond and Patcharaporn Weerachawanasak, ***"Catalytic transfer Hydrogenation of Furfuryl alcohol to γ-Valerolactone by using Y zeolite and Cu/Y zeolite"***. PACCON 2023, General Sampao Chusri Building: E4, Mae Fah Luang University, Chiang Rai, Thailand.